

Development and proof of concept of a biological vascularized cell-based drug delivery system

Entwicklung und Proof of Concept eines biologischen, vaskularisierten,
zellbasierten Drug-Delivery-Systems



Dissertation zur Erlangung des
naturwissenschaftlichen Doktorgrades
der Julius-Maximilians-Universität Würzburg

vorgelegt von
Sebastian Kreß

geboren in Aschaffenburg

Würzburg, 2018

Eingereicht am: 08.11.2018

Mitglieder der Promotionskommission:

Vorsitzender: Prof. Dr. Markus Engstler

Gutachter: Prof. Dr. Heike Walles

Gutachter: Prof. Dr. Georg Krohne

Tag des Promotionskolloquiums: 27.03.2019

Doktorurkunde ausgehändigt am:

“Sometimes science is a lot more art than science.”

- Rick Sanchez

ABSTRACT

A major therapeutic challenge is the increasing incidence of chronic disorders. The persistent impairment or loss of tissue function requires constitutive on-demand drug availability optimally achieved by a drug delivery system ideally directly connected to the blood circulation of the patient. However, despite the efforts and achievements in cell-based therapies and the generation of complex and customized cell-specific microenvironments, the generation of functional tissue is still unaccomplished.

This study demonstrates the capability to generate a vascularized platform technology to potentially overcome the supply restraints for graft development and clinical application with immediate anastomosis to the blood circulation.

The ability to decellularize segments of the rat intestine while preserving the ECM for subsequent reendothelialization was proven. The reestablishment of a functional arteriovenous perfusion circuit enabled the supply of co-cultured cells capable to replace the function of damaged tissue or to serve as a drug delivery system. During *in vitro* studies, the applicability of the developed miniaturized biological vascularized scaffold (mBioVaSc-TERM®) was demonstrated. While indicating promising results in short term *in vivo* studies, long term implantations revealed current limitations for the translation into clinical application. The gained insights will impact further improvements of quality and performance of this promising platform technology for future regenerative therapies.

ZUSAMMENFASSUNG

Eine kontinuierlich steigende Inzidenz chronischer Krankheiten stellt eine immer größer werdende therapeutische Herausforderung dar. Der anhaltende Funktionsverlust von Geweben erfordert die bedarfsgerechte Verfügbarkeit von Wirkstoffen, deren kontinuierliche Bereitstellung und Verteilung über die Blutzirkulation von implantierbaren Pharmakotherapie-Produkten gelöst werden kann. Trotz der Fortschritte und Erfolge mit Zelltherapien sowie der Nachbildung der Zell-eigenen Nischen konnten bisher noch keine funktionellen Gewebe für die medizinische Anwendbarkeit hergestellt werden.

Diese Studie zeigt die Möglichkeit zur Herstellung einer vaskularisierten Plattform-Technologie um die Beschränkung der Nährstoff-Versorgung zu überwinden für die Entwicklung von Transplantaten für die klinische Anwendung und deren sofortige Anastomose an die Blutzirkulation.

Die Möglichkeit Rattendarmsegmente zu dezellularisieren, die Extrazellulärmatrix und das interne Gefäßsystem dabei jedoch zu erhalten um diese Strukturen wiederzubesiedeln wurde bewiesen. Das Wiederherstellen des funktionellen arteriovenösen Perfusionskreislaufs ermöglichte die Versorgung von Ko-kultivierten Zellen um damit funktionalen Gewebeersatz bzw. -modelle aufzubauen oder als Medizin-Produkt Einsatz zu finden. *In vitro*-Studien zeigten eindrucksvoll Reife und Anwendbarkeit des hier entwickelten miniaturisierten, biologischen, vaskularisierten Scaffold (mBioVaSc-TERM®). Während in *in vivo*-Studien zunächst vielversprechende Ergebnisse erzielt wurden, zeigten Langzeit Implantationen die aktuellen Grenzen zur Translation in die klinische Anwendung. Die gewonnenen Erkenntnisse werden dazu dienen Qualität und Funktionalität dieser vielversprechenden Plattform-Technologie zu verbessern um zukünftige regenerative Therapien zu ermöglichen.

TABLE OF CONTENTS

Abstract	I
Zusammenfassung	II
Table of Contents	III
List of Abbreviations and Units	VIII
Lists of Figures	X
List of Tables	XI
1. Introduction	1
1.1 Tissue homeostasis – maintaining tissue function	1
1.2 Therapeutic strategies to restore or substitute tissue functionality	2
1.3 Tissue Engineering and Regenerative Medicine.....	3
1.3.1 Definition of Tissue Engineering	4
1.3.2 Definition of Regenerative Medicine.....	4
1.3.3 Scaffolds for Tissue Engineering and Regenerative Medicine.....	5
1.3.4 Cell sources for tissue engineering strategies	6
1.3.5 Clinical applications of tissue engineered scaffolds	7
1.4 Vascularization	8
1.4.1 Vascular development and vessel composition	8
1.4.2 The necessity for vascularization	10
1.4.3 Vascularization strategies in TE.....	11
1.5 BioVaSc – Biologically vascularized scaffold	12
1.6 Aim of the thesis	14
2. Materials	16
2.1 Biological materials.....	16
2.2 Equipment and consumables	17
2.3 Chemicals and cell culture reagents.....	22
2.4 Media, solutions, and buffers	26
2.5 Commercially obtained kits.....	28
2.6 Lentiviral expression systems	29
2.7 Oligonucleotides	30
2.8 Antibodies.....	30
2.9 Software	31

3. Methods	33
3.1 Murine intestinal tissue preparation.....	33
3.1.1 Scaffold explantation	33
3.1.2 Decellularization.....	33
3.1.3 Bile acid evaluation.....	34
3.1.4 Biocompatibility assay	34
3.1.5 DNA purification from tissue.....	34
3.1.6 Graft implantation.....	35
3.1.7 Animal stress scoring.....	35
3.2 Cell culture	36
3.2.1 Cell culture conditions	36
3.2.2 Primary dermal microvascular endothelial cell isolation.....	36
3.2.3 Primary dermal fibroblast cell isolation.....	37
3.2.4 Cell count and cellular vitality	37
3.2.5 Passaging of adherent cells	38
3.2.6 Freezing of cells.....	38
3.2.7 Thawing of cells.....	38
3.2.8 Liver-like organoid formation	38
3.2.9 Viability assay via membrane leakage	39
3.2.10 Viability assay via mitochondrial reductase activity.....	39
3.2.11 Viability assay via mitochondrial dehydrogenase activity	40
3.2.12 Viability assay via quantification of cellular ATP	40
3.2.13 Graft vascularization	40
3.2.14 Bioreactor setup.....	41
3.3 Histological staining.....	41
3.3.1 Fixation and paraffin embedding	41
3.3.2 De-wax and rehydration.....	42
3.3.3 Haematoxylin and eosin (H&E) stain.....	42
3.3.4 Feulgen stain	43
3.3.5 Elastica van Gieson stain	43
3.3.6 Trichrome stain according to Masson Goldner	44
3.3.7 Immunohistochemistry	45
3.3.8 Immunofluorescence (IF)	46
3.3.9 Light sheet fluorescence microscopy.....	46
3.3.10 Preparation for transmission electron microscopy.....	46

3.4 Characterization of vascular barrier function	47
3.4.1 FITC-dextran barrier permeability.....	47
3.4.2 Trans-endothelial electrical resistance (TEER)	47
3.4.3 Intravital microscopy	48
3.4.4 LDL uptake	48
3.4.5 Myography.....	48
3.5 Bacterial culture	49
3.5.1 Casting of agar plates.....	49
3.5.2 Bacteria culture conditions.....	49
3.5.3 Bacterial transformation by heat shock	49
3.5.4 Mini prep.....	50
3.6 Molecular genetics	50
3.6.1 Chromosomal DNA determination	50
3.6.2 PCR.....	51
3.6.3 DNA purification from agarose gel or PCR.....	51
3.6.4 Cloning.....	51
3.6.5 Transfection for virus production.....	52
3.6.7 Viral transduction	53
3.7 Proteomic analysis.....	53
3.7.1 Protein precipitation.....	53
3.7.2 SDS Gel and Coomassie-stain	54
3.7.3 Western blotting.....	55
3.7.4 Elastin ELISA	55
3.7.5 Collagen ELISA.....	56
3.7.6 Glucose stimulated insulin secretion.....	56
3.7.7 Insulin ELISA.....	56
3.7.8 Activin A ELISA.....	57
3.7.9 Myostatin ELISA.....	57
3.7.10 Bioactivity assay of Activin A / Myostatin	58
3.8 Statistical analysis.....	58
4. Results.....	59
4.1 Establishment of the mBioVaSc-TERM®.....	59
4.1.1 Explantation of a rat jejunal segment.....	59
4.1.2 Decellularization and structural characterization of the mBioVaSc-TERM®...	61
4.2 Revascularization capacity of the mBioVaSc-TERM®	64

4.2.1	Characterization of genetically modified endothelial cells	64
4.2.2	Revascularization capacity of ECs to repopulate the mBioVaSc-TERM®	67
4.2.3	Demonstrating vascular barrier integrity by perfusion analysis	70
4.2.4	Analysis of the differentiation capacity of hPSC-derived mesothelial cells towards ECs, pericytes, and aSMA ⁺ cells within the mBioVaSc-TERM®	74
4.3.	Biocompatibility of the mBioVaSc-TERM® for tissue development	77
4.3.1	Setup of co-culture conditions enabling the generation of tissue culture	77
4.3.2	Distribution of bioactive compounds throughout the vascular system	81
4.4	<i>In vivo</i> application demonstrating proof of concept in a small animal rat model..	85
4.4.1	Anastomosis of the mBioVaSc-TERM® with the blood circulation	85
4.4.2	Confirmation of <i>in vivo</i> biocompatibility after graft implantation.....	87
4.4.3	Successive overgrowth of the scaffolds during the implantation period	89
4.4.4	Fading of functional markers on ECs and liver-like organoids	91
5.	Discussion.....	95
5.1	Identification of a suitable tissue for miniaturization of the BioVaSc-TERM®	96
5.2	Establishment of a decellularization protocol for rat intestine	98
5.3	Scaffold characterization upon cell removal, structural preservation, and biocompatibility	100
5.4	Reestablishment of the vascular system.....	102
5.4.1	Revascularization-capacity of the vascular structures with primary ECs.....	103
5.4.2	Maturation of the vascular barrier by arteriovenous perfusion culture.....	105
5.4.3	iPS technology depicts an alternative cell source for vascularization	108
5.4.4	Advancements for mBioVaSc-TERM® revascularization.....	109
5.5	Application of the mBioVaSc-TERM® as a platform for multicellular co-culture	111
5.5.1	Example of mBioVaSc-TERM® application for liver-like organoid culture	112
5.5.2	Example of mBioVaSc-TERM® application as drug delivery system.....	113
5.5.3	Example of mBioVaSc-TERM® application as endocrine tissue graft	114
5.5.4	Advancements for tissue graft generation and maintenance	116
5.6	Clinical relevance and capacity of the mBioVaSc-TERM® for <i>in vivo</i> application	117
5.6.1	Immediate and leakage-free vascular anastomosis of the mBioVaSc-TERM®	118
5.6.2	Potential integration of the mBioVaSc-TERM® into surrounding tissue.....	119
5.6.3	Alternative implantation sites avoiding the risk for peritoneal adhesion.....	121
5.6.4	Barriers guarding the graft from ECM remodeling and deposition	122
5.6.5	Vascular regression during long-term mBioVaSc-TERM® implantation.....	124

5.6.6 <i>In vivo</i> implantation demonstrated proof of concept but need for optimization towards a functional tissue graft or drug delivery system.....	127
5.8 Summary	129
5.9 Conclusion	129
5.10 Outlook on future perspectives	130
References.....	133
Appendix.....	148
Copyright permission of reprints	149
Affidavit.....	150
Eidesstattliche Erklärung.....	150
Danksagung.....	151

LIST OF ABBREVIATIONS AND UNITS**Abbreviations**

3D	three dimensional
ADME	absorption, distribution, metabolism and elimination
Ang-1	angiopoietin-1
aSMA	alpha-smooth muscle actin
ATMP	Advanced Therapy Medicinal Product
bFGF	basic fibroblast growth factor
BioVaSc	biologically vascularized scaffold
CCh	carbachol
CD	cluster of differentiation
CHO	chinese hamster ovary
CK	cytokeratin
DNA	deoxyribonucleic acid
ECs	endothelial cells
ECM	extracellular matrix
e.g.	<i>exempli gratia</i>
ELISA	Enzyme-linked Immunosorbent Assay
EMA	European Medicines Agency
et al.	<i>et alii</i>
FACS	fluorescence-activated cell sorting
Fig.	figure
FDA	Food and Drug Administration
FDA/PI	fluorescein diacetate / propidium iodide
FITC	fluorescein isothiocyanate
GFP	green fluorescent protein
GLP	good laboratory practice
GMP	good manufacturing practice
hdm	human dermal microvascular
HPLC	high performance liquid chromatography
iPS cell	induced pluripotent stem cell
LPS	lipopolysaccharide
MCAM	melanoma cell adhesion molecule
MTT	3-(4,5-dimethylthiazol-2-yl)-2,5-diphenyl tetrazolium bromide
NG	neural/glial antigen
NICC	neonatal islet-like cell clusters
o/n	over night
PDGF	platelet-derived growth factor
PECAM	platelet endothelial cell adhesion molecule
PSC	pluripotent stem cell
RFP	red fluorescent protein
RM	regenerative medicine
RT	room temperature
SEM	scanning electron microscopy
SD	standard deviation
SMC	smooth muscle cell
TCP	tissue culture plate

TE	tissue engineering
TEER	transendothelial electrical resistance
TEM	transmission electron microscopy
TGF- β	transforming growth factor beta
VEGF	vascular endothelial growth factor
WST	water-soluble tetrazolium salt

Abbreviations of countries

AT	Austria
CH	Switzerland
DE	Germany
DK	Denmark
SE	Sweden
UK	United Kingdom
USA	United States of America

Units

$^{\circ}\text{C}$	degree Celcius
Ω	ohm
A	ampere
bp	base pairs
d	day(s)
Da	Dalton
g	gram
h	hour(s)
l	liter
m	meter
M	molar
min	minutes
rcf	relative centrifugal force
rpm	rounds per minute
s	seconds
U	units
w/v	weight/volume

Prefixes

μ	micro
c	centi
k	kilo
m	milli
n	nano

LISTS OF FIGURES

Figure 1. Concept of Tissue Engineering	4
Figure 2. Blood vessels – types and composition.	10
Figure 3. Porcine- and rat-derived biologically vascularized scaffolds.	14
Figure 4. Cannulation and explantation of the mBioVaSc-TERM®.	60
Figure 5. Qualitative and quantitative characterization of the acellular rat jejunal segment.	63
Figure 6. Endothelial cell characterization.....	66
Figure 7. mBioVaSc-TERM® revascularization by vascular perfusion.....	68
Figure 8. Revascularization of the mBioVaSc-TERM®.....	69
Figure 9. Venous return profile at different stages of mBioVaSc-TERM® establishment	71
Figure 10. Vascular perfusion of the EC-repopulated mBioVaSc-TERM®.	73
Figure 11. Composition of differentiated mesothelial cells within the mBioVaSc-TERM®.	76
Figure 12. Establishment of intraluminal co-culture conditions.....	78
Figure 13. Liver-like organoid implementation in the reendothelialized mBioVaSc- TERM®.....	80
Figure 14. <i>In vitro</i> drug secretion from the mBioVaSc-TERM®.....	82
Figure 15. Vascularized endocrine pancreatic tissue generation with functional insulin secretion.	84
Figure 16. Anastomosis of the mBioVaSc-TERM® to a host vasculature.	87
Figure 17. Monitoring and scoring of experimental animals.	89
Figure 18. Macroscopic evaluation of the implanted mBioVaSc-TERM®.	90
Figure 19. Graft explantation and immunohistological examination.	93

LIST OF TABLES

Table 1. Cell lines employed.	17
Table 2. Laboratory equipment.....	17
Table 3. Laboratory consumables.	20
Table 4. Chemicals and cell culture reagents.	22
Table 5. Composition of cell culture media.	26
Table 6. Composition of solutions and buffers for biochemical and histological analysis.	27
Table 7. Commercially obtained kits.....	28
Table 8. Lentiviral expression vectors.	29
Table 9. PCR primer oligonucleotides employed for cloning.....	30
Table 10. Primary antibodies employed for immunohistological staining.....	30
Table 11. Secondary antibodies employed for immunohistological staining.	31
Table 12. Software employed.....	31
Table 13. Score sheet.	36
Table 14. Paraffin embedding.	41
Table 15. Haematoxylin and eosin (H&E) stain.....	42
Table 16. Feulgen stain.	43
Table 17. Elastica mit van Gieson stain.....	44
Table 18. Trichrome stain according to Masson Goldner.	44
Table 19. Dehydration.....	46

1. INTRODUCTION

1.1 Tissue homeostasis – maintaining tissue function

The extracellular space, mainly consisting of water, proteins, and polysaccharides, depicts the non-cellular component of tissues and organs¹. It provides not only framework and thereby the architecture, but also elicits biochemical and biomechanical effects on cells².

During organogenesis, tissue environment is highly fluctuating due to continuous and extensive extracellular matrix (ECM) deposition, degradation, and structural organization as well as cellular proliferation, migration, and differentiation¹.

For tissue-specific function, ECM-architecture and cellular homeostasis are critical³. However, tissue homeostasis is hardly static but a dynamic reciprocity between cells and ECM. The bidirectional interactions result in continuous ECM remodeling eliciting mechanical forces and biochemical mediators bound to the matrix triggering cellular responses affecting cell-signaling and ECM architecture⁴ by secretion of ECM components or ECM-degrading enzymes⁵.

The main classes of ECM macromolecules are proteoglycans and fibrous proteins. Proteoglycans mainly constitute hydrated gels depicting functional properties in hydration and buffering of mechanical force⁶. The major fibrous ECM proteins are collagens, elastins, fibronectins and laminins, predominantly deposited by fibroblasts. Fibroblasts are primarily responsible for ECM remodeling: both, buildup and degradation. Secreted matrix metalloproteinases counterbalance ECM protein synthesis⁷.

When wounded or during disease the tissue homeostasis between ECM degradation and deposition as well as cellular proliferation, differentiation, and ECM remodeling is unbalanced⁸. During wound repair homeostasis is gradually recovered. Regeneration is usually orchestrated by a sequence of cytokines recruiting cells for matrix formation, immunocompetent cells, tissue-specific cells repopulating the newly formed tissue, as well as neovascularization⁹. If this process is impaired scar formation replaces functional tissue regeneration. However, the major therapeutic challenges are chronic wounds, increasing in incidence due the prevalence of diabetes, obesity and vascular disorders in an aging society⁹.

1.2 Therapeutic strategies to restore or substitute tissue functionality

For replacement of an endocrine function, it is not necessarily required to restore the whole organ but only the respective cells or their secretome.

The cellular secretory function can be substituted and/or regeneration can be stimulated by drug delivery. The disadvantage of classical pharmacological treatment is that it is usually manually applied and has to be strictly surveyed as, in contrast, endocrine cells have an intrinsic feedback mechanism regulating the secretion¹⁰.

Furthermore, technical devices for drug delivery get increasingly applied¹¹. Typically equipped with a sensor to measure e.g. blood glucose level and a pumping device loaded with the respective compounds. These devices are commonly either externally attached to the patient with a needle penetrating the skin or implanted subcutaneously. The problem for the implanted device besides encapsulation is the repeated surgical intervention when reloading the compounds. The external devices bear the risk of infection due to the needle permanently piercing the skin.

An alternative is the transplantation of the respective cells/organoids or organs. However, facing drawbacks as donor compatibility and availability as well as immunosuppression¹² in addition to the need for a suitable implantation site to ensure graft survival¹³. Moreover, after islet transplantation in type 1 diabetes patients, the success rate is only at about 50 % over three years¹⁴.

To circumvent the use of allo- or xenografts, gene therapy could be utilized to genetically manipulate autologous cells to secrete the respective compounds. Apart from regulatory and safety concerns¹⁵, it is extremely laborious to also implement the respective feedback mechanisms to ensure an intrinsic regulation for secretion. An alternative source for transplantable organs was promised by tissue engineering (TE) providing *in vitro* generated autologous grafts. However, the generation of functional full thickness organs is still not achieved, yet¹⁶.

Currently in development are prevascularized biological drug delivery systems intended to circumvent foreign body response and to provide an optimized microenvironment for cellular functionality, direct connection to the blood circulation, as well as a protective barrier around the implemented cells¹⁷. Preclinical data in mice describe the restoration

of glycemic homeostasis by implementation of human embryonic stem cell-derived pancreatic endoderm cells in a subcutaneously established prevascularized pouch¹⁷.

1.3 Tissue Engineering and Regenerative Medicine

In tissue engineering (TE) and regenerative medicine (RM), therapeutic approaches are being developed to alleviate healthcare problems related to the diseases of cellular deficiency, including loss of tissue/organ functionality. Tissues and organs are damaged by disease (acute and chronic), trauma, or congenital defects. The aim is to support the innate healing capabilities to recover tissues or to replace them by *in vitro* generated grafts (Fig. 1).

While the current definitions of TE and RM were determined in the late twentieth century, the basic principles and ideas date back more than 10,000 years¹⁸ ago. 10,000 before Christ (BC) the principles of RM have been applied using linen, gut, or heads of large biting ants as synthetic, natural, and biological materials, respectively, to enable or support wound healing¹⁹. The first known transplantation of live skin grafts was conducted by an Indian surgeon Susruta²⁰ around 2,500 BC. The most classical example of RM dates back to around 1,500 BC guiding regeneration of skin wounds with cell-supportive scaffolds. Lint, grease and honey were applied onto skin wounds providing a fibrous scaffold with a barrier against pathogens and a hypertonic antibiotic function, respectively²¹. The first conveyed description of *in vivo* regeneration dates back to about 700 years BC in ancient Greek mythology²².

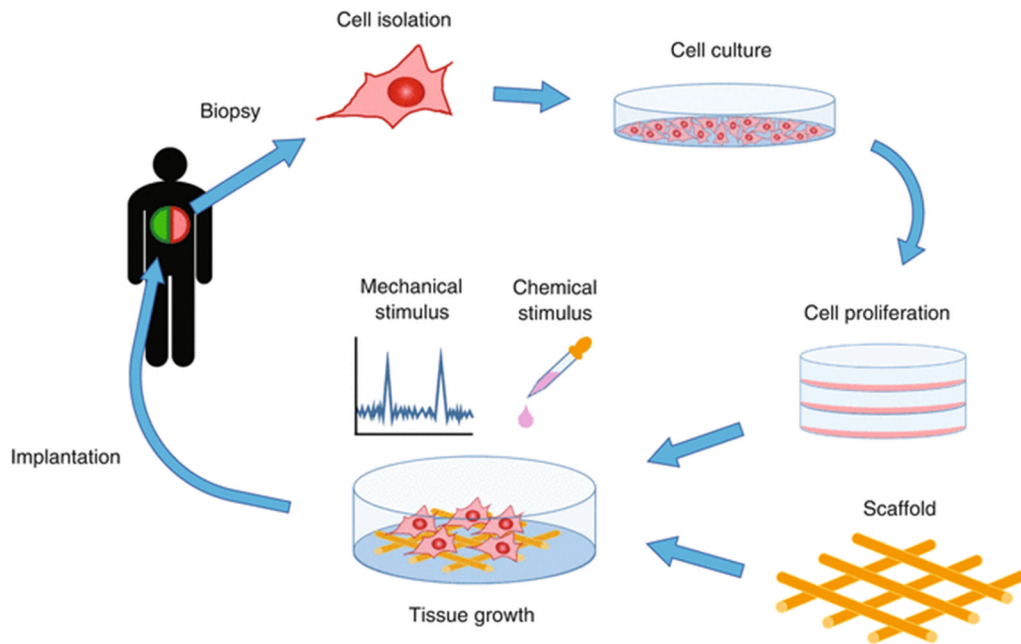


Figure 1. Concept of Tissue Engineering.

The classical concept of TE describes the generation of functional, autologous grafts to replace deficient tissues. To produce autologous tissue grafts with the constituting organ functionality, the relevant cell types are isolated from biopsies and expanded *in vitro*. The combination of cells with scaffolds enables 3D organotypic culture, while chemical and mechanical stimuli promote functional maturation. Finally, the *ex vivo* established autologous grafts are transplanted into the patient to restore or substitute lost tissue and/or function. Alternatively, the grafts are utilized as personalized test systems for drug screening or the evaluation of therapeutic strategies. Copyrighted reprint²³.

1.3.1 Definition of Tissue Engineering

TE aims at the production of functional tissue substitutes to replace deficient tissues^{24,25} and thereby restore tissue homeostasis. Engineered tissues can serve as model for further investigations on development, homeostasis, and pathogenesis. This is often achieved by a combination of preferably autologous cells, soluble or coupled molecules²⁶, synthetic or natural scaffolds, and bioreactors²⁷.

1.3.2 Definition of Regenerative Medicine

The main focus in RM aims on the stimulation or reactivation of innate developmental processes or the endogenous regenerative capacity initiating repair and regeneration until restoration of cellular/tissue homeostasis and functionality^{28,29}. A combination of

scaffolds with cellular and pharmacological therapies or products are generated *ex vivo* but applied to stimulate the *in vivo* healing process^{18,30}.

1.3.3 Scaffolds for Tissue Engineering and Regenerative Medicine

Critical-size-defects or loss of functions of an organ cannot be compensated naturally, thus, for reconstruction, replacement is the only viable treatment option. Approaches in TE combine living cells and/or growth factors with materials providing an appropriate microenvironment for cells to pursue their native function. Thereby, the generation of tissue substitutes providing the required structures and components enable to replace or to stimulate the innate regenerative capabilities and restore the original tissue. Consequently, when generating tissues *in vitro*, it is critical to provide an environment mimicking cell-specific cues, including physical properties and morphogens guiding cellular behavior. Dependent on the tissue, the material and mechanical properties of the scaffold such as mechanical rigidity or flexibility can vary widely serving various purposes either by retention, presentation, or controlled release of growth factors; or by enabling cell attachment and/or facilitating migration as well as guiding cellular differentiation³¹. Further requirements for the materials utilized as implants demand to be biocompatible, non-toxic, non-immunogenic, non-carcinogenic, nor dislocate or erode over time but integrate into the adjacent tissues³².

Synthetic biomaterials used in TE are mainly polymers^{33,34}, of which many have regulatory approval for medical application. Manifold other materials and technologies, e.g. structured macroporous hydrogels³⁵, electrospinning^{36,37}, and bioprinting^{38,39} emerged within the last years to generate scaffolds for TERM. During chemical synthesis, the material properties can be customized upon the aggregation state, injectability, transparency, topography, porosity, and resorption. However, cellular toxicity is still a challenge to overcome for most polymers.

Natural scaffolds comprise ECM components such as proteins and polysaccharides. On the one hand, they exhibit high biocompatibility, on the other hand, they potentially provoke immunogenicity upon implantation, especially in combination with allogenic or xenogenic cells or cellular remnants. Nevertheless, progress was made with skin⁴⁰, cartilage⁴¹, heart^{42,43} and heart valves^{44,45}, liver⁴⁶, and lung^{46,47}.

The most recently ascending natural scaffolds are decellularized tissue matrices. By removing the tissue's cells and remnants thereof, immunogenic reactions are avoided⁴⁸ while preservation of the natural ECM in structure, composition, and mechanical integrity enables the generation of a native-like cellular environment for tissue generation and regeneration⁴⁹. Therefore, the cellular phenotype can be maintained and cell attachment, motility, and differentiation⁵⁰ is facilitated. Furthermore, its biological nature assures to be non-toxic and biocompatible⁵¹. To restore tissue functionality, the scaffold is ideally reseeded with autologous cells. Tissue maturation is enabled by specifically designed bioreactors providing physiological conditions and applying mechanical stimuli⁵². In contrast to *de novo* engineering of tissues, decellularized tissue matrices take advantage of the preservation of the whole original tissue framework, especially vascular networks⁵³. While considered for clinical application, there are mainly bioengineered hollow organs, such as bladder^{54,55} and tracheal⁵⁶ grafts available. Preliminary full thickness whole organs, such as kidney⁵⁷, liver⁴⁶, lungs⁵⁸ or limbs⁵⁹, are in progress for rodent transplantation.

1.3.4 Cell sources for tissue engineering strategies

Tissue functionality mostly requires specialized cell types, often a distinct spatial organization and an orchestrated interaction between different cells and cell types. The utilization of the specific cell source is critical for the generation of *in vitro* engineered tissue.

Most prevalent is the use of cell lines, indefinitely proliferating cells that can usually be traced back to one single immortalized cell. There are manifold cell lines from plenty of tissues available. However, the immortalization is based on mutations in the genome that can alter the biology of the cell.

Primary cells are freshly isolated from tissue and therefore closely reflect the natural cellular behavior and function. In contrast to cell lines, primary cells should only be cultured for a few population doublings to ensure an *in vivo*-representative cellular character.

Stem cells proliferate almost indefinitely and have the capacity to differentiate into specialized cell types⁶⁰. However, the availability is limited and in the case of embryonic stem cells tightly restricted by law⁶¹.

Since autologous cells, either primary differentiated or multipotent adult stem cells⁶², are preferred for therapeutic intervention due to immunologic tolerance. However, primary cells are often not applicable due to tissue/cellular impairment and respective stem cells are lacking. Furthermore, stem cells require a defined niche to maintain their specific properties⁶³. Therefore, induced pluripotent stem cells (iPSC) emerged as an alternative cell source⁶².

Since iPSCs were first described in 2006 when differentiated adult cells were reprogrammed to a pluripotent embryonic-like state with the capacity to differentiate into cells of all embryonic lineages⁶⁴ it was promised to be able to unlock hidden regenerative potential of organs similar to fish, amphibians, and reptiles⁶⁵. Pluripotency describes the capacity of a stem cell to differentiate in any of the three germ layers: endoderm – developing e.g. the gastrointestinal tract and the lungs; mesoderm – developing e.g. muscle, bone, and blood; and ectoderm – developing e.g. epidermal tissues and the nervous system⁶⁶. However, most applications of stem cells in RM are inefficient and the anticipated hopes to cure degenerative diseases were not achieved, yet. Nevertheless, iPSCs can theoretically be differentiated into any cell type applicable for cell-based TE⁶⁷.

1.3.5 Clinical applications of tissue engineered scaffolds

The first clinically applied bioengineered tissue was a trachea analogon⁶⁸. However, this seemingly simple tissue such as a straight tubular windpipe to be replaced by a prosthetic substitute took almost a century of research until its implantation.

Solid or nonporous prosthetic materials failed in clinical application due to infection, dislodgement, migration, extrusion, and stenosis, as well as non-re-epithelialization, precluding long term incorporation³².

Employing tracheal allografts instead of synthetic windpipes still caused immunological rejection⁶⁹. Chemical pre-treatment of tracheal allo- and xenografts reduced immunogenicity and necrosis⁷⁰, however, also resulted in poor cartilage and epithelial

constitution⁷¹. Animal studies demonstrated the reduced immunogenic rejection after cryopreservation^{72,73} but elicited ischemia in the grafts^{74,75}.

The final success to generate a functional replacement was achieved employing a decellularized matrix for tracheal reconstruction⁷⁶. A decellularized porcine jejunal segment was reseeded with autologous costal chondrocytes, smooth muscle cells, respiratory epithelium, and endothelial progenitor cells. Bioreactor technology was employed for cellular, and consequently, tissue maturation by applying physiological stimuli to emerge into a multi cell layered *in vitro* vascularized bioartificial scaffold with tracheal functional elements including respiratory epithelium cilia movement⁷⁷.

The fails of cell-free scaffolds and the clinical success of the multi cellular biologically vascularized scaffold made clear that only living vascularized tissue can substitute for functional regeneration.

1.4 Vascularization

Despite success in early TE, around the 1980s, with relatively avascular tissues and low cellular metabolic rates that could be met by nutrient diffusion, the generation of complex tissues still fails in majority. The main problem in the development of complex functional tissue is due to the fact of proper nutrition while orchestration of homotypic and heterotypic cell-cell interactions in a spatially controlled micrometer scaled environment. The vascular network provides the infrastructure to supply the cells the required nutrients and oxygen but also enables the metabolic exchange of factors, substrates and products and maintains the water and protein balance between intra- and extravascular compartments. Furthermore, the vascular wall functions as a barrier preventing pathogens or harmful materials circulating in the blood from spreading into tissues⁷⁸.

1.4.1 Vascular development and vessel composition

The importance of vascularization is reflected in its developmental priority being the first functional organ developed in the vertebrate embryo. During embryonic development, the coordinated orchestration of movement and differentiation of cell lineages form blood vessels, originating together with the heart⁷⁹. Thereby, the supply-infrastructure for tissue nutrition is established and even before the uptake of vascular functions, inductive

signals for patterning and organogenesis are provided by vasculogenic ECs⁸⁰. Before further maturation of the vascular network, arteries and veins composed solely of ECs are morphologically not discriminable, but on molecular level the angioblasts are already primed by distinct signaling pathways whether forming arteries or veins^{81,82}. In later stages, further ECs arise from already existing endothelial cells integrated in the vascular structure⁷⁹. During maturation of the vascular network a gradual transition from arteries to arterioles to capillaries, enabling nutrient exchange, merging into venules and veins is established (Fig. 2).

Vasculogenesis describes the *de novo* formation of blood vessels, mainly occurring during embryogenesis⁸³. Whereas during angiogenesis, new vessels predominantly sprout from existing vessels. During angiogenesis, the cells reorganize their vessel structure by migration and proliferation forming and stabilizing new vascular lumen⁸⁴. Major trigger for vascular sprouting are mechanical stimuli such as changes in blood flow, velocity, hydrostatic pressure, and resistance in the vascular bed⁸⁵.

Besides endothelial cells composing the inner surface of blood and lymphatic vessels, pericytes are recruited to the endothelial layer to enhance blood vessel stabilization⁷⁹. The vascular cells, then, deposit collagenous and elastic fibers assembling the vessel walls. Smooth muscle cells compose a major part of the wall of large blood vessels and facilitate vascular contractility⁸⁶.

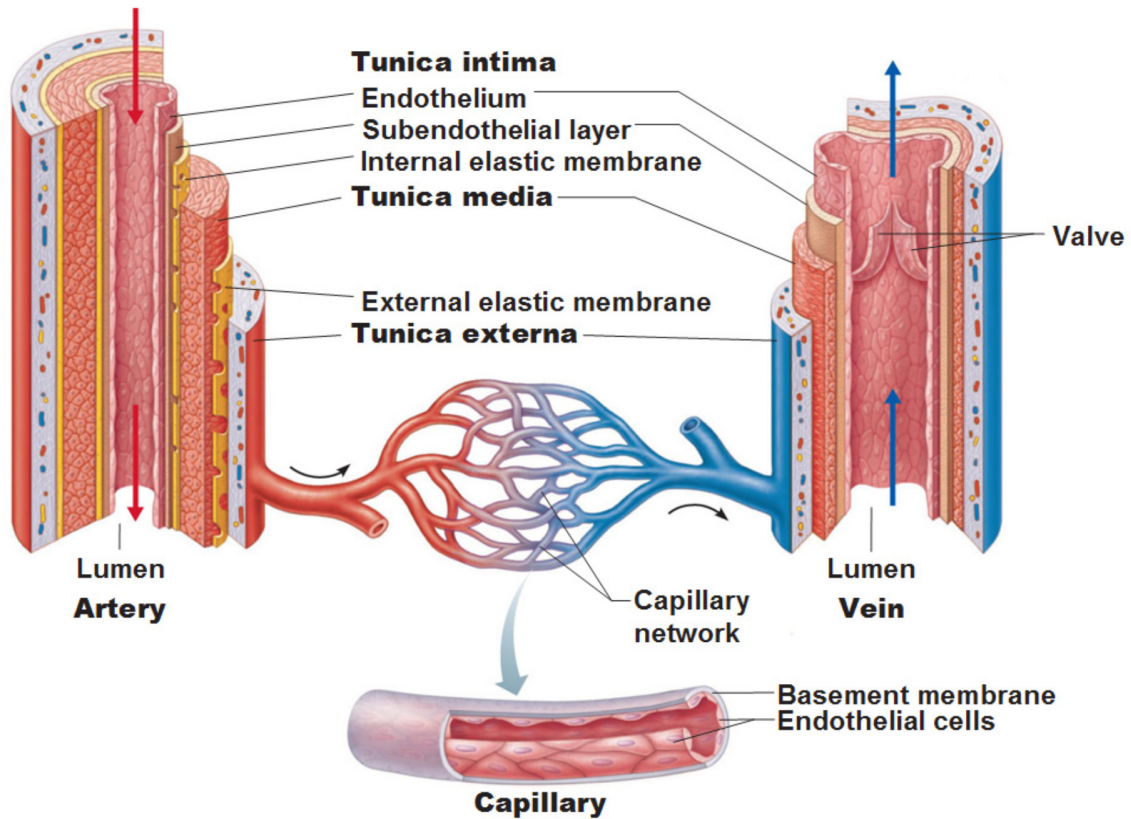


Figure 2. Blood vessels – types and composition.

Vascular wall composition of artery, vein, and capillaries. Capillaries are composed of only an EC layer on a basement membrane with few dispersed pericytes dependent on the capillary type. Arterioles and venules are additionally covered by a layer of smooth muscle cells (SMCs). Arteries and veins depict the largest vessels in terms of lumen diameter and wall thickness, typically composed of three layers embedding SMCs and fibroblasts in collagen and elastic fibers to withstand and regulate the blood pressure. Copyrighted reprint⁸⁷.

1.4.2 The necessity for vascularization

Graft integration is critical to functionally and structurally substitute for the original tissue, thereby, the interconnection with the host vasculature is inevitable as a cell-based graft needs to be supplied. Aside of few exceptions as e.g. cartilage, in the body, most cells are not more than 100-200 μm away from a capillary assuring sufficient diffusion and exchange of nutrients, oxygen, and waste products from the bloodstream⁶⁶. Thereby, the viability of cells and tissues is maintained, furthermore, making regeneration possible.

Tissue-engineered dense complex 3D structures quickly exceed the nutrient diffusion limit, thereby becoming inadequately supplied, ultimately leading to necrosis⁸⁸. Without the implementation of an adequate infrastructure for mass transfer, tissue-engineered structures will not exceed a size necessary for clinical application. Therefore, it is critical

that engineered tissues are vascularized to grant the embedded cells access to nutrition supply and metabolic factors.

Besides the indispensability of vascular structures when attempting to generate living thick tissues *in vitro*, the lack of vascularization also impedes the graft integration and functional tissue restoration *in vivo*⁸⁹. Furthermore, the co-culture of endothelial cells (EC) with tissue-specific cells not only grants better integrated vascularized grafts but also improves tissue-specific function⁹⁰.

1.4.3 Vascularization strategies in TE

Despite early awareness of proper gas and nutrient supply in biology, initial TE products developed in material sciences lacked the integration of living cells or a strategy for their nutrition. Subsequently, various vascularization strategies arose approaching the task with diverse methods such as scaffold functionalization, microfluidic systems, cell-based techniques, modular assembly, and *in vivo* systems⁹¹.

Scaffold functionalization comprised either various structural methods of increasing scaffold porosity up to the formation of channels to form perfusable elements within the scaffold⁹² or biochemical modifications of the material surface presenting or releasing angiogenic factors to initiate angiogenesis⁹³ and promote vascular ingrowth *in vivo*, which was demonstrated to improve graft survival⁹⁴.

Cell-based techniques describe the implementation of ECs or endothelial progenitor cells to establish a pre-vascularization of a construct in order to provide a functional vasculature⁹⁵. The degrees of pre-vascularization vary from *in vitro* establishment before implantation⁹⁶ to *in vivo* self-assembly of vascular structures⁹⁷. Furthermore, co-cultures of ECs and a combination of tissue-specific cell types, enable to establish vascularized tissues⁹⁸. The integration of ECs is achieved either as multicellular spheroids^{99,100} or simple loose mixing of the cells in the scaffold¹⁰¹. ECs, especially in spheroidal culture, produce capillary-like sprouts, increased in presence of angiogenic factors¹⁰² and fibroblast co-culture¹⁰³. This characteristic is utilized for scaffold pre-vascularization.

An *in vivo* approach is the formation of an arteriovenous loop with a host vessel and subsequent embedding in a tissue chamber. The ECM in between the shunt loop within the chamber becomes densely vascularized by a sprouting capillary network¹⁰⁴.

Alterations in scaffold material, pore size, and biochemical loading improve, direct, and control neoangiogenesis in the ECM embedded within the loop¹⁰⁵. The addition of tissue-specific cells in the matrix within the loop before implantation allows the generation of vascularized functional tissue up to a thickness of 2 mm¹⁰⁶. Bigger more complex 3D tissues might be generated in large animal models¹⁰⁷. However, for the generation of large tissues by this loop-approach, the formation of vascularization in between the loop needs to be promoted *in vitro* by prevascularization or biochemical scaffold modification¹⁰⁸. However, human application of this method is critical as it either requires repeated surgical interventions until full autologous graft vascularization or if vascularized in an animal model the graft will be xenograft requiring immunosuppression.

Approaching the connection between scaffold vascularization and host circulation, it was demonstrated that pre-vascularization of scaffolds accelerated the adhesion of the vascular networks¹⁰⁹. The thereby created vascular pedicles for engineered tissues facilitated subsequent transplantation and thereby integration into the implantation site¹¹⁰, however requires multiple surgeries. Regarding clinical applicability, most approaches for graft vascularization are still only viable for small tissues as vascular ingrowth or self-assembly in a dense tissue takes too long until full functional vascularization is established within a voluminous tissue, thereby risking necrosis. Large, thick tissue substitutes require an immediate and full perfusion with nutrients and oxygen to survive and be maintained. Nevertheless, for *in vivo* application, the functional anastomosis with the host circulation for an immediate functional perfusion remains a critical unmet task.

1.5 BioVaSc – Biologically vascularized scaffold

Gathering the mentioned properties and concerns, an ideal scaffold should provide a microenvironment for 3D tissue-like cell culture with an embedded vascular network that can be anastomosed to the blood circulation of a patient when considered for transplantation. The so far most promising engineered tissue combining the before mentioned advantages in one tissue graft was the BioVaSc-TERM®. The BioVaSc-TERM® is based on a decellularized porcine jejunal segment explanted with adjacent vascular structures.

During explantation of the intestinal segments for the BioVaSc-TERM®, the preservation of all vessel structures was highly critical. Also the decellularization protocol was established to preserve the vasculature. The subsequently established acellular luminal intestinal structure served as a scaffold for 3D cell culture with a preserved vascular network. Once revascularized with autologous ECs, it provided a vascular network for nutrient supply. The vessels comprised a diameter from about 200 µm until about 2–20 µm in the capillary bed of the lumen. The cannulation before explantation and consecutive preservation of mesenteric arterial and venous vessels allowed the connection of the vasculature to a perfusion bioreactor. Thereby, the pedicles served as a feeding input and draining outlet for perfusion culture and mass transfer throughout the scaffold^{111,112}. The vascular structures were repopulated and matured ensuring a sufficient nutrient supply for further implemented cells to establish tissue-specific cocultures on the luminal ECM ultimately generating vascularized tissue grafts (Fig. 3). Cell viability and functionality of tissue-specific cells was proven *in vitro*. The scaffolds' intrinsic properties allowed tissue reconstruction *in vitro* proving subsequent vascular tightness upon *in vivo* anastomosis¹¹³. Furthermore, the preserved mesenteric vessels allowed for immediate anastomosis and connection to a host vascular circulation impeding tissue degeneration upon implantation^{112,113}.



Figure 3. Porcine- and rat-derived biologically vascularized scaffolds.

Decellularized ECM scaffolds with preserved vascular structures derived from porcine respectively rat jejunum. The BioVaSc-TERM® and miniaturized mBioVaSc-TERM® serve as platform technology for the generation of bioartificial tissue grafts or as drug delivery system.

1.6 Aim of the thesis

Full tissue vascularization still depicts a major problem in TE for the generation of clinically relevant grafts. Pre-vascularization of cell-based scaffolds significantly improved tissue integration upon implantation. However, for tissues bigger than micro-scaled, an immediate connection to the host circulation is required for sufficient nutrient supply and graft vitality. The BioVaSc-TERM® meets the mentioned requirements. Nevertheless, the full potential of this technology has not been exploited yet. Its scale causes the requirement of vast amounts of specific cellular material for recellularization limiting its applicability, in particular in basic research and preclinical utilization as well the implantation in small animal models.

The aim of this study was to establish a miniaturized biological vascularized scaffold with a mature functional vascular network enabling tissue-specific recellularization with less cells necessary as well as implantation in small animal models for preclinical animal studies. Furthermore, the utilization of the vessel system and its applicability as a delivery system by secretion of bioactive drugs into the vascular circulation was to be demonstrated. *In vivo* studies were designed to indicate the capacity and proof of concept of the platform technology.

The first part of the thesis was to establish a decellularization protocol for rat intestinal segments, to remove host cells and preserve the biological ECM components and architecture. Next, the embedded innate vascular system had to be reendothelialized to develop a tight vascular barrier enabling arteriovenous circulation. Therefore, a dynamic perfusion bioreactor setup promotes vascular maturation and provides physiological gas and nutrient supply distributed via afferent feeding and efferent draining vessels.

To demonstrate the capacity to maintain co-cultures, various tissue-specific cells were cultured in close proximity to the capillaries embedded inside the luminal ECM. Thereby, the *ex vivo* generation of tissue-like grafts was promoted. Demonstrating physiological metabolic functions and the secretion of biologically active compounds into the vascular circulation indicated the capability to potentially serve as a drug delivery system.

Finally, *in vivo* studies demonstrated the feasibility of vascular anastomosis to the blood circulation of a host animal facilitating implantation in small animal models to examine clinical applicability and functionality.

2. MATERIALS

2.1 Biological materials

Biological scaffolds were dissected from Wistar and Lewis rats. *In vivo* implantation was performed on female NIH-Foxn1nu rats. All rats were at an age of about 8 weeks and obtained from Charles River, Sulzfeld, Germany. All animals were kept on a standard diet and water ad libitum at a 12 day and night cycle. All animals received humane care in compliance with the guidelines by the FELASA, WHO and FDA (WHO-TRS978 Annex3 und FDA-OCTGT Preclinical Guidance) and §§4 & 8 Protection of Animals Act and in consent after approval from our institutional animal protection board, University Würzburg. Organ explantation was performed under registration reference number # 55.2 2532-2-256 and *in vivo* animal studies were performed under registration reference number #2532-2-12. Anesthesia during surgery was administered by Isoflurane inhalation, pain management was treated with Carprofen (dosage and application was 5 mg/kg s.c.) according to the recommendation of: 'Pain therapy for laboratory animals GV-SOLAS'-guideline by the Committee for anesthesia and analgesia, in 2015. Upon termination of the experiments, animals were sacrificed in accordance with the ethical committee approval and received an overdose of CO₂ with a subsequent cardiocentesis as approved.

In vitro cell cultures and revascularization were established from primary human dermal microvascular ECs isolated from prepuce. Additionally, fibroblasts were isolated from the same source as ECs. Considered as a source of β -cell replacement, neonatal pig islet-like cell cluster (NICCs) were isolated from piglets and kindly provided by Prof. Dr. Eckhard Wolf (Molecular Animal Breeding and Biotechnology, LMU München, Munich, DE). hPSC-derived mesothelial cells and their respective differentiation and culture media were kindly provided by Prof. Dr. Stephen Dalton (Center for Molecular Medicine, University of Georgia, Georgia, USA). Further cell lines were employed as stated in Table 1.

Table 1. Cell lines employed.

Cell line	Supplier / manufacturer
Human embryonic kidney cells HEK293T	LGC Standards GmbH, Wesel, DE
Chinese hamster ovary cells CHO	LGC Standards GmbH, Wesel, DE
Human upcyte® hepatocytes	Medicyte GmbH, Heidelberg, DE
Human upcyte® liver sinusoidal endothelial cells	Medicyte GmbH, Heidelberg, DE
Human upcyte® mesenchymal stem cells (MSC)	Medicyte GmbH, Heidelberg, DE

Upcyte® hepatocytes, liver sinusoidal ECs and MSCs were stably transduced with lentiviral constructs carrying sequences which code for certain proliferation-inducing factors¹¹⁴. The upcyte® process allowed almost unlimited cell proliferation of cells from one donor with a performance similar to the original primary cells¹¹⁵.

2.2 Equipment and consumables

Utilized laboratory equipment and consumables are listed below.

Table 2. Laboratory equipment.

Designation	Specification	Manufacturer
Aspiration system	Vascusafe	Integra Biosciences, Biebertal, DE
Autoclaves	Tecnoklav	Biomedis, Giessen, DE
	TableTop Autoclave	Systec, Wettenberg, DE
	Varioklav	H+P, Hackermos, DE
Cell culture safety cabinet	Safe2020	Thermo Fisher Scientific, Dreieich, DE
CO ₂ incubator	Hot-Air Disinfectable Gassed Incubator BBD 6220	Haraeus, Hanau, DE
	Bioreactor incubator system	Chair TERM, JMU Würzburg, Würzburg, DE
Centrifuge	Multifuge X1R	Thermo Fisher Scientific, Dreieich, DE

	Microcentrifuge 5417R	Eppendorf, Hamburg, DE
	Minicentrifuge	Hartenstein, Würzburg, DE
	Heraeus Pico 17 Centrifuge	Thermo Fisher, DE
Cold-storage room		Genheimer, Höchberg, DE
Drying oven for microscopy slides	TDO 66	Medite, Dietikon, CH
Electrode	Chopstick Electrode STX3	Merck, Darmstadt, DE
Epithelial Volt-Ohm Meter	Millicell® ERS-2	Merck, Darmstadt, DE
Erlenmeyer flask	Glass	VWR, Ismaning, DE
Forceps	Standard Micro-Adson Dumont #5	Fine Science Tools, Heidelberg, DE
Freezers	-20 °C	Liebherr, Biberach, DE
	-80 °C	Kendro, München, DE
Freezing container	Mr. Frosty	ThermoFisher Scientific
Fume hood		Prutscher Laboratory Systems, Neudörfel, AT
Gel casting tray		Peqlab, Darmstadt, DE
Gel combs	10 well, 1.5 mm 20 well, 1.5 mm 34 well, 1.5 mm	Peqlab, Darmstadt, DE
Gel electrophoresis system	PerfectBlue	Peqlab, Darmstadt, DE
Gel system power supply	EV243	Peqlab, Darmstadt, DE
Hemocytometer	0.1 mm, 0.0025 mm ²	Hartenstein GmbH, Würzburg, DE
Ice machine	AF-80	HIBU Eismaschinen GmbH & Co.KG, DE
Immersion thermostat	Alpha A	Lauda, Lauda-Königshofen, DE
Liquid nitrogen tank	MV 815 P-190 -180 °C	Jutta Ohst german-cryo GmbH, DE
Microplate reader	Infinite M200	Tecan Deutschland GmbH, DE
Microscopes	Biorevo BZ-9000	KEYENCE, Neu-Isenburg, DE
Microwave	NN-E205W	Panasonic, Hamburg, DE

Mounting pins	for ring preparations	DMT, Aarhus, DK
Muscle strip Myograph system	820MS	DMT, Aarhus, DK
Orbital shaker	KM-2 Akku	Edmund Bühler, Hechingen, DE
PCR UV cabinet	Captair Bio	Erlab, Köln, DE
pH meter		Mettler Toledo, Giessen, DE
Pipets	0.5-10 µl 10-100 µl 100-1,000 µl	Eppendorf, Hamburg, DE
Pipetting aid	Pipetboy	Brand, Wertheim, DE
Rocking platform		neoLab, Heidelberg, DE
Scales	Precision balance PCB Microbalance SE2 Ultra	Kern, Balingen-Frommern, DE Sartorius Stedium Biotech, Göttingen, DE
Scissors	Iris Surgical	Fine Science Tools, Heidelberg, DE
Septophag		Hesse, Emmerich, DE
Sliding microtome	SM 2010R	Leica, Wetzlar, DE
Steam Cooker	MultiGourmet	Braun, Kronberg/Taunus, DE
Thermal shaker	Thermomixer comfort	Eppendorf AG, DE
Thermocycler	Thermocycler 48	SensoQuest, Göttingen, DE
Tissue embedding center	EG1150H	Leica, Wetzlar, DE
Tissue float bath	GFL 1052	Medax, Kiel, DE
Tissue processor	Microm STP 120	Thermo Fisher Scientific, Dreieich, DE
TissueRuptor		Qiagen, Hilden, DE
Trans illuminator		Vilber Lourmat, FR
Ultrapure water system		Millipore, Schwalbach, DE
Vortex shaker	Vortex-Genie 2	Scientific Industries via Carl Roth, Karlsruhe, DE
Water bath		Julabo Labortechnik, Seelbach, DE
Western blot imaging	Fluor-Chem Q system	CellBiosciences, DE

Table 3. Laboratory consumables.

Designation	Specification	Manufacturer
Air filter	Minisart® HY Syringe Filter, 0.2 µm hydrophobic PTFE	Sartorius Stedim Biotech GmbH, DE
Autoclaving container	Stainless steel sterilization container	Fine Science Tools, Heidelberg, DE
Blotting membrane	Polyvinylidene Difluoride	ROCHE Deutschland Holding GmbH, DE
Cannulas	Vasofix® Safety 0.70 x 19 mm, G 24 yellow	B. Braun Melsungen AG, Melsungen, DE
Cell culture dishes	Petri dishes 94 mm	Greiner Bio-One, Frickenhausen, DE
Cell culture flask	25 cm ² 75 cm ² 150 cm ²	TPP, Trasadingen, DE
Cell culture multiwell plates	6 well 12 well 24 well 48 well 96 well	TPP, Trasadingen, DE
Cell strainer	40 µm 70 µm	Greiner Bio-One, Frickenhausen, DE
Centrifuge tubes	15 ml 50 ml	Greiner Bio-One, DE
Cover slips for microscopy slides	24 x 60 mm	Menzel-Gläser, Braunschweig, DE
Cryotubes	1.5 ml	ThermoFisher Scientific, Dreieich, DE
Dako Pen		Dako, Hamburg, DE
Embedding cassettes		Klinipath, Duiven, DE
Embedding filter paper		Labonord, Mönchengladbach, DE
Glass-reactor	Bottles Cannulas Corpus	Weckert Labortechnik, Kitzingen, DE
Gloves	Latex Nitril	Kimberly-Clark, Koblenz, DE

Microcentrifuge tubes	0.2 μ l	Biozym, Oldendorf, DE
	0.5 ml	Eppendorf, Hamburg, DE
	1.5 ml	
	2 ml	
Microscopy slides	Polysine Super-Frost Plus	Langenbrinck, Emmerdingen, DE
Microtome blades	A35	pfm medical, Köln, DE
Multiwell plates	96 well black	Greiner Bio-One, Frickenhausen, DE
Parafilm		Sigma-Aldrich, DE
Pasteur pipettes	glass	Brand, Wertheim, DE
Pipet tips	0.5-10 μ l	Nerbe plus, Winsen/Luhe, DE
	10-100 μ l	
	100-1,000 μ l	
Pressure sensor dome	for Transducer SP 844	HJK Sensoren + Systeme GmbH & Co. KG, Merching, DE
Scalpel blades		Hartenstein GmbH, DE
Serological pipettes	5 ml,	Greiner Bio-One, Frickenhausen, DE
	10 ml,	
	25 ml,	
	50 ml	
Sewing Thread	Silkam 4/0	Braun, Melsungen, DE
Staining dish with lid	105 x 85 x 70	Carl Roth, Karlsruhe, DE
Syringes	1 ml Omnifix	Braun, Melsungen, DE
	2 ml Discardit II	BD Biosciences, Heidelberg, DE
	5 ml Discardit II	
	10 ml Discardit II	
20 ml Discardit II		
Syringe filter	0.2 μ m pore size Minisart NML	Sartorius Stedium Biotech, Göttingen, DE
Tubing	PharMed®BPT (Ismaprene)	Ismatec, Wertheim- Mondfeld, DE
	Silicon tubing Tygon 3350	Saint-Gobain, Courbevoie, FR

Tubing connection	Male Luer Integral Lock Ring to 200 Series Barb Female Luer Lug Style to 200 Series Barb Y Tube Fitting with Classic Series Barb each 1/8" (3.2 mm) ID Tubing, Natural Kynar PVDF	Nordson Medical <i>MedNet</i> , Münster, DE
Transwells	Corning® Transwell® polyester membrane cell culture inserts	Sigma-Aldrich, München, DE
Whatmanpaper		Sigma-Aldrich, München, DE

2.3 Chemicals and cell culture reagents

Table 4. Chemicals and cell culture reagents.

Designation	Catalog no.	Manufacturer
2-Propanol	9866.6	Carl Roth, Karlsruhe, DE
Acetic acid	6755.1	Carl Roth, Karlsruhe, DE
Acid fuchsin Ponceau Azophloxin	10180	Morphisto, Frankfurt Main, DE
AcLDL	L35354	Invitrogen, Darmstadt, DE
Acrylamide Rotipherese Gel30	3029	Carl Roth, Karlsruhe, DE
Agar-Agar	2363.2	Carl Roth, Karlsruhe, DE
Agarose LE	840004	Biozym, Hessisch Oldendorf, DE
Albumin fraction V (BSA)	2834.4	Carl Roth, Karlsruhe, DE
Ammonium persulfate	431532	Sigma-Aldrich, München, DE
Antibody Diluent Lab Vision OP Quanto	TA-125-ADQ	Thermo Scientific, Dreieich, DE
β-Mercaptoethanol	M31448	Sigma-Aldrich, München, DE
Benzyl alcohol	24122	Sigma-Aldrich, München, DE
Benzyl benzoate	B6630	Sigma-Aldrich, München, DE

Brilliant blue R 250	3862	Carl Roth, Karlsruhe, DE
Bromophenol blue sodium salt	A512.1	Carl Roth, Karlsruhe, DE
Carbachol	C4382	Sigma-Aldrich, München, DE
Carprofen (Rimadyl®)	779-358	Henry Schein, Melville, USA
Chloroform	C2432	Sigma-Aldrich, München, DE
Citric acid monohydrate	3958	Carl Roth, Karlsruhe, DE
Collagen IV	C5533	Serva Electrophoresis, Heidelberg, DE
DeoxyribonucleaseI from bovine pancreas	DN25	Sigma-Aldrich, München, DE
Diclofenac	D6899	Sigma-Aldrich, München, DE
Dimethylsulfoxid (DMSO)	D2438	Sigma-Aldrich, München, DE
DMEM/F-12, GlutaMAX Supplement	31331-093	Gibco, Darmstadt, DE
DNA ladder plus 100-3000 bp	25-2020	Peqlab, Darmstadt, DE
EDTA	6381-92-6	Sigma-Aldrich, München, DE
Entellan	1079610100	Merck, Darmstadt, DE
Eosin 1% aqueous	10177	Morphisto, Frankfurt Main, DE
Ethanol, denatured, 96 %	T171.2	Carl Roth, Karlsruhe, DE
FCS	FCS.ADD.0500	Bio & SELL GmbH, Feucht, DE
FDA (Fluoresceindiacetat)	F7378	Sigma-Aldrich, München, DE
Fibronektin	33016-015	Thermo Scientific, Dreieich, DE
FITC-coupled albumin 66 kDa	A 9771	Sigma-Aldrich, München, DE
FITC-Dextran 4 kDa	46944	Sigma-Aldrich, München, DE
FITC-Dextran 40 kDa	FD40S	Sigma-Aldrich, München, DE
Fluoromount-G DAPI	SBA-0100-20	Biozol, Eching, DE
GelRed	M3199.0500	Genaxxon, Ulm, DE
D-Glucose	G8270	Sigma-Aldrich, München, DE
Glutaraldehyd	G5882	Sigma-Aldrich, München, DE
Glycerin	3783.2	Carl Roth, Karlsruhe, DE
Glycerol	M6145	Sigma-Aldrich, München, DE
Glycine	3908.3	Sigma-Aldrich, München, DE

H ₂ O ₂	8070.2	Carl Roth, Karlsruhe, DE
Haematoxylin according to Mayer	10231	Morphisto, Frankfurt Main, DE
Haematoxylin according to Weigert	10225	Morphisto, Frankfurt Main, DE
HCl	1.09057.1000	VWR, Darmstadt, DE
Heparin-Sodium 2500		Ratiopharm, Ulm, DE
Isoflurane	1214	Cp pharma, Burgdorf, DE
L-Glutamin	G7513	Sigma-Aldrich, München, DE
Lightgreen- Goldner III	10369	Morphisto, Frankfurt Main, DE
Matrigel matrix, Corning	FALC356231	Omnilab, Bremen, DE
Methanol	32213	Sigma-Aldrich, München, DE
Mowiol	0713.1	Carl Roth, Karlsruhe, DE
MSCGM™ Mesenchymal Stem Cell Growth Medium	PT-3001	Lonza, Basel, CH
MTT (3-(4,5-Dimethyl-2-Thiazolyl)-2,5-Diphenyl-2H-Tetrazolium bromide)	20395	SERVA, Heidelberg, DE
Na ₂ /EDTA	E5134	Sigma-Aldrich, München, DE
NaCl	HN00.3	Carl Roth, Karlsruhe, DE
NaOH	6771.3	Carl Roth, Karlsruhe, DE
N ω -Nitro-L-arginine methyl ester	N5751	Sigma-Aldrich, München, DE
NP40	68412-54-4	AppliChem, Darmstadt, DE
NucBlue Live ReadyProbes	R37605	Invitrogen, Darmstadt, DE
Orange G	11602	Morphisto, Frankfurt Main, DE
Osmiumtetroxid	E19100	Science Services, München, DE
Paraffin Roti-Plast	6642.6	Carl Roth, Karlsruhe, DE
Paraformaldehyd 4 %	A3813	
PBS-	D8662	Sigma-Aldrich, München, DE
PBS+	D8537	Sigma-Aldrich, München, DE
Penicillin-Streptomycin (100x)	P4333	Sigma-Aldrich, München, DE
PI (Propidiumiodid)	P4170	Sigma-Aldrich, München, DE

Picric fuchsine	3925	Carl Roth, Karlsruhe, DE
Polybrene	H9268	Sigma-Aldrich, München, DE
Propylenoxid	20401	Science Services, München, DE
Protein Marker PeqGold 14.4-116 kDa	16893941	Peqlab Biotechnology, Erlangen, DE
Protein Marker Quadcolor 4 6-300 kDa	830537	Biozym, Hessisch Oldendorf, DE
Proteaseinhibitor	5892791001	Sigma-Aldrich, München, DE
Puromycin	A1113803	Life Technologies, Darmstadt, DE
Roticlear	A538.5	Carl Roth, Karlsruhe, DE
Schiff reagent	3952016	Sigma-Aldrich, München, DE
Sodium deoxycholat	D6750	Sigma-Aldrich, München, DE
Sodium disulfite	407410	Sigma-Aldrich, München, DE
Sodium Dodecyl Sulfate (SDS)	CN30.3	Carl Roth, Karlsruhe, DE
Sodium phosphate dibasic	S7907	Sigma-Aldrich, München, DE
Sodium phosphate monobasic	S8282	Sigma-Aldrich, München, DE
Sodium Pyruvate (100mM)	11360039	Life Technologies, Darmstadt, DE
TE buffer pH 8.0	A2575	AppliChem, Darmstadt, DE
TEMED	2367.2	Carl Roth, Karlsruhe, DE
Tissue lysis reagent QIAzol	79306	Qiagen, Hilden, DE
TRIS base	T6066	Sigma-Aldrich, München, DE
TRIS-HCl	9090.1	Carl Roth, Karlsruhe, DE
Triton-X 100	3051.2	Carl Roth, Karlsruhe, DE
Trizma hydrochloride (Tris- HCl)	T5941	Sigma-Aldrich, München, DE
Trypan blue	T8154	Sigma-Aldrich, München, DE
Trypsin-EDTA 10x	59418C	Sigma-Aldrich, München, DE
Tryptone	8952.4	Carl Roth, Karlsruhe, DE
Tween 20	8.22184.0500	VWR, Darmstadt, DE
upcyte® Hepatocyte Growth Medium		Medicyte GmbH, Heidelberg, DE
upcyte® liver organoid culture medium		Medicyte GmbH, Heidelberg, DE

upcyte® LSEC Medium		Medicyte GmbH, Heidelberg, DE
VascuLife VEGF-Mv Endothelial Complete Kit	LL-0005	CellSystems Biotechnologie Vertrieb GmbH, Troisdorf, DE
Versene	15040	Life technologies, Carlsbad, USA
WST-1	11644807001	Roche, Basel, CH
X-treme Gene9	06365787001	Roche, Basel, CH
Xylene	A538.2	Carl Roth, Karlsruhe, DE
Yeast extract	2363.2	Carl Roth, Karlsruhe, DE

2.4 Media, solutions, and buffers

Table 5. Composition of cell culture media.

Medium		Composition
CHO culture medium	10 % (v/v)	Ham's F12 FBS
hdmEC	5 ng/ml 50 µg/ml 1 µg/ml 10 mM 15 ng/ml 5 ng/ml 5 ng/ml 0.75 U/ml 5 % (v/v)	Vasculife basal medium rh FGF basic Ascorbic acid Hydrocortisone hemisuccinate L-glutamine rh IGF-1 rh EGF rh VEGF Heparin sulfate FBS
Fibroblasts	10 % (v/v)	DMEM FBS
HEK293T	10 % (v/v) 2 mM	DMEM FBS L-glutamine
NICC	0.5 % (v/v) 10 mM 50 µM 1 x 1 x 10 mM 1.6 mM	Ham's F10 BSA Glucose IBMX Pen/Strep Glutamine Nicotinamide CaCl ₂ ·2H ₂ O

Table 6. Composition of solutions and buffers for biochemical and histological analysis.

Buffer	Composition	
DNaseI solution (decellularization)	250 ml 100 mg	PBS DNaseI
Sodium deoxycholat solution	4 % (w/v)	Sodium deoxycholate
BSA blocking buffer (histology)	1 x 5 % (w/v)	PBS BSA
Citrate buffer (10 x)	42 g/l 17.6 g/l	Citric acid NaOH pellets pH 6.0
Citrate buffer for antigen retrieval	10 % (v/v)	Citrate buffer (10 x)
PBST washing buffer (histology)	1 l 0.5 % (v/v) fill up to 10 l	PBS (10 x) Tween-20 Deionized water
Agarose gel	10 % (v/v) 0.6 – 1.2 % (w/v)	TAE buffer (10 x) Agarose
Master mix for PCR	18.7 µl 6 µl 1 µl 1 µl 0.3 ml 1 µl 1 µl	Deionized water Mango Taq buffer MgCl ₂ dNTPs Polymerase Forward primer 5 pmol/µl Reverse primer 5 pmol/µl
TAE buffer (10 x) (nucleic acid gel electrophoresis)	0.4 M 0.2 M 3.72 g/l	Tris Acetic acid EDTA sodium salt
APS (40 %) (SDS gel)	4 g 10 ml	Ammoniumperoxodisulfate Deionized water
Coomassie Brilliant Blue	1.25 l 250 ml 1 l 6.25 g	Deionized water Acetic acid Methanol Brilliant Blue R 250
Coomassie destain	10 % (v/v) 10 % (v/v)	2-propanol Acetic acid
Lower Tris buffer (SDS gel electrophoresis)	1.5 M 0.4 % (w/v)	Tris base SDS pellets

Reducing sample buffer (5x)	1.5 M	Tris base
	10 % (w/v)	Glycerin
	2 % (w/v)	SDS pellets
	0.01 % (w/v)	Bromphenol blue
	5 % (v/v)	β- mercaptoethanol
RIPA lysis buffer	50 mM	Tris base
	137 mM	NaCl
	1 mM	EDTA
	1 % (v/v)	Triton-X 100
	1 % (w/v)	Sodium deoxycholate
	0.1% (w/v)	SDS pellets
Running buffer (10 x) (SDS gel electrophoresis)	250 mM	Tris base
	1.9 M	Glycine
	1.5 % (w/v)	SDS pellets
TBS (10 x)	150 mM	NaCl
	25 mM	Tris base
TBST washing buffer	1 l	TBS (10 x)
	0.05 % (v/v)	Tween-20
	fill up to 10 l	deionized water
Transfer buffer (10 x) (western blot)	25 mM	Tris base
	192 mM	Glycine
Transfer buffer (western blot)	10 % (v/v)	Transfer buffer (10 x)
	20 % (v/v)	Methanol
Upper Tris buffer (SDS gel electrophoresis)	0.5 M	Tris base
	0.4 % (w/v)	SDS pellets

2.5 Commercially obtained kits

Table 7. Commercially obtained kits.

Designation	Catalog no.	Manufacturer
Activin A DuoSet ELISA Development kit	DY338	R&D Systems, Minneapolis, USA
CellTiter 96® AQueous One Solution Cell Proliferation Assay	G3582	Promega, Madison, USA
CellTiter-Glo® Luminescent Cell Viability Assay	G7570	Promega, Madison, USA
Collagen Assay - Sircol™	S1111	Biocolor, Carrickfergus, UK

DC Protein Assay (Western Blot)	500-0116	Bio-Rad Laboratories, München, DE
DCS Super Vision 2 HRP-Polymer- Kit	PD000KIT	DCS Innovative Diagnostik- Systeme, Hamburg, DE
DNeasy Blood & Tissue Kit	69504	Qiagen, Hilden, DE
Elastin Assay - Fastin™	F2000	Biocolor, Carrickfergus, UK
GDF-8/Myostatin Immunoassay Quantikine® ELISA	DGDF80	R&D Systems, Minneapolis, USA
Gel Extraction Kit	28704	Qiagen, Hilden, DE
Glycosaminoglycan Assay - Blyscan™	B1000	Biocolor, Carrickfergus, UK
Insulin ELISA	10-1200-01	Mercodia, Uppsala, SE
KAPA HiFi PCR Kit	KR0368	KAPA biosystems, Wilmington, USA
PCR Purification Kit	28104 28004	Qiagen, Hilden, DE
Plasmid Miniprep Kit	27104	Qiagen, Hilden, DE
Quant-iT™ PicoGreen® dsDNA Reagenz	P7589	Invitrogen, Carlsbad, USA
Total Bile Acids Enzyme Cycling Method kit	DZ042A	Diazyme, Poway, USA
WesternBright Chemiluminescence substrat Quantum	541015	Biozym, Hessisch Oldendorf, DE

2.6 Lentiviral expression systems

Table 8. Lentiviral expression vectors.

Plasmid	Vector type	Marker	Catalog no.	Manufacturer
pCDH-CMV-MCS- EF1-Puro	Cloning and Expression	Puro	CD510B-1-SBI	BioCat GmbH, Heidelberg, DE
pCDH-CMV-MCS- EF1-GFP-T2A-Puro	Cloning and Expression	GFP + Puro	CD513B-1-SBI	BioCat GmbH, Heidelberg, DE

psPAX2	Packaging	12260	Addgene, Cambridge, USA
pMD2.G	Envelope	12259	Addgene, Cambridge, USA

2.7 Oligonucleotides

Table 9. PCR primer oligonucleotides employed for cloning.

Gene	NCBI RefSeq	Primer sequence	Inserted digestion site	Transcript size [bp]	Melting Temp. [°C]
hMSTN	NM_005259.2	ggagaatctagacatgcaaaa actgcaactctg	XbaI	1,127	60
		gagagagaattcaggggaaa accttccatgtt	EcoRI		
hINHBA	NM_002192	ggagaatctagagcagggcct tttaaaaaggc	XbaI	1,280	60
		gaaggagaattcgacaactct tgctcccttc	EcoRI		

2.8 Antibodies

Table 10. Primary antibodies employed for immunohistological staining.

Antigene	Host	Clone	Concentration	Manufacturer	Isotype
aSMA	mouse	1A4	1 µg/ml	Abcam, Cambridge, UK	IgG2a
Caspase-3, activated	rabbit	polyclonal	2 µg/ml	Abcam, Cambridge, UK	Serum
CD31	mouse	JC70A	35 ng/ml	DakoCytomation, Glostrup, DK	IgG1

CD31	mouse	P2B1	1 µg/ml	Abcam, Cambridge, UK	IgG1
CD90	rabbit	YG031111 C	1:250	Abcam, Cambridge, UK	IgG
CK18	mouse	C-04	200 ng/ml	Abcam, Cambridge, UK	IgG1
Glucagon	rabbit	EP3070	1:1000	Abcam, Cambridge, UK	IgG
Insulin	Guinea Pig	polyclonal	1:100	DakoCytomation, Glostrup, DK	
Ki67	rabbit	SP6	1:100	Abcam, Cambridge, UK	IgG
NG2	mouse	HMB45	1:100	Abcam, Cambridge, UK	IgG1
vWF	mouse	F8/86	100 ng/ml	DakoCytomation, Glostrup, DK	IgG1
vWF	rabbit	polyclonal	1:100	Abcam, Cambridge, UK	IgG

Table 11. Secondary antibodies employed for immunohistological staining.

Antigene	Dye	Host	Dilution	Manufacturer
Mouse	Alexa Fluor 488	Donkey	1:400	ThermoFisher Scientific GmbH, DE
Rabbit	Alexa Fluor 488	Donkey	1:400	Invitrogen, Darmstadt, DE
Guinea Pig	Alexa Fluor 488	Goat	1:400	Invitrogen, Darmstadt, DE
Mouse	Alexa Fluor 555	Donkey	1:400	Invitrogen, Darmstadt, DE
Rabbit	Alexa Fluor 555	Donkey	1:400	Invitrogen, Darmstadt, DE
Mouse	Alexa Fluor 647	Donkey	1:400	Invitrogen, Darmstadt, DE
Rabbit	Alexa Fluor 647	Donkey	1:400	Invitrogen, Darmstadt, DE

2.9 Software

Table 12. Software employed.

Software	Developer
Bio-Rad CFX Manager	Bio-Rad Laboratories, München, DE
Clone Manager 6	Sci-Ed Software, Denver, USA

Image J	Wayne Rasband, NIH, USA
Imaris	Bitplane, Zurich, CH
Keyence BZ II Analyzer Keyence BZ II Viewer	KEYENCE, Neu-Isenburg, DE
Origin	OriginLab, Northampton, USA
Visio	Microsoft Corporation, Redmond, USA

3. METHODS

3.1 Murine intestinal tissue preparation

3.1.1 Scaffold explantation

The abdominal wall was disinfected and cut open by a median laparotomy (Fig. 4). The intestine was set aside at first to expose the mesenterica superior, the vessels supplying duodenum, jejunum, and ilium. Vessels were uncovered carefully removing adjacent lymph nodes and possible fat and connective tissue to facilitate cannulation with a 24 gauge catheter. Arteria mesenterica superior and vena mesenterica superior were individually cannulated and the cannulas fixed with a surgical thread to prevent dislocation. Heparin (100 IE/kg) was administrated into the feeding artery via the placed cannula and flushed through the intestinal vascular tree. Flow and blood clearance was monitored visually. A flushed 5 to 10 cm long jejunal segment was chosen for explantation. Redundant adjacent vessels were ligated to allow flow only through the isolated segment. The segment was additionally flushed with PBS. Venous return affirmed full circulation. Subsequently, the ligated segment with its cannulated feeding artery and draining vein was resected and extracted. Another washing step assured integrity, proper explantation of the segment, and flushed residual blood inside the vasculature. Finally, the intestinal lumen was cleared off feces. The resulting scaffold appeared clean but fleshy due to the dense native connective tissue. The specimen were stored at 4 °C until further processing.

3.1.2 Decellularization

The explanted scaffold was decellularized with a modified protocol based on a previously described method^{116,117}. Both, the intestinal lumen and the vascular tree were continuously perfused for detergent delivery and mechanical removal of cellular debris using a roller pump at a turnover of 1 rpm equivalent to 0.6 ml/h. For decellularization the scaffold was successively perfused with deionized water 4 °C for 24 h, followed by perfusion with 4 % sodium deoxycholate at RT for 4 h, and finally with 1 mg/ml DNase-I and 1 % P/S in PBS⁺ at 37 °C for 3 h. Every step was followed by a 30 min PBS wash with

a final washing step over night at 4 °C. After treatment the scaffolds were sterilized by 25 kGy gamma-irradiation and stored in PBS at 4 °C.

3.1.3 Bile acid evaluation

Following the Total Bile Acids kit protocol, 180 µl reagent 1 were rendered per well into a 96 well plate. 2.7 µl of each, sample, control, and calibrator, were added. After 3 min of incubation at 37 °C samples a blank value was set at 405 nm. Thereafter, 60 µl of reagent 2 were added and further incubated at 37 °C with bile acid values to be determined after 60 and 120 s. The difference between the 120 and 60 s value was incorporated into the calculation for the total bile and deoxycholic acid concentration:

$$conc. = \frac{\Delta_{sample} - \Delta_{blank}}{\Delta_{calibrator} - \Delta_{blank}} * 50 \mu M$$

3.1.4 Biocompatibility assay

Biocompatibility of the acellular mBioVaSc-TERM® was performed in compliance with DIN EN ISO 10993-5 for medicinal products. The acellular scaffold was incubated in 1 ml cell culture medium per 3 cm² for 72 h at 37 °C on a rocking shaker. Pure cell culture medium incubated alongside served as control. Meanwhile, about 20,000 target cells were cultured for 24 h in a 96 well format. Culture medium was discarded on the cells and replaced by the incubated culture media, fresh culture medium, 1% SDS, as well as 4 % sodium deoxycholate and incubated for another 24 h. Cell viability was determined adding 20 µl CellTiter 96® AQueous One Solution Reagent onto 100 µl of fresh culture medium. The 120 µl mix replaced the culture medium on the cells and was incubated for 1h at 37 °C. Absorbance was recorded at 490nm using a 96-well plate reader.

3.1.5 DNA purification from tissue

Up to 25 mg tissue was cut into pieces and combined with 180 µl of ATL buffer and 20 µl proteinase K solution in a microcentrifuge tube. Until thorough lysis the mix was incubated at 56 °C on a shaking heating block and vortexed occasionally. Then, 200 µl buffer AL and 200 µl 96 % ethanol were added and vortexed each time. The mixture

was transferred into a DNeasy spin column and centrifuged over 6,000 rcf for 1 min. The flow through was discarded, 500 µl of AW1 solution were added to the column, and centrifuged for 1 min at over 6,000 rcf. The flow through was again discarded, 500 µl of AW2 solution were added to the column, and centrifuged for 2 min at 20,000 rcf. For DNA elution, the flow through was discarded, 200 µl buffer AE were pipetted directly onto the membrane of the column, and centrifuged for 1 min at over 6,000 rcf.

3.1.6 Graft implantation

Surgical implantations of the mBioVaSc-TERM® were conducted by Dr. Johannes Baur (Department of General, Visceral, Vascular and Pediatric Surgery, University Hospital Würzburg, Würzburg, DE). For graft implantation into the regio abdominalis, female NIH-Foxn1nu rats were employed. During the procedure, general anesthesia was induced by continuous isoflurane inhalation-anesthesia with subcutaneous preoperative carprofen analgesia of 5 mg/kg. The abdominal cavity was opened by a median laparotomy (Fig. 14). The infrarenal aorta abdominalis and the infrahepatic vena cava were dissected from fat and connective tissue. After clamping the vessels proximal and distal, an incision of about 3 mm was cut into the vessels for the subsequent anastomosis of the mBioVaSc-TERM® onto the host circulation. The mBioVaSc-TERM® arterial vessel was anastomosed side-to-end to the aorta abdominalis and the scaffolds vein to the vena cava. After examination of the patency of the anastomosis and the pervading of the scaffold with blood the abdominal cavity was closed occluding the abdominal musculature and closure of the skin with sutures. After surgical intervention, carprofen was administered as well as the following three days.

3.1.7 Animal stress scoring

Animals were monitored on a daily basis upon indications of general condition, body weight, posture, overall social behavior, and in case of doubt clinical indications were examined. Dependent on the score, the experiments were executed as planned or stopped prematurely to minimize harm for the animal.

Table 13. Score sheet.

Criteria	Score			
	0	1	2	3
Bodyweight	Unaffected or gain	Loss between 5 and 10 %	Loss between 10 and 20 %	Loss above 20 %
General condition	Clean orifices and eyes	Lightly encrusted orifices or eyes	Unnatural posture, encrusted orifices or eyes	Paralysis, breathing difficulties
Behavior	Typical behavior	Increased rest	Lethargy	Apathy
Clinical indication	Typical body temperature, breathing, and pulse	Slightly Increased respiratory rate	Irregular respiratory rate	Strongly reduced feeding and water uptake, animal feels cold
Actions to undertake	Nothing	Thorough observation	If one criterion persists for more than two days or two criteria appear at the same time: termination	Termination

3.2 Cell culture

3.2.1 Cell culture conditions

If not otherwise stated cells were maintained in a controlled humidified incubator at 37 °C with 5 % CO₂ in cell specific culture medium.

3.2.2 Primary dermal microvascular endothelial cell isolation

Skin biopsies from human prepuce were washed with PBS and redundant fat and connective tissue was removed. The tissue was then cut into strips of 2 to 3 mm width and incubated in dispase o/n at 4 °C. For the isolation of microvascular endothelial cells from

the dermis the epidermal part of the skin was detached with forceps. The dermal strips were washed with Versene and then incubated for 40 min at 37 °C in trypsin/EDTA. The enzymatic reaction was stopped by adding of 1 % FCS to the volume and the strips were transferred into pre-warmed Vasculife medium. Each dermal strip was scratched eight times with light pressure with a scalpel to isolate the ECs therefrom. The cell suspension was transferred into a cell strainer and subsequently centrifuged for 5 min at 1,200 rpm. Cells were seeded in a density of 1×10^4 cells/cm². Medium was exchanged every third or fourth day. To eliminate fibroblasts from the isolated ECs Vasculife was removed and replaced by Versene incubating for 4 to 10 min until fibroblasts were detached.

3.2.3 Primary dermal fibroblast cell isolation

For fibroblast isolation skin biopsies from human prepuce were treated similarly to EC isolation. Briefly, dermis and epidermis were cut in stripes, separated from each other and if desired ECs enzymatically and mechanically detached from the dermal part. The dermis was further cut into 3x3 mm cubic pieces and incubated in collagenase solution for 45 min at 37 °C. The pellet was washed twice by centrifugation at 1,200 rpm for 5 min in cell culture medium. Finally, the dermal pieces were transferred and dispersed in a cell culture flask with cell culture medium. The medium level should not allow for the tissues to detach from the flask to allow cell outgrowth. After 5 d cells were grown out of the tissue and the skin pieces were washed out of the flask for subsequent cell culture.

3.2.4 Cell count and cellular vitality

An aliquot of a cell suspension was mixed with trypan blue and about 10 µl of the suspension were transferred into a Neubauer chamber. Placed under a microscope, in each of the four big squares white appearing living cells and the dead cells appearing blue were counted. Determining cell number per ml, the mean of all four square were calculated, multiplied by the dilution factor of the original cell suspension with trypan blue, as well as multiplied with the volume of the chamber:

$$\text{cell count per ml cell suspension} = \text{mean of living cells} * \text{dilution factor} * 10,000$$

Relative cellular vitality results from the amount of living cells compared to dead cells:

$$vitality[\%] = \frac{\text{amount of living cells}}{\text{amount of dead cells}} * 100$$

3.2.5 Passaging of adherent cells

Cells cultured adherent were washed with PBS before Trypsin/EDTA incubation at 37 °C for up to 5 min until cells have detached. Detachment can microscopically be controlled upon their morphology. After all cells have detached, enzymatic reaction was stopped by addition of 10 % FCS to the total volume. Cell suspension was centrifuged to form a pellet and subsequently resuspended in fresh cell culture medium, counted, and subcultured into a new cell culture flask in desired concentration.

3.2.6 Freezing of cells

Cells were detached from adherent culture, counted, and cell suspension adjusted to about $1 \cdot 10^6$ cells/ml of fresh cell culture medium supplemented with 10 to 20 % FCS and 10 % DMSO serving as cryoprotectant. Finally, the suspension was transferred into cryotubes, placed into Mr. Frosty, which in turn was stored at -80 °C o/n. For long term storage, the cryo-vials were transferred into a liquid nitrogen tank.

3.2.7 Thawing of cells

Frozen cells were transferred into a 37 °C prewarmed water bath. Thawed cell suspension was transferred into prewarmed cell culture medium, centrifuged for 5 min at 1,200 rpm if not recommended otherwise, resuspended in fresh prewarmed cell culture medium to replace the cell toxic DMSO supplemented medium, and transferred into a cell culture flask.

3.2.8 Liver-like organoid formation

Liver-like organoid formation was performed as previously described by Ramachandran et al.¹¹⁸. Hepatocytes, liver sinusoidal endothelial cells¹¹⁹ and bone marrow-derived mesenchymal stem cells were cultured in upcyte® Hepatocyte Growth Medium, upcyte®

LSEC Medium and MSCGM™ Mesenchymal Stem Cell Growth Medium, respectively. For liver organoid formation, cells were mixed in liver organoid growth medium, and cultured on Matrigel™-coated plates until the formation of liver organoids by self-organization. After 3 d in culture, the spheroidal organoids were carefully transferred from the matrigel culture placed inside the revascularized lumen to be integrated and supplied by the mBioVaSc-TERM®.

3.2.9 Viability assay via membrane leakage

Dilution of 1 µl of 0.5 mg/ml FDA as well as 9 µl of 0.05 mg/ml PI in 990 µl PBS-. FDA/PI solution was added to cells and fluorescence was examined after 10 s with an appropriate microscope within 30 min before cells become impaired by the cytotoxic solution. Non-fluorescent fluoresceindiacetate was examined when converted to fluorescein by living cells with an excitation wavelength of 467 to 498 nm and an emission wavelength of 513 to 556 nm. Propidiumiodide, on the other hand, was examined when entered the cells via damaged cell membranes and bound to nucleic acids with an excitation wavelength of 542 to 582 nm and an emission wavelength of 604 to 644 nm.

3.2.10 Viability assay via mitochondrial reductase activity

For qualitative analysis, MTT reagent was diluted to 1 mg/ml with fresh cell culture medium. The solution was added to the cells and incubated for 90 min under cell culture conditions. When the tetrazolium dye MTT was reduced to purple insoluble formazan, the solution was discarded and the cells washed with PBS+ before photo-documentation.

For quantitative determination 3 mg MTT /ml purified water was diluted further 1:1 with fresh cell culture medium. Onto cultured cells, medium was replaced by 250 µl of MTT solution in a 96 well and incubated for 4 h under cell culture conditions to allow reduction of MTT to insoluble formazan and its intracellular deposition. The solution was then discarded and 200 µl DMSO with 25 µl glycine buffer (0.1 M glycine, 0.1 M NaCl, pH 10.5) were added per well to solubilize the purple formazan. Absorbance was examined at 570 nm.

3.2.11 Viability assay via mitochondrial dehydrogenase activity

Culture medium on cells, typically 5×10^3 per 96 well as guiding value in 200 μ l cell culture medium, was replaced by 200 μ l of test-media, fresh culture medium serving as negative control, and culture medium with 1 % SDS as positive control. After 24 h incubation at 37 °C and 5 % CO₂ all media were replaced by 200 μ l of a WST-1 solution diluted 1:10 in PBS⁺ and kept in the incubator for 1 h until analysis. Absorbance was determined at 450 nm with reference wavelength of 620 nm after shaken for 1 min.

3.2.12 Viability assay via quantification of cellular ATP

Cells were cultured in a 96 well plate until confluency. Cells were washed with PBS⁺ and subsequently 100 μ l fresh culture medium were added as well as 100 μ l CellTiter Glo reagent. The Tecan luminescence reader allowed for shaking the culture plate for 2 min, and subsequent incubation in the dark for 10 min before luminescence determination using an integration time of 1 s, with the luminescent signal directly proportional to the intracellular ATP.

3.2.13 Graft vascularization

For revascularization, detached ECs were successively injected through the arterial and venous cannulas into the vascular tree of the scaffold. Allowing cell adherence to the vascular walls, infusion was followed by a 1 h static incubation until a subsequent injection into both vessels and another 1 h static incubation. Dependent on scaffold size, 0.5 to 1 ml of a 1×10^6 cells/ml EC suspension was introduced per injection with an infusion rate of 4 ml/min. To allow maturation and functional lining of the endothelial barrier on the vascular bed the scaffold was connected to a bioreactor in which the vascular system was perfused dynamically mimicking physiological blood pressure. For standardization and reproducibility the perfusion in the bioreactor was computer controlled. Temperature, CO₂ concentration and pressure were monitored and adjusted as well as the dynamic perfusion was controlled in order to achieve physiological blood circulating conditions.

3.2.14 Bioreactor setup

Glass cannulas were fixed in a glass reactor and connected via tubes with glass bottles storing culture medium and serving as pressure compensation. Both glass bottles were interconnected via two tubing systems. One of them allowing media flow via a peristaltic pump, the other one clamped serving as bypass. The pressure compensation bottle was connected to the arterial inflow with a pressure dome to sensor the inflow pressure (represented by the scheme in Fig. 7C).

3.3 Histological staining

3.3.1 Fixation and paraffin embedding

Samples were fixed in 4 % PFA for 2 h and subsequently placed in cassettes for dehydration and embedding in paraffin as described in table 14.

Table 14. Paraffin embedding.

Reagent incubation	Time [h]
Tap water	2
Ethanol 50 %	1 to o/n
Ethanol 70 %	1
Ethanol 90 %	1
Ethanol 96 %	1
Isopropanol	1
Isopropanol	1
Isopropanol/ Xylene 1:2	1
Xylene	1
Xylene	1
paraffin	o/n
paraffin	o/n

3.3.2 De-wax and rehydration

Microtome sections of paraffin embedded samples on glass slides were stored for 1 h at 60 °C until paraffin was melted. To de-wax the samples they were incubated in xylene twice for 10 min each. For rehydration of the samples, they passed through a descending alcohol series ranging from 96 % ethanol, to 80 %, to 70 %, to 50 % dipped in three times until arriving in purified water.

3.3.3 Haematoxylin and eosin (H&E) stain

Microtome sections of paraffin embedded samples were de-waxed and rehydrated. Stain was conducted as described in table 15.

Table 15. Haematoxylin and eosin (H&E) stain.

Reagent incubation	Time [min]
Haematoxylin according to Mayer	6
Purified water	Gently flowing until no more dye washed off
Tap water	5
Eosin	6
Purified water	Gently flowing until no more dye washed off
Ethanol 70 %	Dip in twice
Ethanol 96 %	2
Isopropanol	5
Isopropanol	5
Xylene	5
Xylene	5
Entellan® mounting	

Haematoxylin stained the nuclei blue by binding of the dye-metal complex to basophilic DNA. Most positively charged intracellular and extracellular proteins were stained red or pink by eosin.

3.3.4 Feulgen stain

Sodium disulfite washing solution was prepared as followed: 95 ml purified water, 5 ml sodium disulfite, and 1 ml HCl. Samples were prepared by common de-paraffination and successively rehydrated. Stain was conducted as described in table 16.

Table 16. Feulgen stain.

Reagent incubation	Time [min]
Tap water	10
HCl	50
Purified water	2
Purified water	2
Schiffs reagent	60
Sodium disulfite washing	3
Sodium disulfite washing	3
Purified water	2
Purified water	2
Ethanol 50 %	1
Ethanol 70 %	1
Ethanol 80 %	1
Ethanol 99 %	1
Xylene	1
Entellan® mounting	

DNA and other chromosomal material was semi-quantitatively stained red. The background can be counterstained if desired but was unstained otherwise.

3.3.5 Elastica van Gieson stain

Samples were prepared by common de-wax and successively rehydrated. Stain was conducted as described in table 17.

Table 17. Elastica mit van Gieson stain.

Reagent incubation	Time [min]
Haematoxylin according to Weigert	15
Tap water	5
picric fuchsine solution	2
Purified water	Gently flowing until no more dye washed off
Ethanol 70 %	Dipping in three times
Ethanol 96 %	5
Isopropanol	5
Xylene	5
Xylene	5
Entellan® mounting	

Nuclei were stained dark brown, elastic fibers red to dark violet.

3.3.6 Trichrome stain according to Masson Goldner

Microtome sections of paraffin embedded samples were de-waxed and rehydrated. Staining was conducted as described in table 18.

Table 18. Trichrome stain according to Masson Goldner.

Reagent incubation	Time [min]
Haematoxylin according to Weigert	5
Purified water	0.1
Tap water	8, flowing
Acid fuchsine Ponceau	4
Acidic acid 1 %	0.1
Orange G	5
Acidic acid 1 %	0.1
Lightgreen Goldner III	6
Acidic acid 1 %	0.1

Tap water	1, flowing
Ethanol 96 %	2
Ethanol 96 %	2
Isopropanol	2
Xylene	5
Xylene	5
Entellan® mounting	

Haematoxylin stains the nuclei blue by binding of the dye-metal complex to basophilic DNA. Acid fuchsin Ponceau stained the cytoplasm red. Lightgreen stained collagen fibers of the connective tissue green.

3.3.7 Immunohistochemistry

10x Citrate buffer was prepared by dissolving 42 g/l citric acid monohydrate into purified water. pH was adjusted to 6.0 with 5 M NaOH. Washing buffer was prepared with 0.5 % Tween-20 in PBS. Paraffin sections were de-waxed and rehydrated. Thereafter, antigen epitopes were heat-induced demasked in 1x citrate buffer at 100 °C for 20 min. In case of intracellular antigens cells were additionally permeabilized with 0.3 % Triton-X100 in PBS for 10 min. Intracellular peroxidase was blocked by incubation with 3 % H₂O₂ in purified water for 10 min and washed for 5 min thereafter. Unspecific binding was blocked by 5 % BSA in antibody dilution solution during at least 30 min. Primary antibody was incubated o/n at 4 °C. Before and after 10 min polymer enhancer incubation at RT samples were washed three times 5 min in washing buffer. HRP polymer was incubated for 20 min at RT and washed afterwards three times 5 min. DAB solution was incubated for about 5 min until staining. Slides were transferred into washing buffer, then counterstained in haemalaun for 30 to 45 s and tap water for 60 to 90 s. Transferred in purified water, the samples were successively dehydrated as described in table 19.

Table 19. Dehydration.

Reagent incubation	Time [min]
Ethanol 70 %	Dipping inside twice
Ethanol 96 %	2
Isopropanol	2
Xylene	3
Xylene	3
Entellan® mounting	

3.3.8 Immunofluorescence (IF)

Paraffin sections were de-waxed and rehydrated. Thereafter, antigen epitopes were heat-induced demasked in citrate buffer at 100 °C for 20 min. In case of intracellular antigens cells were additionally permeabilized with 0.3 % Triton-X100 in PBS for 10 min. Unspecific binding was blocked by 5 % BSA in antibody dilution solution during at least 30 min. Primary antibody was incubated o/n at 4 °C. Before and after 1 h secondary antibody incubation at RT samples were washed three times 5 min in washing buffer. Samples were mounted in Fluoromount G + DAPI.

3.3.9 Light sheet fluorescence microscopy

Whole mount sections were fixed and stained by immunofluorescence as described before. Optical clearing for light sheet microscopy was performed by a two-step process¹²⁰ involving a 2 h incubation in n-hexane followed by three times 30 min incubation in a 1:3 benzyl benzoate / benzyl alcohol solution.

3.3.10 Preparation for transmission electron microscopy

0.1 M phosphate buffer was prepared using 10.9 g/l sodium phosphate dibasic, 3.2 g/l sodium phosphate monobasic, and pH was adjusted to 7.3. Cells and tissue models were washed properly with PBS before fixed at 4 °C o/n in 0.1 M phosphate buffer,

4 % PFA, and 1 % glutaraldehyde. Samples were washed afterwards three times in phosphate buffer for 10 min each. Then, osmiumtetroxide was diluted to 1 vol.-% in phosphate buffer and samples were incubated for 1 h with subsequent washing steps of 5 min with phosphate buffer twice and once 5 min with purified water. After washing, samples were successively dehydrated in 30, 50, 70, and 96 % ethanol for 5 min each followed by 10 min in 100 % ethanol, twice. Then samples were incubated in propylenoxide for 10 min, twice, and o/n in a 1:1 propylenoxide/epon mixture. The next day, samples were incubated in epon for 2 h, then embedded in epon. Polymerization occurs at 55 to 60 °C during 24 to 72 h. Ultra-thin sections were cut and contrasted using uranyl acetate for 20 min and iron citrate for 7 min followed by 30 min air dry.

3.4 Characterization of vascular barrier function

3.4.1 FITC-dextran barrier permeability

A sterile filtered 0.25 mg/ml FITC-dextran solution in cell culture medium was prepared and prewarmed to 37 °C. The culture medium of the barrier models was removed and replaced with fresh medium in the basolateral compartment and with the FITC-dextran solution in the apical compartment. It was critical to establish a similar medium level in both compartments. The models were cultured for 30 min on an orbital shaker at 37° in the CO₂ incubator. 200 µl of the basolateral compartment were transferred in a black 96 well plate and analyzed upon fluorescent particles passing the barrier by a fluorescence reader with an absorption of 490 nm and an emission of 525 nm. Fresh culture medium and the FITC-dextran solution served as control. The cell culture models could be cultured further afterwards with a full fresh medium exchange.

3.4.2 Trans-endothelial electrical resistance (TEER)

For barrier model maintenance it is crucial that the electrode was disinfected with 70 % ethanol for 15 min before application. For reproducible analysis the Millicell® ERS-2 system was calibrated before each usage, the electrode was equilibrated in fresh cell-specific culture medium, and culture medium of the constructs was exchanged beforehand. With the models placed on a heating plate to ensure 37 °C the electrodes were

applied to the compartments separated from the cellular barrier and the electrical resistance determined. For each condition, the measurement was performed in triplicates. Cell free inserts served as negative control. Evaluation of the actual TEER-value from the determined resistance was calculated as:

$$TEER \text{ value } [\Omega * cm^2] \\ = (\text{sample resistance } [\Omega] - \text{blank resistance } [\Omega]) * \text{culture area}[cm^2]$$

After measurement, the models were cultured further in the incubator. The electrode was disinfected in 70 % ethanol for 5 min.

3.4.3 Intravital microscopy

To analyze vessel integrity and microvascular permeability real-time fluorescence intravital microscopy was employed as described previously¹²¹. The graft was placed under a standard inverted microscope and perfused with carbogen-gassed PBS solution at 37 °C. Intravital real-time fluorescence was detected after infusion of either FITC-coupled dextran or albumin solution in PBS or blood directly into the vasculature via the arterial pedicle. For *in vivo* analysis the animal was kept under anesthesia while the jugular vein was prepared for infusion with the dye and the vascular perfusion was observed under a fluorescence microscope as described.

3.4.4 LDL uptake

Endothelial cells incorporate LDL through receptor-mediated endocytosis. To demonstrate the metabolic function the ECs inside the vessel structures the graft was exposed to 10 µg/ml AcLDL for 4 h at 37° C by infusing the solution through the arterial pedicle of the vascularized scaffold. Nuclei were stained by incubation of 2 drops of NucBlue™ Live ReadyProbes™ per 1 ml assay solution for 30 min. A standard fluorescence microscope was employed for visualization.

3.4.5 Myography

Segments of reendothelialized vessels were dissected and mounted on pins inside a myograph organ bath system to determine vascular contraction. The chambers of the

myograph were washed with distilled water, preheated to 37 °C with freshly prepared krebs henseleit buffer solution, and constantly gassed with carbogen. Reendothelialized vessels of the mBioVaSc-TERM® were dissected from surrounding connective tissue and a segment of about 3 mm was mounted on the pins of each chamber. The pins were tightened and the vessel segments incubated in the chambers. After 1 h of equilibration, vasodilation was inhibited by 3 µM diclofenac and 200 µM N-nitro-L-arginine methyl ester. Vasoconstriction was stimulated by increasing concentrations of 0.1 µM, 1 µM and 10 µM carbachol.

3.5 Bacterial culture

3.5.1 Casting of agar plates

10 g tryptone, 5 g yeast extract, and 10 g NaCl were dissolved into 500 ml purified water provided in a volumetric flask placed on a magnetic stirrer. pH was set to 7.5 and the volume was stocked with purified water to a final volume of 1 l. The generated LB medium was split into two 500 ml bottles, to each 3.25 g agar-agar was added, and brought for autoclaving immediately. Agar dissolved while autoclaving. Afterwards, the hot LB medium with agar was cooled a little but while still liquid cast in petri dishes. Desired antibiotics were added right before casting.

3.5.2 Bacteria culture conditions

Bacteria were cultured in LB medium in an Erlenmeyer flask in a stirring shaker at 37 °C typically overnight.

3.5.3 Bacterial transformation by heat shock

While bacterial transformation foreign DNA was introduced into bacteria in order to store and replicate introduced plasmids. Frozen *E. coli* were thawed on ice and 100 ng plasmid DNA was mixed in. In case of prior ligation, the whole preparation was added. After DNA addition, bacteria and DNA were incubated on ice for 5 min followed by a heat shock for 45 s at 42 °C. Afterwards, after another cool down for 5 min on ice to allow membrane

closure 800 µl of LB medium were added and transformed bacteria cultured at 37 °C for 30 to 60 min to allow antibiotic resistance coded on the plasmid to be translated. Bacteria were seeded onto agar plates that were pre-warmed to RT and cultured o/n at 37 °C to grow cultures of bacteria successfully transformed. The following day cultures were picked and transferred into a liquid stirring culture to allow for bacterial growth and subsequent plasmid isolation.

3.5.4 Mini prep

Overnight bacterial culture was harvested by centrifugation at 6,000 rcf for 15 min at 4 °C. The bacterial pellet was resuspended in 0.3 ml buffer P1. 0.3 ml buffer P2 were added, mixed by inverting 4 to 6 times, and incubated for 5 min. 0.3 ml prechilled Buffer P3 were added, mixed by inverting 4 to 6 times, incubated for 5 min on ice, and then centrifuged for 10 min at 14,000 to 18,000 rcf. Meanwhile, a QIAGEN-tip 20 was equilibrated with 1 ml buffer QBT. After equilibration, supernatant was applied to the tip and after flown through, the tip was washed twice with 2 ml buffer QC each. DNA was eluted with 0.8 ml buffer QF and precipitated by adding 0.56 ml isopropanol and centrifuging at 15,000 rcf for 30 min at 4 °C. Supernatant was discarded, the pellet washed with 1 ml 70 % ethanol, and centrifuged at 15,000 rcf for 10 min. The resultant DNA pellet was air dried for 5 to 10 min and dissolved in TE buffer.

3.6 Molecular genetics

3.6.1 Chromosomal DNA determination

A standard curve was prepared by serial dilution in advance ranging from 25 pg/ml to 25 ng/ml in a low range or from 1 ng/ml to 1 µg/ml in a high range. 100 µl of standard, blank, and samples were applied in duplicates into a black 96 well plate. To each, 100 µl pico green reagent was added and incubated together for 2 to 5 min while protected from light to minimize photobleaching. Fluorescence was measured with an excitation of 480 nm and emission of 525 nm. Quantification of DNA amount is determined on the basis of the standard curve.

3.6.2 PCR

For amplification of DNA fragments 10 μ l of 5x KAPA HiFi buffer was mixed with 1.5 μ l 10 mM KAPA dNTP mix, 1.5 μ l 10 μ M forward primer, 1.5 μ l reverse primer, up to 100 ng DNA template, and 1 U KAPA HiFi DNA polymerase filled up to 50 μ l PCR grade water. PCR was performed following a cycling protocol with an initial denaturation step at 95 °C for 3 min followed by 15 to 30 cycles of 20 s denaturation at 98 °C, 15 s annealing at 60 to 75 °C depending on the primers used, and 15 to 60 s per kb DNA to be extended at 72 °C. Final extension was performed at 72 °C for 1 min per kb DNA.

3.6.3 DNA purification from agarose gel or PCR

Excised DNA from gel after electrophoresis was placed in microcentrifuge tube and per 10 mg gel 10 μ l membrane binding solution was added, vortexed and incubated at 50 to 65 °C until complete dissolving of the gel.

To PCR amplified DNA fragments an equal volume of membrane binding solution was added.

DNA in membrane binding solution was transferred to the SV minicolumn, incubated for 1 min, and centrifuged at 16,000 rcf for 1 min to allow DNA to bind to the column. The flowthrough was discarded. For washing 700 μ l wash solution was centrifuged through the column at 16,000 rcf for 1 min. Washing was repeated with 500 μ l wash solution centrifuging for 5 min and then without wash solution for 1 min but with the lid open to allow evaporation of any residual ethanol. DNA was eluted with 50 μ l nuclease free water centrifuging 1 min at 16,000 rcf after a 1 min incubation.

3.6.4 Cloning

Cloning allowed the insertion of properties into cells such as drug resistance markers or specific protein expression via DNA insertion. Digestion of DNA from a plasmid source with the appropriate restriction enzymes allowed DNA fragment generation for immediate unidirectional insertion into a vector. Alternatively, PCR primers were designed with restriction sites to allow unidirectional cloning into a vector. Restriction digestion was performed adding 10 units of restriction enzyme, 1 μ g DNA, and 5 μ l of

10x NEBuffer up to a total volume of 50 μ l and incubated for 1 h at the restriction enzyme dependent temperature. Using fast digestion enzymes, a total volume of 20 μ l was prepared with 2 μ l of 10x fast digest buffer, 1 μ g DNA, and 1 μ l fast digest enzyme incubated for 5 min at 37 °C. Vectors were digested the same way as the inserts. To prevent self-ligation of vectors, dephosphorylation was performed using 5 units of Antarctic phosphatase with 1 to 5 μ g of digested vector DNA in 2 μ l of 10x buffer in a total volume of 20 μ l for 15 min at 37 °C. Reaction was heat inactivated for 5 min at 70 °C. Vector and insert were purified before ligation by fragment size separation in an agarose gel and subsequent excision and retrieval. Ligation was performed using a molar ratio of vector to insert of 1:3. A total of about 100 ng DNA was mixed with 10 μ l of 10x T4 ligase buffer and 1 μ l T4 DNA ligase in a total volume of 20 μ l incubated for 5 min at RT. All volumes were added up to the recommended volume with nuclease free water.

The coding sequences of *ActivinA* and *Myostatin* were cut out of bacterial plasmids using restriction enzymes. The same enzymes were used to cleave the vector plasmids before ligation of vector and gene of interest. Control digests of the newly ligated vector plasmids resulting in the expected fragment sizes were analyzed by gelelectrophoresis. Subsequently, HEK293T cells were transduced with the vector plasmid along with plasmids encoding lentiviral encapsulation and packaging proteins. The thereby produced virus particles were afterwards used to transfect CHO cells introducing the gene of interest into the host cell genome.

3.6.5 Transfection for virus production

HEK 293T cells were passaged and cultured until a confluency of 70 to 80 %. Lentiviral packaging and envelope vector as well as the transfer vector containing the gene of interest to be integrated were mixed in a molar ratio of 2:1:1 to a final mass of 2 μ g in 200 μ l of serum free cell culture medium, typical for a 6 well format. Per 1 μ g DNA added, 3 μ l transfection reagent were added and mixed gently and then incubated for 25 min at RT to form complexes. Meanwhile, medium was exchanged onto the HEK cells and into the fresh medium the DNA mix was added dropwise. It was compulsory to wear protective equipment and follow safety precautions. The next day, medium was exchanged onto the HEK cells and replaced with fresh culture medium supplemented with 30 % FCS to enhance virus production for the following 48 h. Virus containing supernatant was

harvested and filtered with a 0.45 μm filter with low protein binding capacity or centrifuged at 2,000 rpm to eradicate cellular remnants. Virus was used immediately for transduction or stored at $-80\text{ }^{\circ}\text{C}$.

3.6.7 Viral transduction

Before transduction, antibiotic selection was tested on the cells to determine the minimal concentration necessary for cell death. The cell layer should be about 20 to 50 % confluent therefore when assayed. Additionally, polybrene compatibility was investigated beforehand on the cells as its application improved transducability.

For viral transduction, cells to be transduced were seeded typically in a 6 well format to be at 60 to 70 % confluency 72 h thereafter. Then, virus was applied to the cell layer as well as fresh cell culture medium up to 2 ml, yet at least one third of the total volume to be cell culture medium. It was compulsory to wear protective equipment and follow safety precautions. Virus was incubated for 24 to 72 h to allow for gene introduction until fresh medium exchange to allow for proliferation of the transduced cells. 3 to 5 d after transduction cells were selected upon the implemented antibiotic in the beforehand determined concentration. If no antibiotic resistance was integrated but fluorescence was, selection could be conducted via FACS sorting.

Evidence of residual virus availability in the culture medium was investigated at the earliest after 3 passages. Therefore, supernatant of the transduced cells was transferred onto HEK 293T cells at about 50 % confluency. Past 72 h of incubation, cells were investigated upon viral integration via ELISA, PCR, or fluorescent protein expression detection.

3.7 Proteomic analysis

3.7.1 Protein precipitation

To precipitate protein four times the volume of $-20\text{ }^{\circ}\text{C}$ acetone was added, vortexed, incubated for 60 min at $-20\text{ }^{\circ}\text{C}$, and then centrifuged for 10 min at 13,000 to 15,000 rcf. Supernatant was carefully discarded without disrupting the protein pellet. Subsequently,

acetone was allowed to evaporate for 30 min. Protein pellet was dissolved with buffer appropriate for the downstream process and stored at -20 °C.

3.7.2 SDS Gel and Coomassie-stain

Buffers were prepared as follows in purified water:

10x SDS running buffer consisted of 250mM tris base, 1.9 M glycine, and 1.5 % SDS.

5x reducing sample buffer consisted of 1.5 M tris base, 2 % SDS, 10 % glycerol, 0.01 % bromophenol blue sodium salt, and 5 % β -mercaptoethanol. For non-reducing buffer, β -mercaptoethanol was left out.

Lower tris consisted of 1.5 M tris base and 0.4 % SDS.

Upper tris consisted of 0.5 M tris base and 0.4 % SDS.

APS stock solution for SDS gels was prepared diluting 40 %-w/v ammonium persulfate. 1 ml aliquots were stored at -20 °C.

Coomassie stain solution was filtered after solving of 250 ml acetic acid, 1,000 ml methanol, 6.25 g brilliant blue in 1,250 ml purified water.

Destain solution consisted of 10 %-v/v isopropanol and 10 %-v/v acetic acid.

10 ml 10 % resolving gel sufficient for two gels consisted of 2.5 ml lower tris, 3.3 ml acrylamide, 2.2 ml purified water, 2 ml glycerol, 14 μ l APS, and 14 μ l TEMED. Cast gel immediately after addition of APS and TEMED before gel polymerization.

5ml stacking gel consisted of 1.25 ml upper tris, 0.5 ml acrylamide, 3.2 ml purified water, 12 μ l APS, and 12 μ l TEMED. Cast gel immediately after addition of APS and TEMED before gel polymerization.

For each gel prepared, two glass slides were washed with purified water and 70 % ethanol. Spacers were placed in between the glasses and placed as one into the clamping system. Resolving gel was cast up to two thirds in between the glass slides and covered with purified water to ensure a straight horizontal line after polymerization for 30 min. Water was then removed and stacking gel was cast and sealed with a comb creating the pockets after polymerization for 30 min. Gels in glass slides were clamped in the electrophoresis system. 1x running buffer was filled into the chambers and combs removed. Samples were mixed with 5x loading buffer to end up with 1x loading buffer,

heated for 5 min at 95 °C, and spun down. 20 to 30 µl of sample were introduced into each pocket. 5 µl marker was used for size indication. Voltage and output power were set to maximum and current was set to 25 mA per gel. After the run, the gel was removed from the electrophoresis system as well as from the glasses and transferred into Coomassie stain for at least 1 h incubation on a rocking shaker. To remove excessive Coomassie staining the gel was incubated in destain solution until visualization of the specific staining.

3.7.3 Western blotting

After protein separation via SDS gel electrophoresis, gels were rinsed with transfer buffer and transferred onto the blotting chamber into a sandwich consisting of three whatman paper, blotting membrane, the gel, another three whatman paper. Whatman paper were soaked with transfer buffer. Closing the lid, blotting was performed for 1 to 1.5 h at 3 mA/cm² of gel. Successful blotting was visible by transfer of the stained marker from the gel onto the membrane. The membrane was then transferred into blocking solution for 1 h to inhibit unspecific antibody binding. Primary antibody was diluted in 5 to 10 ml of blocking solution and incubated on the blot for 1 to 2 h at RT or o/n at 4 °C. Blots were washed afterwards three times for 10 min each in TBST, then incubated in HRP coupled secondary antibody for 1 h at RT. Blots were again washed twice for 5 min each and developed immediately after. For blot development, the blot was covered with a mixture of 1 ml peroxide solution and 1 ml luminol enhancer solution. After 30 to 60 s of incubation the signal was acquired.

3.7.4 Elastin ELISA

For determination of α-elastin content, tissue samples were incubated in 750 µl of 0.25 M oxalic acid at 100 °C for 60 min. After cooling down to room temperature the samples were centrifuged for 10 min at 10,000 rpm to collect the supernatant. The procedure was repeated for two more times until the tissue was digested. Of each digest duplicates of 100 µl were mixed with 100 µl ice cold elastin precipitation reagent by vortexing. After precipitation for 15 min samples were centrifuged for 10 min at 12,000 rpm. The supernatant was discarded while the pellet was vortexed with 1 ml dye

reagent. Reaction between elastin and dye was allowed while 90 min incubation on a rotational shaker. After centrifugation for 10 min at 12,000 rpm unbound dye was discarded. 250 μ l dye dissociation reagent added, shortly vortexed, and incubated for 10 min to disassociate bound dye from elastin. 200 μ l were transferred into a transparent 96 well plate and examined at 513 nm. Elastin amount directly proportional to the dye is calculated from a standard curve typically ranging from 0 to 60 μ g. Blank value was subtracted from all determined values.

3.7.5 Collagen ELISA

Test samples, standard, and blanks were prepared in microcentrifuge tubes and filled up to 100 μ l volume. 1 ml Sircol Dye Reagent was added, mixed by inverting and placed in a mechanical shaker for 30 min to allow formation of collagen-dye complexes. The bound collagen was centrifuged for 1 min at 12,000 rpm and the supernatant was discarded. Unbound dye was removed with 750 μ l ice-cold Acid-Salt Wash Reagent. Before discarding the wash reagent it was centrifuged for 10 min at 12,000 rpm. To recover the dye bound to collagen 250 μ l Alkali Reagent were added, vortexed, incubated for 5 min to allow for proper dye release. 200 μ l were transferred into a 96 well plate, absorbance was determined at 555 nm.

3.7.6 Glucose stimulated insulin secretion

Insulin secretion of pancreatic islets was stimulated by glucose incubation after deprivation with KRB buffer. Therefore, the islets were pre-incubated in 3 mM glucose for 30 min before glucose stimulated insulin secretion incubating the cells with 3, 5, and 10 mM glucose. Supernatant was taken and analyzed by ELISA.

3.7.7 Insulin ELISA

In a 96 well format 25 μ l insulin ELISA calibrator standards, controls, and samples were mixed with 100 μ l enzyme conjugate solution and incubated for 2 h on a plate shaker with about 800 rpm at RT. The plate was washed six times with wash buffer. Subsequently

200 μ l TMB substrate were added and incubated for 15 min. After addition and proper mixing of 50 μ l stop solution optical density was determined at 450 nm.

3.7.8 Activin A ELISA

Capture antibody was diluted in PBS to working concentration and immediately used to coat a 96 well microplate with 100 μ l per well. The sealed plate was incubated o/n at RT. The wells were then washed three times with washing buffer. To block unspecific binding sites 300 μ l reagent diluent were incubated for at least 1 h and subsequently again washed three times. For assay procedure, 100 μ l sample respectively standards were added per well together with 100 μ l of 1 M urea. The plate was mixed gently, covered, and incubated for 2 h at RT. After another triple washing step 100 μ l detection antibody was added and covered for another 2 h at RT with another subsequent triple washing step. Afterwards, 100 μ l streptavidin-HRP was added and incubated for 20 min at RT avoiding direct light. After subsequent washing, 100 μ l substrate solution were added and incubated for 20 min at RT avoiding direct light. Then, 50 μ l stop solution were added and thoroughly mixed in. Optical density was determined immediately using a microplate reader set to 450 nm with correction set to 540 or 570 nm. Protein concentration was calculated by means of the standard curve.

3.7.9 Myostatin ELISA

Upon reagent preparation, samples were activated to remove the GDF-8 pro-peptide. All reagents were at RT. 1 N HCl was added to the sample, mixed, and incubated for 10 min at RT. 1.2 N NaOH/0.5 M HEPES and calibrator diluent RD5-26 were added to the mix. Activated samples were assayed within 2 h. 50 μ l assay diluent was added to microplate strips with 50 μ l samples, controls, and serial diluted standards were added and incubated for 2 h on a horizontal orbital microplate shaker set at 500 rpm. Washing was performed four times with wash buffer. 200 μ l GDF-8 conjugate were added and incubated for another 2 h shaking with subsequent washing. 200 μ l substrate solution were added and incubated for 30 min protected from light. 50 μ l stop solution were added to each well. Thorough mixing was indicated by color change from blue to yellow. Optical density was determined using a microplate reader set to 450 nm with correction set to 540 or 570 nm.

Protein concentration was calculated by means of the standard curve. The dilution factor from sample activation was calculated in the concentration determined off the standard curve.

3.7.10 Bioactivity assay of Activin A / Myostatin

Cells virally transduced to produce Activin A respectively Myostatin were cultured and protein secreted into the supernatant was collected. For both proteins, Activin A as well as Myostatin, their impact on cell proliferation of mouse plasmacytoma cell line (MPC)-11¹²² was utilized. Both proteins were described in literature to inhibit MPC-11 cellular proliferation, Activin A with an EC₅₀ of around 0.75 to 3 ng/ml and Myostatin with an EC₅₀ of around 30 to 40 ng/ml. To Test Biological activity, protein supernatant was transferred as a dilution series onto MPC-11 cultured in a 96 well format. After 48 h incubation cellular viability was determined giving an indication of the biological activity of the secreted protein, its EC₅₀ and thereof its present concentration in the supernatant.

3.8 Statistical analysis

All results are expressed as mean \pm standard deviation (SD). Differences between experimental groups were analyzed using the one-tailed independent samples t-test. A value of $p < 0.05$ was considered as statistically significant (*), $p < 0.01$ as statistically highly significant (**). $p > 0.05$ was considered as statistically not significant.

4. RESULTS

The aim of this thesis was to generate a scaffold of rat intestine that resembles the structural properties of the BioVaSc-TERM®. After establishing a suitable explantation strategy, a protocol for detergent-based perfusion decellularization of the scaffold was developed. The miniaturized version of the BioVaSc-TERM®, that is referred to as the mBioVaSc-TERM®, was characterized on its structure and composition by histological and protein biochemical analyses. Preservation of an intact vascular system was analyzed by reendothelialization of the vessel structures, thereby demonstrating scaffold biocompatibility *in vitro*. Scaffold revascularization was utilized to maintain complex multicellular co-cultures viable to perform functional metabolic conversion and protein secretion analysis. Finally, implantation into rats demonstrated *in vivo* survival of the mBioVaSc-TERM® and highlighted its potential as biological scaffold for clinical application.

4.1 Establishment of the mBioVaSc-TERM®

The overall base of this work was to determine an optimal rat jejunal segment to obtain a biological scaffold similar to the porcine BioVaSc-TERM®. Focus was on an easy preparation strategy of the tissue, the preservation of its native ECM characteristics, as well as an accessible vascular system.

4.1.1 Explantation of a rat jejunal segment

Homologue to the porcine BioVaSc-TERM®, the mBioVaSc-TERM® was generated from rat jejunal segments. The explantation is depicted in figure 4, indicating the incisions made for a laparotomy (Fig. 4A) to gain access into the abdominal cavity and the subsequent preparation of the cannulation and dissection of the intestinal segment. The mesenteric vessels (Fig. 4B; highlighted by arrowheads), which branch off from the abdominal aorta and leading into the hepatic portal vein, were dissected from surrounding connective tissue and fat. The superior mesenteric artery and antidromic vein, supplying and draining the small intestine, respectively, were prepared for cannulation (Fig. 4C and D) to grant access to the vascular network enabling its perfusion

with PBS, thereby flushing out the blood before coagulation. Full clearance from blood by PBS perfusion indicated an intact, perfusable arteriovenous loop. A jejunal segment cleared from blood was ligated (Fig. 4E) to prevent leakage and to enable maintenance of an intact arteriovenous circulation after extraction.

Hence, a miniaturized homologue to the BioVaSc-TERM® with an accessible vascular circulation was obtained from the rat (Fig. 4F).

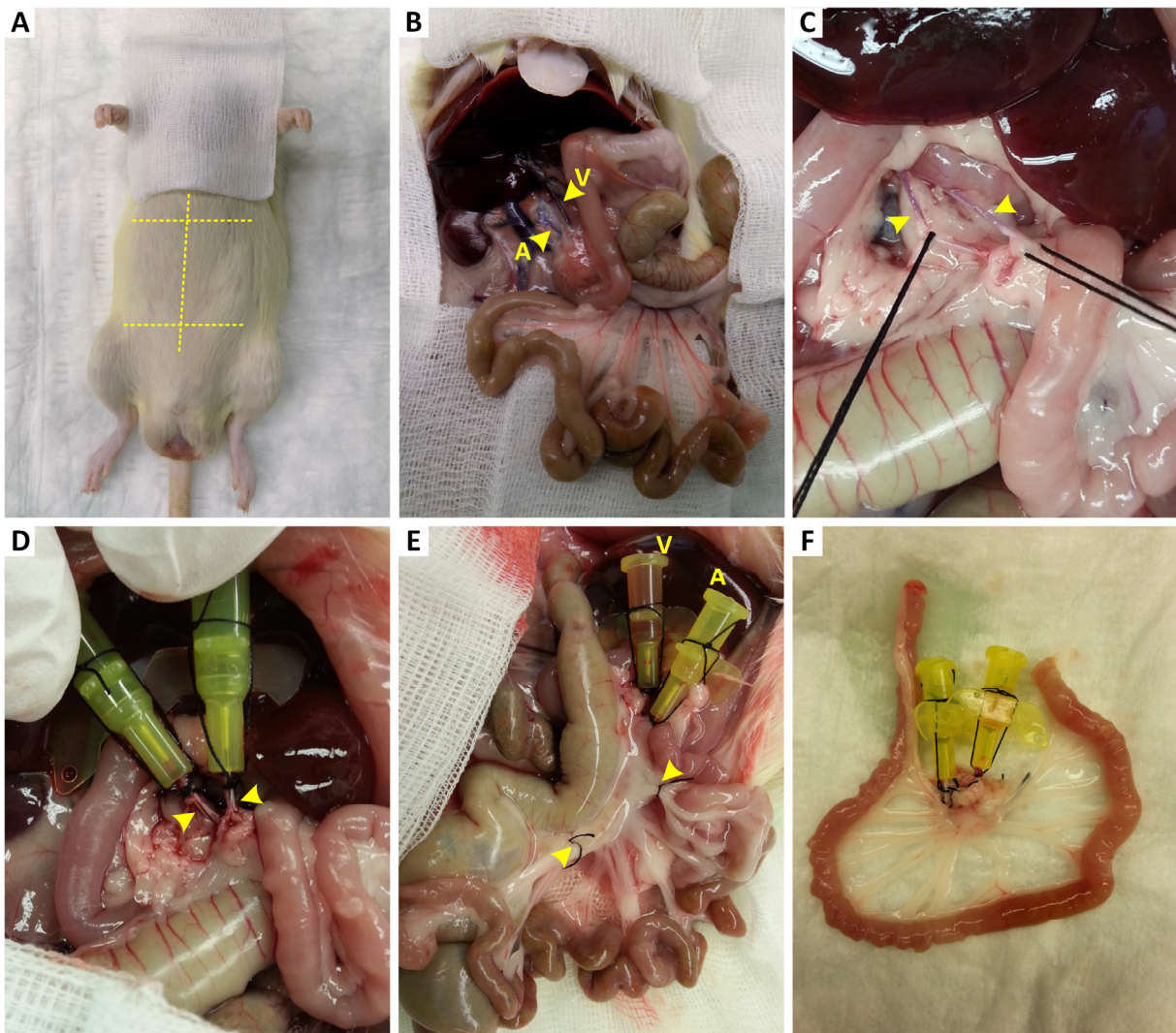


Figure 4. Cannulation and explantation of the mBioVaSc-TERM®.

A jejunal segment was explanted from rat intestine. (A) The abdominal cavity of an euthanized rat was opened with a median laparotomy and vertical relief cuts (represented by dotted lines). (B) The superior mesenteric artery (indicated by 'A') and the superior mesenteric vein (indicated by 'V') were dissected from surrounding connective tissue. (C) Surgical silk threads were prepared to immediately tie (D) the cannula inserted in the superior mesenteric artery and vein. (E) The vasculature was rinsed through the arterial cannula to wash out residual blood. A jejunal segment was determined, ligated (indicated by arrowheads) and (F) extracted. The lumen of the scaffold was subsequently cleaned from blood and feces.

4.1.2 Decellularization and structural characterization of the mBioVaSc-TERM®

For further processing of the explanted native tissue, the host cells were removed to avoid immune reactions when used for transplantation strategies¹²³. To reach this aim existing decellularization protocols were adopted and modified accordingly.

Based upon a literature survey referring to decellularization methods of intestinal structures, relevant protocols^{116,117}, mainly using sodium deoxycholate (SDC) and DNase for perfusion decellularization, were initially reproduced and subsequently optimized upon the devices in-house as well as the structural ECM preservation and cell removal.

Thereby, a detergent-based protocol for perfusion decellularization of both, the vascular system and the scaffold lumen, was established (Fig. 5A): the explanted scaffold was consecutively exposed to distilled water for 24 h at 4 °C for osmotic cell lysis, SDC for 4 h at RT for chemical lysis, and DNase solution for 3 h at 37 °C for enzymatic DNA cleavage. Multiple washing steps with PBS in between each step and after the procedure ensured the removal of residual cell-toxic detergents. Sterility of the resultant scaffold was attained by γ -irradiation.

Afterwards, histological staining and protein biochemical quantification of residual ECM components and DNA were performed for scaffold characterization to demonstrate the preservation of ECM components and architecture but removal of host cells.

The macroscopic appearance after decellularization indicated the removal of the cellular mass, leaving a transparent scaffold (Fig. 5B') if compared to the native intestine (Fig. 5B). Hematoxylin and eosin (H and E) staining of the decellularized scaffold revealed an overall ECM preservation and its structural integrity (Fig. 5C and C'). No remaining cells were observed compared to the native structure (Fig. 5C and C').

To highlight the removal of cells, residual DNA was investigated. Feulgen staining (Fig. 5D and D') qualitatively proved DNA clearance. Fluorometric and spectral photometric quantification confirmed that more than 80 % of the DNA was removed to a content of 25 ng DNA /mg dry weight of the tissue (Fig. 5H). To determine whether the remaining DNA was of high or low molecular weight, the fragment length was analyzed by gelelectrophoresis. Low molecular weight DNA might not be detrimental but could potentially implicate immunoproliferative effects on host lymphocytes¹²⁴, whereas high molecular weight DNA evokes immunogenic rejection upon transplantation¹²⁵.

The gelelectrophoretic analysis of the residual DNA proved the absence of high molecular DNA, indicating removal of cells, but cannot exclude the presence of low molecular fragments or nucleotides due to the detection limit below 100 base pairs (bp) (Fig. 5G). However, also gelelectrophoresis with concentrated DNA revealed only a faint smear indicating the residual DNA irrelevant.

Summarizing, with an average amount of less than 25 ng DNA/mg ECM dry weight and a fragment length below 100 bp of remaining DNA, the generated ECM scaffold potentially fulfills all necessary criteria for an intended medical application¹²⁶.

Despite an expected loss of overall matrix mass during decellularization, Masson's trichrome staining (Fig. 5E and E') confirmed the conservation of the major ECM components such as collagen as well as the removal of cell cytoplasm. Besides the structural components providing a framework for cells, functionality of the scaffold is determined by elastic fibers (Fig. 5F and F'). In addition to the histological evaluation of the scaffold, quantitative determination by protein biochemical analysis revealed the extent of matrix protein preservation. In contrast to DNA removal, the majority of the analyzed ECM proteins were retained. About 70 % of total collagen (Fig. 5I), the most abundant structural protein constituting the scaffolds connective tissue¹²⁷, was confirmed to be preserved after decellularization. Again, considering a loss of matrix, about 60 % of the elastic fibers was preserved compared to the native tissue (Fig. 5J). Furthermore, electron microscopic analysis (Fig. 5L-N) revealed the preservation of intact ECM structures, such as the basement membrane.

In summary, after explantation of a rat-derived intestinal segment, host cells were removed via an established perfusion decellularization protocol through the luminal as well as the vascular compartment. Structural ECM proteins could mostly be preserved, including the vascular basement membrane serving as structural and functional guide for neovascularization, resulting in an acellular scaffold of plain ECM that enabled its therapy-dependent cellular reconstruction while avoiding immune reactions upon transplantation¹²³.

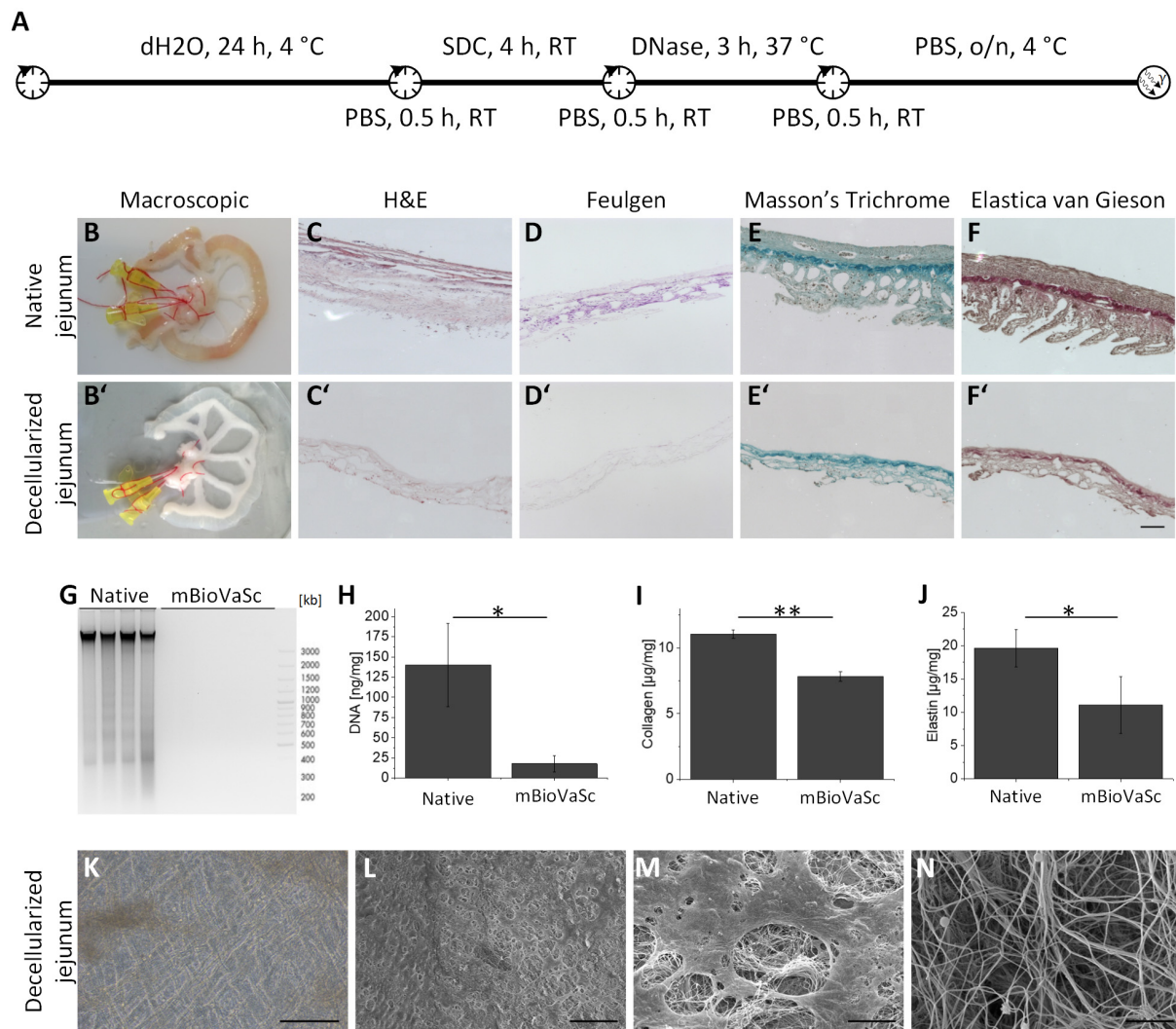


Figure 5. Qualitative and quantitative characterization of the acellular rat jejunal segment.

The cannulated intestinal segments were decellularized preserving ECM and vascular framework to serve as a cell-free scaffold supporting prevascularized cellular reconstruction. (A) Workflow of the decellularization protocol. (B+B') Representative macroscopic pictures of the scaffold. In contrast to (B) the native jejunal segment, (B') the decellularized scaffold appeared transparent. (C-F') Histological analysis of (C-F) the native rat jejunal segment in comparison to (C'-F') the decellularized mBioVaSc-TERM®: (C+C') Representative pictures of H&E staining. (D+D') Feulgen-stained samples depict DNA residues. (E+E') Masson's Trichrome staining representing residual collagen (turquoise), muscle fibers (dark red), as well as cell cytoplasm (pink) between the scaffold and native tissue. (F+F') Elastica vanGieson reaction eliciting elastic fibers within the matrix. (G) DNA fragment length separation via gelectrophoretic analysis. (H) Quantitative determination of the DNA amount in the native and decellularized tissue. (I+J) Quantification of the major ECM components: (I) Collagen and (J) Elastin before and after decellularization. (K-N) ECM network depicted by (K) light microscopy and (L-N) scanning electron microscopy (SEM). Scale bars: (C-F') 100 μm, (K) 1000 μm, (L) 50 μm, (M) 5 μm, (N) 1 μm. Error bars: mean ± SD; *, $p < 0.05$; **, $p < 0.01$; t-test. Copyrighted reprint¹²⁸; modified.

4.2 Revascularization capacity of the mBioVaSc-TERM®

After verifying the preservation of the ECM structure and biochemical components, the next aim was to analyze the integrity of the preserved vessel system and its capacity for reendothelialization.

4.2.1 Characterization of genetically modified endothelial cells

To investigate the preservation of the decellularized vessel system in the mBioVaSc-TERM®, the acellular vascular network was repopulated with human dermal microvascular endothelial cells (hdmEC).

Endothelial cells were isolated from human foreskin, separated from other cell types, and expanded according to an in-house established protocol. Furthermore, the isolated hdmECs were lentivirally transduced either with a green fluorescent protein (GFP) containing expression vector or with the DNA sequence for GFP clonally replaced for red fluorescent protein (RFP), to express either GFP or RFP, respectively. Thereby, non-invasive live imaging of the reendothelialized vascular structures was feasible. To ensure the endothelial character after genetic modification, the cells were subsequently characterized upon their growth kinetics, protein expression profile, and barrier formation capacity to assure vessel formation capability and functionality.

At first, characteristic marker genes of hdmECs that proof their cellular identity and functionality after genetic modification were analyzed quantitatively by FACS analysis. Figure 6A shows that 96.9 % of the examined cells expressed the platelet endothelial cell adhesion molecule (PECAM)-1 also known as cluster of differentiation (CD) 31. 97.6 % of the cells analyzed, expressed the membrane glycoprotein CD105. The angiopoietin receptor TIE2 was detected on 67.8 % of the cells. CD34, characteristic for capillary endothelial cells, was verified on 95.1 % of the hdmECs. VE cadherin was proven to be expressed on 98.7 %. CD146, the melanoma cell adhesion molecule (MCAM), was verified on 94.7 % of the hdmECs. Only vascular endothelial growth factor (VEGF)-receptor 2 could not be identified by FACS.

Besides the presence of functional EC surface proteins, the ability of the genetically modified hdmECs to form a functional tight endothelial barrier was investigated on a trans-well system, providing information about their functionality.

The proliferative potential of the genetically modified GFP- or RFP-tagged hdmECs was assessed performing a cell viability assay (Fig. 6B).

Further, functionality of the hdmECs to form a tight barrier was investigated by measuring the transendothelial electrical resistance (TEER) of the formed cell layer during a culture period of 35 d (Fig. 6C). With reaching confluence, the TEER value increased consistently until peaking at about $14 \Omega \cdot \text{cm}^2$, similar to the TEER value of hdmEC barriers described in literature¹²⁹.

Furthermore, fluorescein isothiocyanate (FITC)-coupled dextran was applied apically onto the cell layer to evaluate endothelial permeability. Fluorospectrometrical analysis quantified that after two weeks of culture only about 1 % of the FITC-coupled dextran passed the established endothelial barrier (Fig. 6D). Thereafter, the barrier integrity remained stable throughout the culture period of 35 d preventing most of the low molecular weight compound to pass the endothelial barrier.

Characterizing the genetically modified GFP-/RFP-tagged hdmECs, the cells exhibited endothelial markers specific for cell-cell junctions, cell-ECM adherence, blood vessel formation, and angiogenesis. Furthermore, confluent endothelial layers established functional barrier properties. Subsequently, both, the native hdmECs as well as the GFP- or RFP-tagged hdmECs were used to repopulate the vascular structures of the mBioVaSc-TERM® in upcoming experiments.

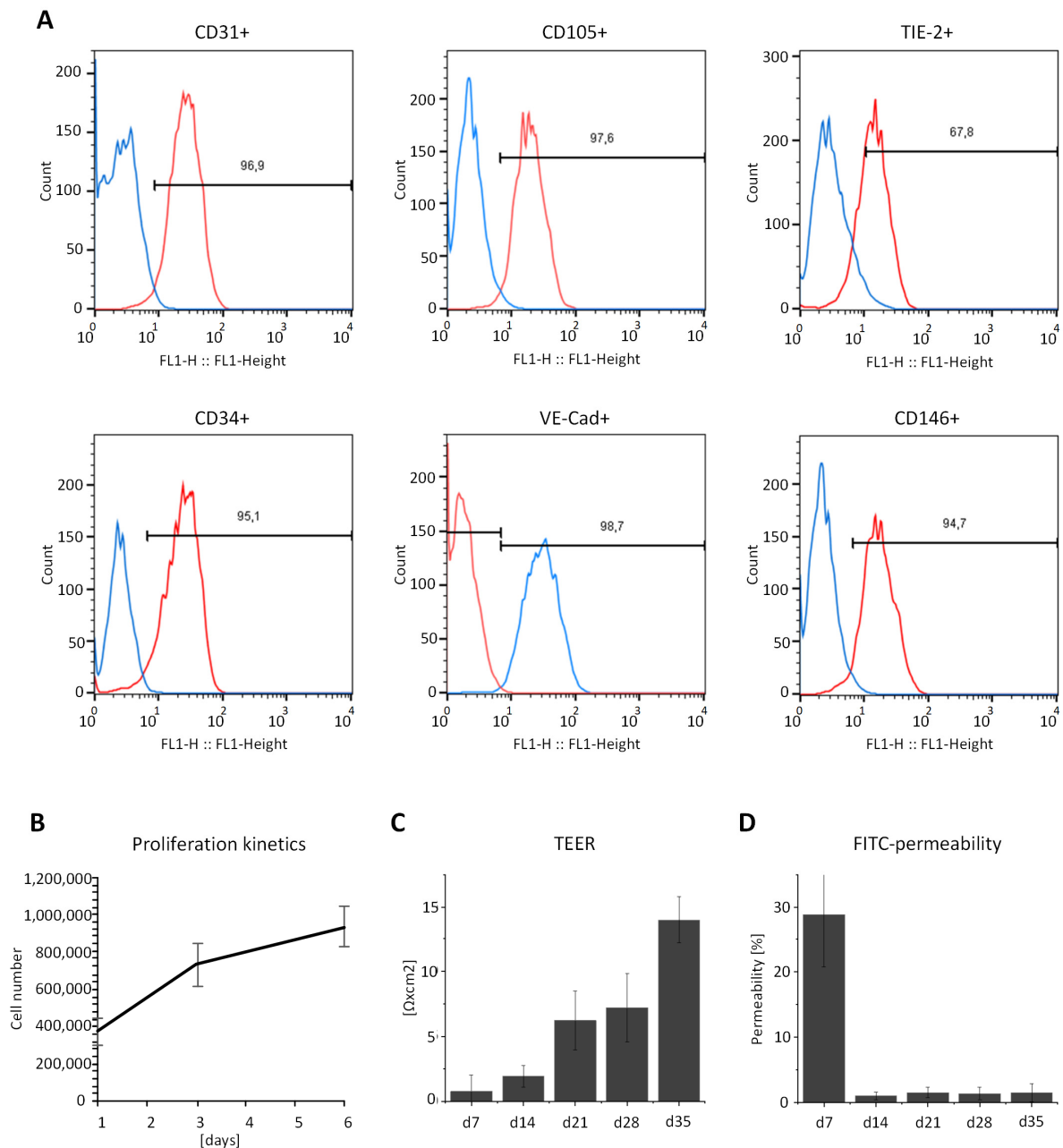


Figure 6. Endothelial cell characterization.

Primary human dermal microvascular and GFP/RFP-tagged hdmECs were analyzed upon cell type-specific properties. (A) FACS analysis revealed EC-characteristic markers for angiogenesis (CD31 and CD105), blood vessel formation (TIE2), and cell adhesion (VE-Cad, CD34, and CD146). (B) CellTiter Glo analysis indicated the proliferative potential of the employed ECs. Proving endothelial barrier properties of a confluent EC layer, (C) TEER measurement demonstrated increasing tightness and resistance over time and (D) constantly low permeability for macromolecules was shown as demonstrated for FITC-dextran. Error bars: mean \pm SD; t-test.

4.2.2 Revascularization capacity of ECs to repopulate the mBioVaSc-TERM®

After identification of their functional endothelial character, the isolated primary hdmECs and modified GFP-/RFP-tagged hdmECs, were infused into and dispersed throughout the whole preserved vascular tree of the decellularized scaffold (Fig. 7A and B). After static incubation to enable attachment to the basement membrane, the reendothelialized mBioVaSc-TERM® was connected to a custom-made perfusion bioreactor system (Fig. 7C) mimicking physiological vascular perfusion. The thereby applied shear stress on the ECs is critical for vessel maturation^{130,131}.

To facilitate pulsatile perfusion culture, the custom-made bioreactor technology for the BioVaSc-TERM®, consisting of a glass reactor connected to media reservoirs via a roller pump installed inside an incubator was adapted for the use of the mBioVaSc-TERM® (Fig. 7D). To maintain a physiological pressure profile at all times throughout the culture period, the applied pressure was sensor-controlled and automatically regulated by the implementation of an automated computer-aided feedback mechanism regulating the pumping device. Both, arterial and venous pressure profiles were individually monitored representing their physiological conditions (Fig. 7D).

For the evaluation of vascular leakage, the hdmEC-endothelialized mBioVaSc-TERM® was perfused with phenol red in PBS and with blood. Infusion of phenol red through the arterial pedicle resulted in unobstructed leakage of the fluid through the vascular barrier (Fig. 7E). In contrast, when perfusing the vessels with heparinized blood (Fig. 7F) no leakage was observed but the infused blood passed through the arteriovenous loop of the mBioVaSc-TERM® and left through the venous cannula. However, only the hemoglobin of the red blood cells was macroscopically visible, stating that erythrocytes could not pass the endothelial barrier.

To examine the repopulation capacity of the vascular system and the lining of the arterial and venous vascular networks as well as their junctions, the arterial and venous pedicles were repopulated with either GFP- or RFP-expressing hdmECs, respectively (Fig. 7G). By means of fluorescently tagged cells, it was feasible to monitor the repopulation of the vascular system by live imaging techniques to discriminate the arterial and venous vessels and capillaries of the whole scaffold. Thereby, thorough revascularization could be investigated by non-invasive and non-destructive methods.

Moreover, the capacity of the hdmECs to form a functional tight vascular barrier within the vessel structure of a 3D scaffold as well as the transition from arterial to venous capillaries was proven.

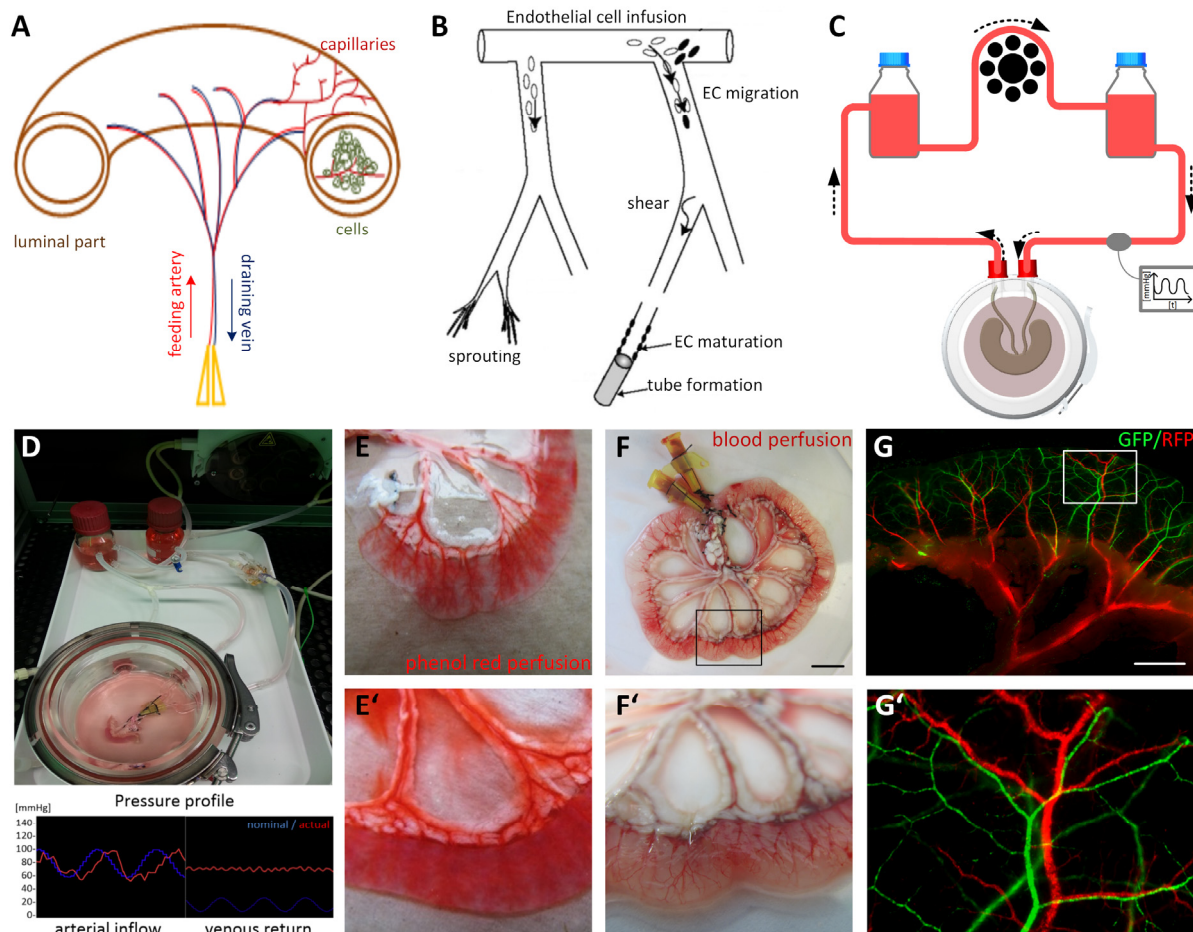


Figure 7. mBioVaSc-TERM® revascularization by vascular perfusion.

The vascular network of the intestinal segment was preserved by conservative perfusion decellularization, enabling the repopulation of the 3D vessel structures with hdmECs via infusion directly into the vascular structures to generate a revascularized scaffold. (A) Cannulas facilitated a direct access to the vascular tree. (B) Static incubation after distribution throughout the whole vascular system facilitated cellular adherence initiating the repopulation. (C) Schematic representation and (D) live setup of the culture setup within a custom-made bioreactor system. An integrated pumping device enabled nutrient supply by physiological pulsatile perfusion and additionally exerting shear stress onto the ECs within the vessels promoting barrier maturation. Continuous monitoring of physiological parameters, such as simulated blood pressure, temperature, and oxygenation enabled constant computer-aided regulation of culture conditions as well as a physiological pressure profile. (E) Phenol red perfusion of the mBioVaSc-TERM®, representing cell culture media perfusion. (F) Culturing the mBioVaSc-TERM® with heparinized blood showed no signs of leakage and allowed a macroscopic identification of the vascular system. (G) Live imaging of GFP- and RFP-tagged hdmECs infused through the arterial and venous pedicle of the mBioVaSc-TERM®, respectively. Scale bars: (E-F) 10 mm, (G) 3 mm. (B) Copyrighted reprint¹³²; modified. (A, D-G) Copyrighted reprint¹²⁸, modified.

Cytocompatibility of the scaffold was assessed by repopulation with hdmECs. Cellular metabolic activity and vitality of hdmECs cultured inside the 3D vascular environment was confirmed by MTT and FDA/PI staining, respectively (Fig. 8A and D). By physiological perfusion culture, the cells were maintained viable within the vascular network lining the inherent vessels throughout seven weeks of *in vitro* cultivation.

Examining whether the cultured hdmECs retained their endothelial character in a 3D vessel environment, the presence of functional endothelial markers was verified. The hdmECs inside the vascular structures were shown to be positive for CD31 (Fig. 8B and E) and vWF (Fig. 8C and F) by immunohistological stainings. However, based on the analysis of the whole mount stainings (Fig. 8E and F), highlighting the hdmECs populating the capillary structures from the top view, the revascularization appeared partially discontinuous, suggesting the capillaries to be either blocked or permeable via paracellular exchange¹³³.

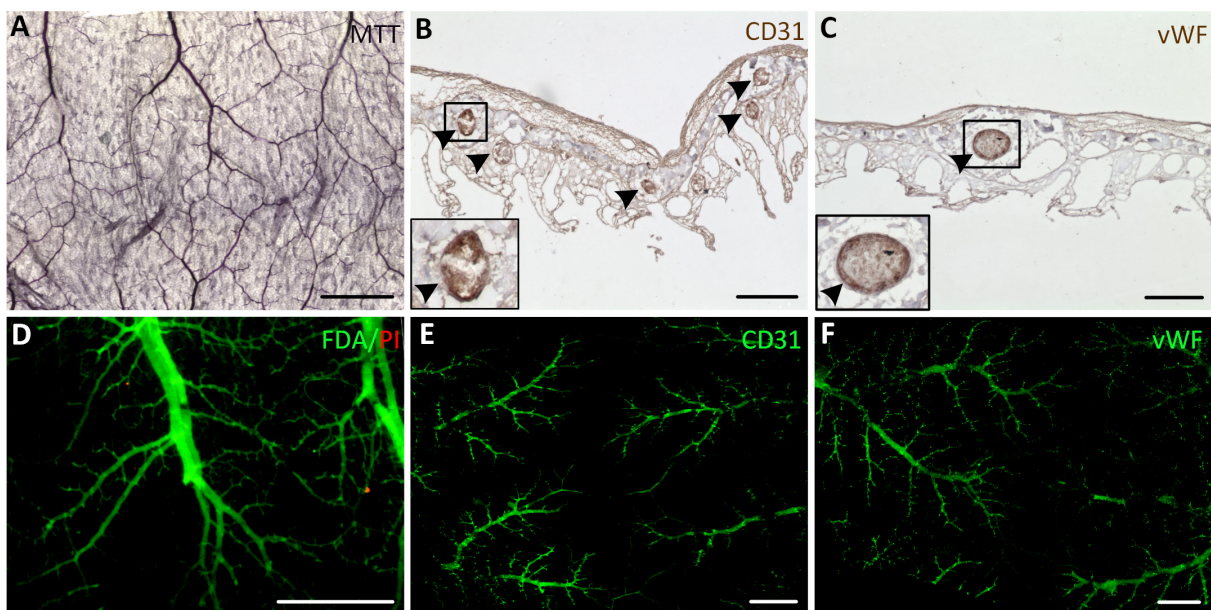


Figure 8. Revascularization of the mBioVaSc-TERM®.

Characterization of hdmECs populating the vascular system of the mBioVaSc-TERM® after maturation in a perfusion bioreactor system. (A) Metabolic activity of the ECs populating the branching capillary network of the mBioVaSc-TERM® by a colorimetric MTT assay. Immunohistological detection of the endothelial marker (B) CD31 and (C) vWF in capillary structures in cross sections of the luminal part of the revascularized mBioVaSc-TERM® (highlighted by arrowheads). (D) Life-dead staining differentiating viable (FDA) and apoptotic/necrotic (PI) ECs. Top view on a whole mount immunofluorescence (IF) staining of the EC-marker (E) CD31 and (F) vWF on the inner luminal surface. Scale bars: (A, D, E, F) 1 mm, (B,C) 200 μ m. Copyrighted reprint¹²⁸; modified.

In summary, hdmECs used for repopulation of the whole vascular network of the mBioVaSc-TERM® were demonstrated to be viable and vital, and to display EC-specific characteristics after infusion and culture within the scaffold during long-term culture. Furthermore, the originally arterial and venous vascular structures could be discriminated within the scaffold by infusion of genetically modified GFP- or RFP-expressing hdmECs through the respective cannulas. The integrity of the vascular network forming a tight barrier in the afferent feeding and efferent draining vessels and its arteriovenous loop was demonstrated by the return of blood through the venous pedicle of the scaffold after arterial infusion. Macroscopically, the blood was clearly visible inside the vasculature, while phenol red leaked out, indicating vascular tightness but permeability for fluids and low molecular weight compounds.

4.2.3 Demonstrating vascular barrier integrity by perfusion analysis

Continuous perfusion through an arteriovenous loop is strongly dependent on an intact EC barrier that is completely removed in decellularized tissues and usually hardly accomplished to be reestablished thoroughly. Therefore, the volume returned from the efferent vessel of the scaffold, referred to as the venous return, was determined after infusion through the arterial vessel.

Already after explantation of the intestinal segment from the donor animal, the decrease in venous return by 30 % was highly significant (Fig. 9; *ex vivo* - blood), presumably due to cutting open vessels upon extraction and altered surrounding tissue pressure onto the vasculature. Perfusion of the scaffold *ex vivo* with PBS instead of blood (Fig. 9; *ex vivo* - PBS) resulted in a significantly declined venous return. Presumably due to missing plasma proteins not exhibiting colloid osmotic pressure thereby reducing fluid extrusion⁶⁶ in the PBS. Clearing the lumen off feces resulted in the infused fluid leaking through the capillary bed into the lumen, thereby further declining the volume passing through the venous cannula (Fig. 9; *ex vivo*, lumen cleared - PBS). Removing all cells and thus the endothelial barrier by decellularization resulted in immediate leakage and thereby a complete loss of the vascular circulation (Fig. 9; mBioVaSc w/o ECs - PBS). Also by infusion of whole blood into the acellular scaffold no perfusion was observed, but confirmed the entire disruption of the vessel integrity (Fig. 9; mBioVaSc w/o ECs - blood). However, when repopulated with hdmECs, the vascular integrity of the scaffold could partially be restored (Fig. 9;

mBioVaSc + ECs - PBS). Perfusing the reendothelialized mBioVaSc-TERM® with blood, the venous return was restored to 30 % of the native *in vivo* situation (Fig. 9; mBioVaSc + ECs - blood).

However, during *in vitro* culture, the perfusion with standard culture media hardly reestablished venous return due to lacking extracellular tissue pressure and no colloid osmotic gradient in between vessel lumen and extravascular space as indicated by Figure 9 (mBioVaSc + ECs - PBS).

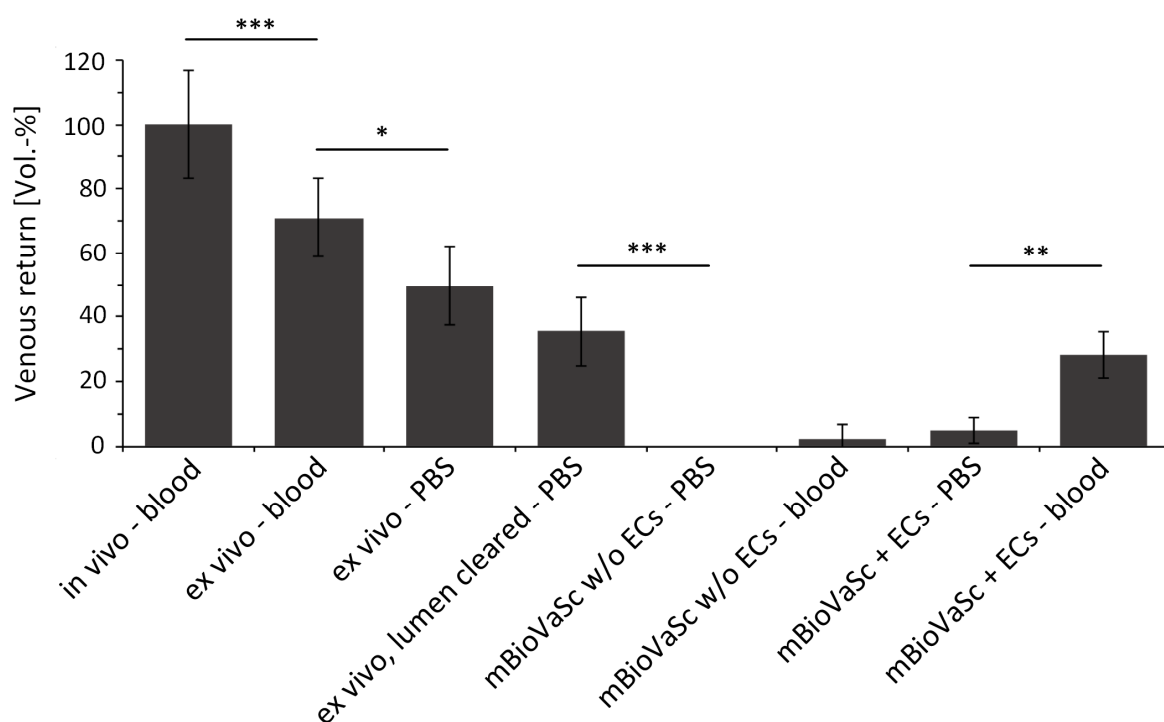


Figure 9. Venous return profile at different stages of mBioVaSc-TERM® establishment

The volume returned through the venous outlet upon arterial infusion through the mBioVaSc-TERM® during stages of scaffold preparation from *in vivo* to decellularization to reendothelialization. Showing a gradual decline of the returned solution when explanted until no return detectable through the venous pedicle when decellularized. After reendothelialization of the vascular system the venous return increased. Error bars: mean \pm SD; * $p < 0.05$, ** $p < 0.01$, *** $p < 0.001$; t-test. Copyrighted reprint¹²⁸; modified.

Beyond the examination of the endothelial character, cellular metabolic activity and vitality, as well as the capacity to form an intact barrier within the vessel structures of the mBioVaSc-TERM®, a functional metabolic cellular uptake was investigated within the

3D vessel environment. LDL uptake demonstrated receptor-mediated endocytosis by the hdmECs. Thereby, hdmEC functionality was demonstrated for cells populating the vascular network of the mBioVaSc-TERM® (Fig. 10A).

After verification of the reproducibility of the revascularization, the end-point examinations were replaced by non-destructive live imaging of the vascular structure.

Investigating the EC barrier integrity of the reendothelialized mBioVaSc-TERM®, the vascular network was perfused with fluorescently coupled dextran and albumin, solved either in PBS or blood, and microscopically evaluated by intravital microscopy live imaging. In detail, the scaffold was perfused with FITC-coupled dextran (~40 kDa) solved in PBS (Fig. 10B), FITC-coupled albumin (~66 kDa) in PBS (Fig. 10C), and FITC-coupled albumin solved in heparinized full blood (Fig. 10D) via the arterial pedicle. Vessels were perfused and monitored for 15 minutes repeatedly washing out and reinjecting with no sign of major leakage out of the vascular bed demonstrating vascular tightness and integrity. Remarkably, while perfusion with blood, the fluorescent particles could be individually detected (Fig. 10D). Thereby, the particles could be tracked following the arterial influx and a delayed efflux in the adjacent venous vessel. The perfusion of the particles inside the whole bloodstream through an intact arteriovenous loop could be assumed.

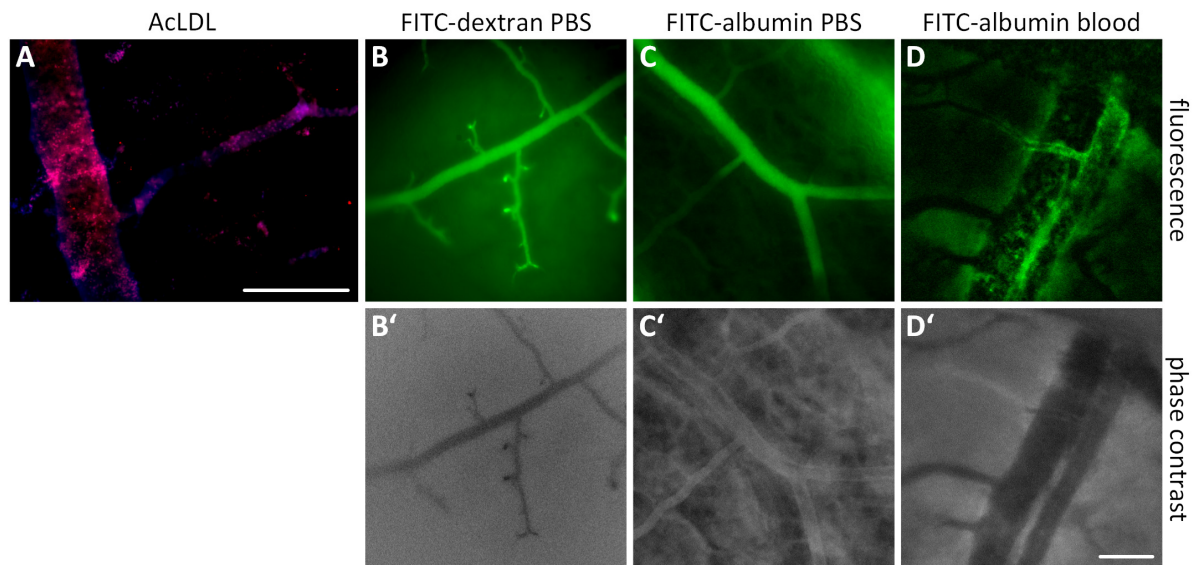


Figure 10. Vascular perfusion of the EC-repopulated mBioVaSc-TERM®.

Perfusion culture of the mBioVaSc-TERM® was performed in a bioreactor system. Vascular functionality and barrier integrity was visualized by live microscopy. (A) AcLDL uptake by hdmECs in the capillary bed of the mBioVaSc-TERM®. Intravital microscopy with (B) FITC-coupled dextran (40 kD), (C) FITC-albumin (66 kDa) resuspended in PBS and (D) FITC-albumin solved in blood perfusion. The perfusion of the fluorescent particles through the capillaries demonstrated no leakage after reendothelialization on a microscopic level under perfusion condition. (B'-D') Respective phase contrast images of the perfused luminal capillaries. Scale bars: (A-D') 100 μm . Copyrighted reprint¹²⁸; modified.

In summary, venous return demonstrated the perfusion of the arteriovenous circulation of the revascularized mBioVaSc-TERM®. Vessel integrity and vascular tightness was confirmed by intravital microscopy of the capillaries within the luminal wall. Besides maturation of hdmECs, thereby establishing a tight endothelial barrier, functional receptor-mediated endocytosis was proven as well as paracellular nutrient exchange in the capillary bed.

In conclusion, establishing a circulation with afferent feeding vessels, a capillary network, and efferent draining vessels by repopulation of the mBioVaSc-TERM® provided the basis for future nutrient supply of luminal cultured cells.

4.2.4 Analysis of the differentiation capacity of hPSC-derived mesothelial cells towards ECs, pericytes, and aSMA⁺ cells within the mBioVaSc-TERM®

In parallel to the generation of the mBioVaSc-TERM®, a cooperation partner developed a protocol to generate human pluripotent stem cell (hPSC)-derived mesothelial cells¹³⁴: multipotent vascular progenitors that can be further differentiated into ECs, pericytes, and smooth muscle cells. They were described to self-assemble to vessel-like structures and support vascularization¹³⁵ and tissue repair¹³⁶ *in vivo*.

Here, hPSCs differentiated towards the mesothelium lineage by Thomas Colunga (Dalton Lab, PI: Prof. Dr. Stephen Dalton, Center for Molecular Medicine, University of Georgia, Georgia, USA), were infused into the mBioVaSc-TERM® connected to the perfusion bioreactor. Within the 3D scaffold, the cells were further differentiated based on the protocol established by T. Colunga.

Whole mount analysis (Fig. 11A and B) of the vessels revealed vascular lining with all three differentiated cells types. Cross sections of different vessels with distinctive diameters demonstrated the cellular composition (Fig. 11C-D''). CD31-positive ECs were lining the inner vascular barrier of all vessels with neural/glial antigen (NG) 2-positive pericytes¹³⁷ in close proximity. In contrast to the ECs, pericytes were distributed only sparsely. Besides ECs and pericytes, capillaries were not enclosed by smooth muscle cells (SMCs). Larger vessels, however, were surrounded by thick layers of alpha-smooth muscle actin (aSMA)-positive cells.

Displaying the presence of all three vascular cell types differentiated from one progenitor, demonstrated the capacity of the hPSC-derived mesothelial cells and the established differentiation protocol to differentiate the cells from one progenitor lineage into three distinct lineages within a 3D *ex vivo* model. The mBioVaSc-TERM® with its inherent vascular network enables the further examination of cellular differentiation in an *in vivo*-like 3D environment resembling the native extracellular vascular architecture. Furthermore, with the mBioVaSc-TERM® connected to the bioreactor setup, further stimulation, such as shear stress by pulsatile perfusion mimicking a physiological *in vivo*-like condition, can be applied onto the cells and its influence on differentiation determined.

With a layer of α SMA-positive cells implemented within the vascular wall of larger vessels, SMC functionality was examined next upon vasoconstriction. As indicated in Figure 11C", larger diameter vessels depicted a thicker layer of α SMA⁺ cells, a segment of the feeding arterial vessel was dissected and mounted in a myograph. However, despite stimulation of the vascular segments with up to 10 mM carbachol (CCh) upon muscular contraction, no relevant increase in applied force was measured besides a baseline (Fig. 11E).

The functional analysis of myography in conjunction with the immunofluorescent staining suggested the incompleteness of the muscular sheet and thereby the inability to perform physiological muscular contraction.

Full vascularization towards densely populated and completely interconnected cellular conjunctions remained to be improved, primarily by enhancing seeding and culture conditions. Nevertheless, mesothelial cells appeared to represent a viable alternative cell source accounting for their potential to differentiate into ECs, pericytes and SMA⁺ cells in a 3D environment to generate functional vascular structures, applicable in TE and regenerative medicine.

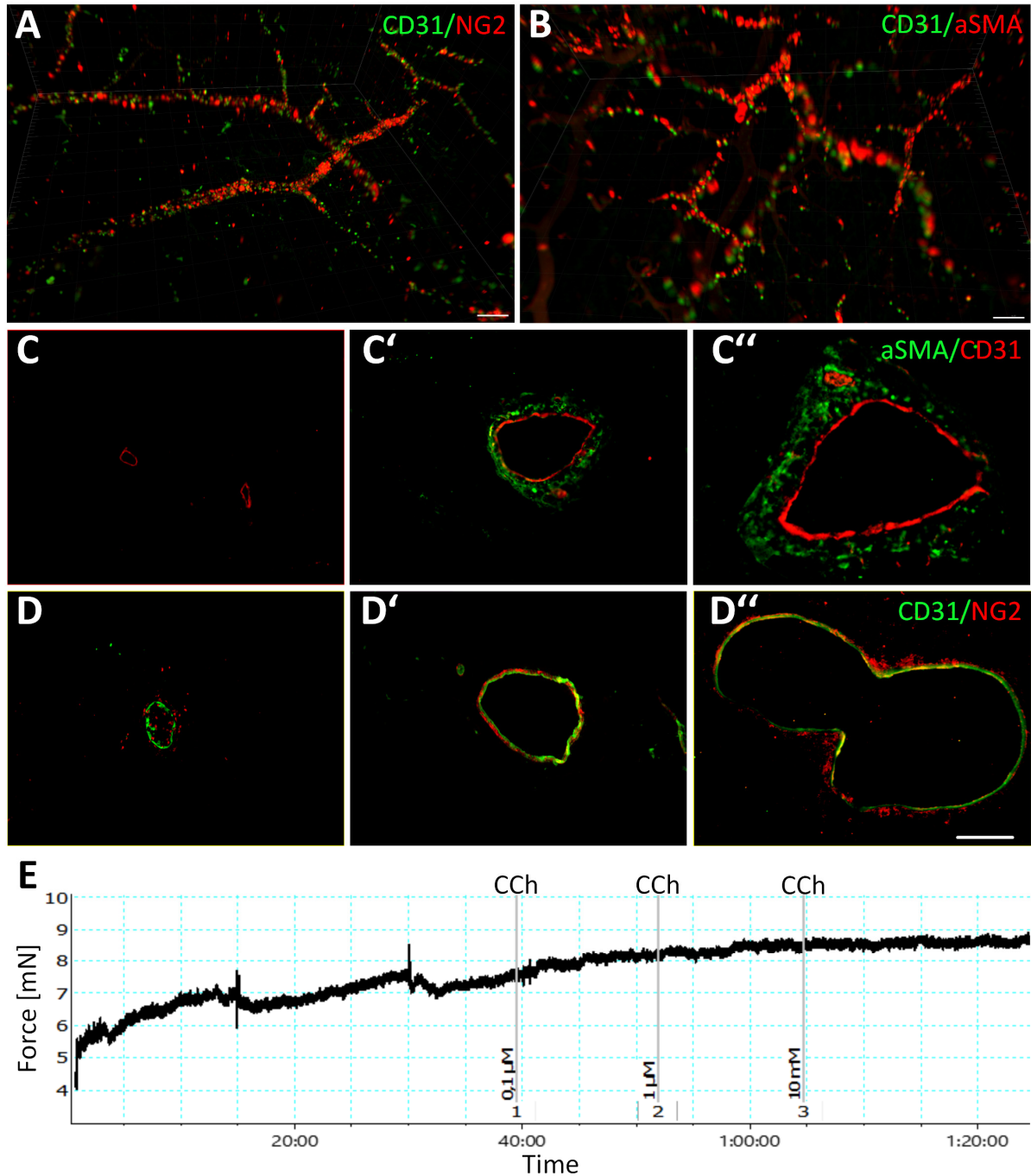


Figure 11. Composition of differentiated mesothelial cells within the mBioVaSc-TERM®.

Mesothelial cells were infused in the vascular structures of the mBioVaSc-TERM® and differentiated towards ECs, pericytes, and SMCs. The cellular character was determined by immunohistological staining against CD31, NG2, and aSMA, respectively. Vascular composition and cellular distribution was examined immunohistologically on (A, B) whole mounts of the vascular network and on (C-D'') cross sections of vessels of different diameter ranging from capillaries to large vessels. (E) Myographic assessment of force applied by muscle contraction of a circular vessel segment after equilibration and upon 0.1 μM , 1 μM , and 10 mM Carbachol (CCh) stimulation. Scale bars: 100 μm .

4.3. Biocompatibility of the mBioVaSc-TERM® for tissue development

After revascularization of the mBioVaSc-TERM® vessel system, co-cultures were established within the luminal compartment of the scaffold to further demonstrate biocompatibility and the capacity to generate functional tissue grafts in future. Implementation of diverse organ-specific cell types with distinct applications verified the capability of the vascular perfusion to maintain co-cultured cells nurtured and to prove the function as a suitable scaffold in TE.

4.3.1 Setup of co-culture conditions enabling the generation of tissue culture

Establishing consecutively a co-culture system of two or more different cell types to generate a functional tissue graft requests great demands on media composition providing critical cues for all employed cells.

At first, the, viability, vitality, and metabolic activity of cells co-cultured in the lumen of the scaffold was analyzed to be maintained throughout long-term culture, indicating biocompatibility of the mBioVaSc-TERM®. This was verified for each cell line used for co-culture as for each cell line an adapted media composition had to be established, confirming cell viability of all implemented cells.

Fibroblasts are the most common cells of connective tissue that are cultured in a basic, less-defined medium without the need of important growth factors like other cell types. They are often used in TE approaches, interacting with other cells and further playing an important role for ECM turnover¹³⁸. Therefore, these cells were used initially to demonstrate the combinability of different cell types with distinct media and supplementations for cell viability when co-cultured within the mBioVaSc-TERM®.

In a first step, the suitability of the mBioVaSc-TERM® for co-culture of hdmECs with Human dermal fibroblasts was analyzed. The fibroblasts were adapted to be cultured in EC culture medium simplifying the media composition applied to the co-culture. The fibroblasts were cultured either directly on the ECM of the inner luminal wall in close proximity to the embedded capillaries (Fig. 12A) or the fibroblasts were enclosed in a collagen gel cast inside the lumen (Fig. 12B). For both luminal culture methods, the cells were analyzed by MTT and FDA/PI demonstrating cellular vitality and viability throughout the whole luminal culture (Fig. 12C) as well as integrated in a collagen gel

(Fig. 12D). Further implemented cell lines for co-culture were analyzed with comparable results, proving luminal co-culture to be viable.

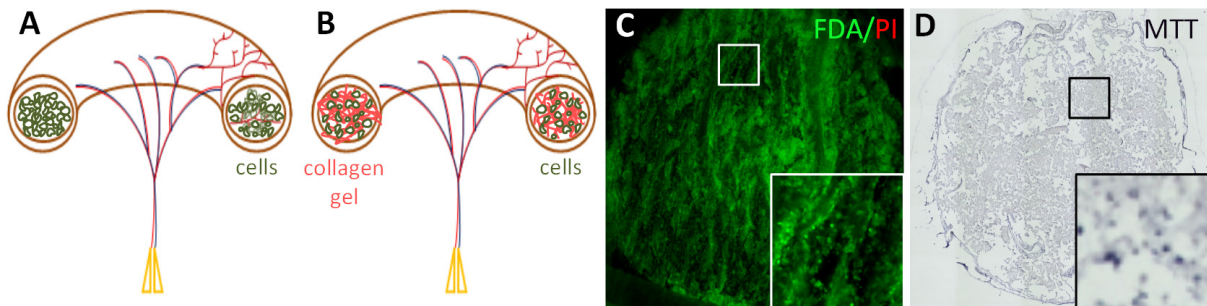


Figure 12. Establishment of intraluminal co-culture conditions.

Schematic representation of cells cultured inside the lumen of the mBioVaSc-TERM® either (A) directly on the luminal ECM adjacent to the capillaries or (B) embedded in a collagen hydrogel cast inside the luminal compartment. (C) Top view on intraluminal cultured cells stained with FDA/PI showing a confluent cell layer of viable cells. (D) MTT analysis on a cross section through the mBioVaSc-TERM® lumen showing metabolic activity of cells cultured in a collagen hydrogel inside the intestinal scaffold.

Culturing fibroblasts inside the luminal compartment, demonstrated the capacity of the revascularized mBioVaSc-TERM® to maintain co-cultures viable and vital over long-term culture. Despite the fact that fibroblasts can play a significant role in tissue culture¹³⁸, the aim was to establish the mBioVaSc-TERM® as a platform technology for complex multicellular tissue or organ culture. Therefore, the demand for optimized media supplementation and sustained nutrient supply was increased by incorporating metabolic highly demanding liver-like organoids inside the scaffold lumen, as the liver is a densely vascularized organ highly active in enzymatic conversion¹³⁹.

Spheroidal liver-like organoids were generated (Fig. 13A and B) as described¹¹⁸ and transferred into the lumen of the revascularized mBioVaSc-TERM®, placed in close proximity to the capillaries embedded in the luminal wall (Fig. 13C). Similar to commercially available perfusion systems¹¹⁸, the organoid culture period was significantly prolonged for up to one week when implemented in the mBioVaSc-TERM® placed in the perfusion bioreactor setup (Fig. 13D) instead of only for a maximum of three days in static conditions. During culture period, cellular viability of the organoid (Fig. 13E) was demonstrated by MTT analysis. Immunohistochemical analysis was performed to confirm of the hepatocyte character by anti-cytokeratin (CK) 18 staining (Fig. 13F).

Hepatocyte functionality was examined by enzymatic conversion of acetaminophen, dextrorphan, 6 β -OH-testosteron, and 4-OH-diclofenac by the cytochromes CYP1A2, CYP2D6, CYP3A4, and CYP2C9, respectively. For enzymatic conversion analysis, the organoids were explanted from the scaffold and exposed to the respective compound to determine the cytochrome conversion rates by high performance liquid chromatography (HPLC). HPLC analysis was performed by Prof. Dr. Angela Mally (Department of Toxicology, University of Würzburg, Würzburg, DE). Comparing the liver-like organoid co-cultures to confluent 2D hepatocyte cultures, enzymatic functionality was shown to remain only on a basal level (Fig. 13G). Pre-incubation with 3-methylcholanthrene and phenobarbital did not significantly increase the hepatic drug-metabolizing enzymatic conversion rate.

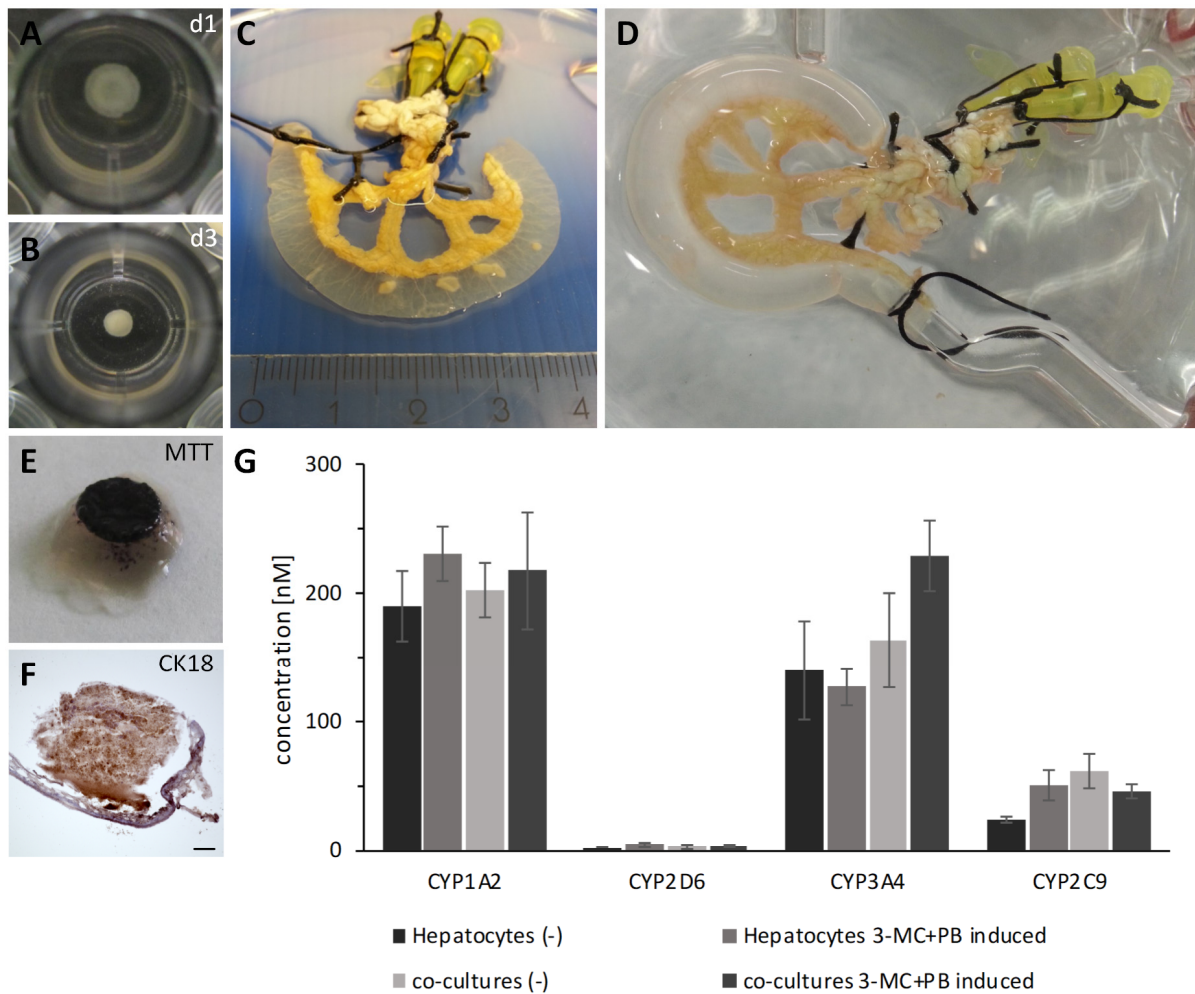


Figure 13. Liver-like organoid implementation in the reendothelialized mBioVaSc-TERM®.

(A+B) Liver-like organoids were generated by self-condensation of a confluent multicellular layer within three days. (C) To sustain the high metabolic need of the organoids, they were implemented in the luminal compartment of the revascularized mBioVaSc-TERM® and (D) connected to the bioreactor setup for perfusion culture. (E) MTT analysis confirmed metabolic activity of the dense cell organoids. (F) Immunohistochemical staining against cytokeratin (CK) 18 on a cross section of a liver-like organoid within the scaffold lumen. (G) Enzymatic conversion demonstrating functionality of the hepatocytes within the co-culture and as mono-culture was demonstrated for liver-typical cytochromes. Scale bars: (F) 100 μ m. Error bars: mean \pm SD; t-test.

In summary, the mBioVaSc-TERM® was reendothelialized with hdmECs and subsequently used to maintain co-cultures within the luminal compartment viable, vital, and functional. Fibroblasts were populating the luminal matrix as cell layer or embedded in a hydrogel cast inside the lumen. Furthermore, dense multicellular organoids were co-cultured. The proof to maintain cells viable and vital inside the luminal part of the mBioVaSc-TERM®, supplied by the adjacent embedded hdmECs, was demonstrated and

basal functionality was maintained. However, ineffective induction of increased enzymatic metabolism revealed the necessity for further optimization of the culture and maturation conditions for the organoids cultured inside the scaffold.

4.3.2 Distribution of bioactive compounds throughout the vascular system

Co-culturing cells inside the luminal part of the scaffold with ECs was shown to be feasible, even with complex and demanding multicellular organoids maintained viable and functional. Beyond nutrient delivery to sustain vitality, the vasculature could also be utilized to distribute drugs secreted by cells cultured in the lumen of the scaffold.

In a pilot experiment, the capacity of the mBioVaSc-TERM® as a scaffold for cells that secrete signaling molecules, such as hormones, cytokines, and growth factors, was investigated.

To achieve this, cells secreting Activin A and Myostatin were generated. Both, Activin A and Myostatin were shown to negatively regulate skeletal muscle growth¹⁴⁰. The respective gene coding for Activin A and Myostatin was cloned into the multiple cloning site of the lentiviral expression vector pCDH-CMV-MCS-EF1-Puro and finally introduced into Chinese hamster ovary (CHO) cells by lentiviral transduction.

For the *in vitro* proof of drug secretion and distribution, the cells were implemented into the luminal compartment of the revascularized mBioVaSc-TERM®. Medium supernatant from all compartments of the bioreactor system, including the vessel compartment was analyzed by ELISA for protein secretion (Fig. 14A). Notably, despite the concentration of secreted protein appeared to be similar, the total amount was up to 200 % higher in the 3D perfusion culture than in static 2D cell culture. Mock transduced CHO cells did not secrete any detectable Activin A nor Myostatin.

The proof of biological activity of the secreted protein was critical for the functionality. Therefore, the inhibitory effect of Activin A and Myostatin on proliferation of responsive cells was utilized in a dose dependent manner¹²². The applied Activin A- and Myostatin-containing supernatant taken from 2D, reactor, and vessel compartment showed the same proliferation inhibitory effect in a dilution series in a bioassay for each protein: with increasing protein concentration administered, the lower cellular proliferation was examined (Fig. 14B).

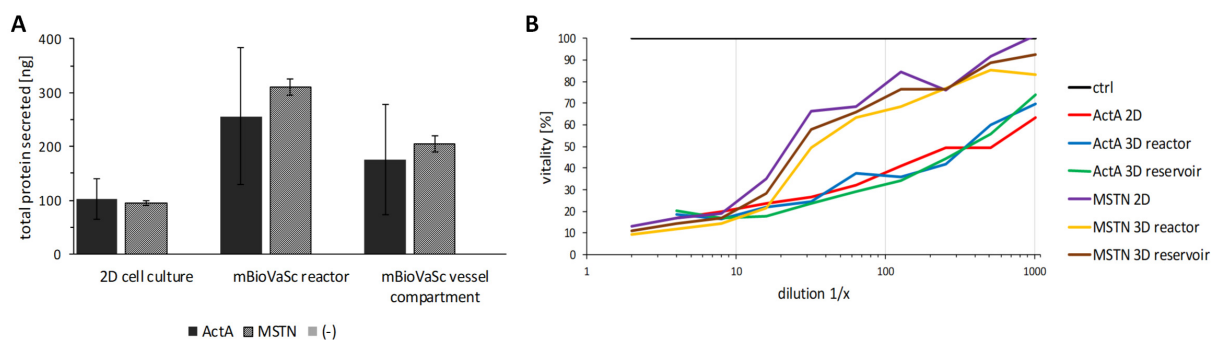


Figure 14. *In vitro* drug secretion from the mBioVaSc-TERM®.

CHO cells genetically modified for Activin A (Act A)/Myostatin (MSTN) secretion were cultured within the luminal compartment of the mBioVaSc-TERM®. (A) Secretion levels were determined from supernatant from standard 2D cell culture flask as well as from the bioreactor and the vascular compartment by ELISA quantification. (B) The secreted proteins were applied in a dose-dependent cell-based assay inhibiting cellular proliferation to determine its biological activity. Error bars: mean \pm SD; t-test. (A) Copyrighted reprint¹²⁸; modified.

Demonstrating maintained viability and sustained release of biologically active proteins from constitutively secreting cells as well as protein distribution throughout the bioreactor system, indicated the applicability of the mBioVaSc-TERM® as a drug delivery system. However, to also demonstrate the capacity of the scaffold to maintain complex native cell cluster naturally secreting proteins upon a highly regulated feedback mechanism viable and functional, pancreatic islets were co-cultured inside the luminal compartment of the revascularized mBioVaSc-TERM®.

Neonatal pig islet-like cell clusters (NICC) represent a cluster of different cell types composing a pancreatic islet isolated that can be utilized for cell therapy in type 1 diabetes patients¹⁴¹ due to their endocrine insulin secretory activity when matured.

NICCs were isolated by Dr. Elisabeth Kemter (Molecular Animal Breeding and Biotechnology, PI: Prof. Dr. Eckhard Wolf, LMU München, Munich, DE), co-cultured in the lumen of the revascularized mBioVaSc-TERM® (Fig. 15A), and investigated for their viability and functionality when cultured *in vitro*.

At first, the amount of NICCs to be cultured per area on the ECM and media supplementation for co-culture with hdmECs was determined. The final media composition consisted of a 1:1 volume mixture of basal Vasculife and Ham's F10 medium including each supplements in their doubled concentration to balance the dilution. Based on the beforehand established culture conditions the NICCs were cultured in the lumen of

the endothelialized mBioVaSc-TERM® accordingly. The metabolic activity of the cell clusters was analyzed by MTT for up to 20 days in culture (Fig. 15B). Noticeable thereby, the islets tended to cluster around the vascular structures. H&E staining on cross sections of the cultured organoids within the scaffold demonstrated that the cells lost their spheroidal shape and rather adhered as a cell layer to the luminal ECM (Fig. 15C). Further immunohistological examination displayed the presence of only few insulin- and glucagon-positive cells (Fig. 15D), presumably due to the not yet fully differentiated but immature neonatal character of the cells¹⁴².

To determine endocrine functionality of the cells, insulin secretion was measured by ELISA analysis of the supernatant. Therefore, the cells were pre-incubated in 3 mM glucose for 30 min before glucose stimulated insulin secretion incubating the islet containing scaffolds with 3, 5, and 10 mM glucose. Comparing the insulin release, there was no significant increase above the basal secretion level determined (Fig. 15E). Moreover, the insulin release declined over time, even though with an overall less steep decline by trend when incubated with 10 mM glucose, indicating insufficient stimulation when cultured under low glucose conditions.

Furthermore, the influence of additional co-cultures on NICC viability and insulin secretion was investigated infusing the NICCs along with ECs and mesenchymal stem cells (MSC) inside the luminal part of the mBioVaSc-TERM® cultured with 10 mM glucose supplementation. Performing an insulin ELISA with the respective supernatants, there was a slight yet insignificant increase in insulin release detected over time (Fig. 15F). This trend was demonstrated to be similar for all co-culture conditions. However, when NICCS were co-cultured with hdmECs or with MSCs and hdmECs, the overall insulin secretion was increased compared to NICCs only and NICCs with MSCs. However, no direct impact of ECs on insulin secretion is described in literature, hypothesizing an indirect effect of ECs on presumably increased vitality or sensitivity of the co-cultured NICCs.

In summary, even though the spheroidal shape was lost, the long-term viability and vitality of NICCs within the mBioVaSc-TERM® was demonstrated. In consideration of the immature character of the neonatal isolated islet-like cell clusters, a sustained basal insulin secretion was maintained when cultured with 10 mM glucose. Less glucose

supplementation indicated a decrease in insulin secretion or a decline in cell viability, whereas co-culture with ECs might increase insulin secretion by elevated NICC vitality.

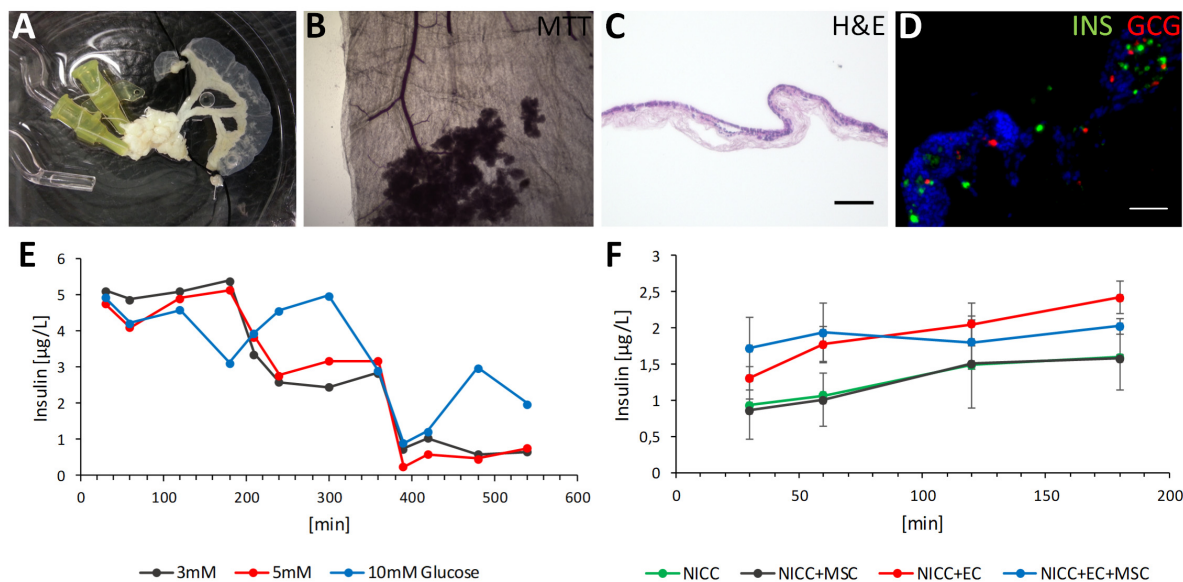


Figure 15. Vascularized endocrine pancreatic tissue generation with functional insulin secretion.

NICCs cultured in the reendothelialized mBioVaSc-TERM® to develop an endocrine tissue. (A) NICCs were cultured inside the luminal compartment in close proximity to the perfused endothelialized capillary network. (B) Colorimetric MTT assay determining metabolic activity revealed a distinct staining of the ECs inside the vascular structures and the islets clustering around vessels. (C) H&E overview stain on cross sections showed a cell monolayer residing on the luminal wall. (D) The presence of insulin- and glucagon-positive cells was demonstrated by immunofluorescence staining. Functional insulin secretion of NICCs was determined by insulin-ELISA (E) after stimulation with 3, 5, and 10 mM glucose as well as (F) after stimulation with 10 mM glucose examining the influence of co-cultures with ECs and MSCs on insulin secretion. Scale bars: (C) 100 µm, (D) 50 µm. Error bars: mean ± SD; t-test.

In summary, the proof of concept was demonstrated for the utilization of the mBioVaSc-TERM® as a platform to maintain co-cultures of complex cellular organoids viable and sustain functional enzymatic conversion as well as secretion of bioactive signaling molecules, however only on a basal level. Functional stimulation to proof increased endocrine secretion based on a feedback mechanism or enhanced enzyme activity still had to be demonstrated to further proof the applicability of the mBioVaSc-TERM® as a drug delivery system.

4.4 *In vivo* application demonstrating proof of concept in a small animal rat model

The vascular tightness was verified and co-cultures inside the lumen were demonstrated to be maintained viable as well as to support sustained biologically active protein secretion showing the applicability and versatility of the scaffold. Thereby, the *in vitro* proof of concept was demonstrated for the mBioVaSc-TERM® to be developed towards a platform technology for endocrine tissue graft generation.

Furthermore, the intended application of the mBioVaSc-TERM® was the translation into clinical practice as a drug delivery system or tissue replacement. As the *in vitro* results were promising, the scaffold was intended to be applied for *in vivo* proof of concept.

For *in vivo* experiments, at first, the mBioVaSc-TERM® was reendothelialized and cultured *in vitro* for up to 14 days until sufficient maturation of the vascular system to ensure its vascular tightness for an implantation in nude rats.

4.4.1 Anastomosis of the mBioVaSc-TERM® with the blood circulation

First transplantations were undertaken to elicit feasibility and to establish a reproducible routine of anastomosis of the arterial and venous vessel of the mBioVaSc-TERM® onto the respective vessels of the rat. All surgical procedures were conducted by Dr. Johannes Baur (Department of General, Visceral, Vascular and Pediatric Surgery, PI: Prof. Dr. C. Otto, University Hospital Würzburg, Würzburg, DE). The caudal part of the abdominal aorta as well as the caudal vena cava proved to be appropriate for the anastomosis with little vascular offset and a high blood flow. Furthermore, the abdominal area provided enough space for an un-compressed positioning at the gut area from where the scaffold was originally extracted.

The rats were kept under constant anesthesia while their abdominal wall was opened by a laparotomy (Fig. 16A) for subsequent implantation. The caudal part of the abdominal aorta as well as the caudal vena cava (Fig. 16B) were prepared for anastomosis of the preserved mesenteric arterial and venous vessels of the mBioVaSc-TERM®, respectively, by clearing and freeing them from connective tissue attached to the vasculature. After end-to-side anastomosis of both vessels to the rat's vasculature (Fig. 16C) the surgical clamps (i.e. serrefines) were removed. Once opened, an immediate blood inflow into the mBioVaSc-TERM® was clearly observable. The bloodstream entered the feeding

vessel flowing through the different branches, guiding the blood flow towards the lumen where it spread out into the vast branching capillaries (Fig. 16D). The constant blood perfusion through the whole vascularization of the scaffold as well as the venous return were proven by manual drainage of the vessels. For this, the blood perfused vessels of the mBioVaSc-TERM® were dissected to branch off the blood inflow with forceps and the retained blood was drained out with another pair of forceps. Subsequently, the branched off blood flow was released and a directed flow was observed from arterial to venous.

Thereby, the methodological technique to reliably ensure an unobstructed anastomosis and directed blood circulation throughout the arteriovenous network of the mBioVaSc-TERM® was verified.

After anastomosis, the blood perfusion through the vasculature of the mBioVaSc-TERM® connected to the animal's circulation was investigated in terms of vascular stability, perfusion, and leakage over a course of 30 minutes (n = 4). In all animals, no visible leakage was detected at any time point nor position, confirming the *in vitro* results when perfusing the scaffold with blood. Additionally performed manual drainages at different positions of the scaffold proved the continuous unidirectional blood flow in feeding arterial and draining venous vessels as well as in the luminal capillaries (Fig. 16D). Representative, in two of the animals, the vascular tightness of the mBioVaSc-TERM® and its perfusion connected to the animal's circulation was further confirmed by real-time intravascular fluorescence microscopy. For this, fluorescently labeled albumin was injected into the jugular vein of the anesthetized animal with the abdomen opened and the mBioVaSc-TERM® anastomosed to the animal's circulation as mentioned before. Thus, the injected tracer was distributed systemically throughout the animal's blood system and was also detected within the vasculature of the anastomosed mBioVaSc-TERM® within less than 1 minute and was distinctly visible thereafter. After cutting off the anastomosis to explant the scaffold (Fig. 16E), immunohistochemical analysis confirmed the presence of CD31-positive cells in all examined vascular compartments of the scaffolds, i.e. in the larger vessel in close proximity to the anastomosis (Fig. 16F), in the distal vascular branches leading towards the lumen (Fig. 16G) and in the luminal capillaries (Fig. 16H).

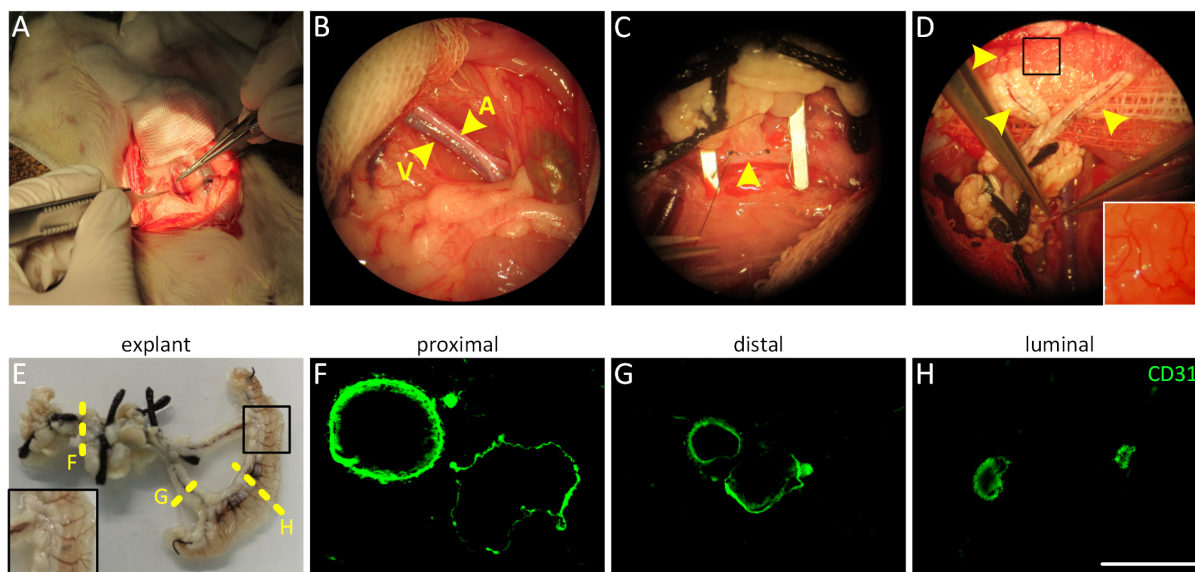


Figure 16. Anastomosis of the mBioVaSc-TERM® to a host vasculature.

The reendothelialized vessels of the mBioVaSc-TERM® were connected to the circulation of a rat. (A) The abdominal wall of the recipient rat was opened by a median laparotomy. (B) The infrarenal part of the aorta abdominalis and the caudal part of the vena cava (indicated by arrowheads) were dissected from surrounding connective tissue. (C) Side-to-end anastomosis of arterial and venous vessels of the mBioVaSc-TERM® with the abdominal vasculature of the animal (highlighted by arrowhead). (D) Blood inflow into the vascular system of the mBioVaSc-TERM® including the capillary network embedded in the luminal wall (highlighted by arrowheads and inset) after release of the clamps. (E) Macroscopic appearance of the implanted mBioVaSc-TERM®. The dotted lines indicated the cross sections for (F-H) immunohistochemical analysis of the endothelialized vessels proximal, distal, and luminal to the anastomosis by anti-CD31 staining. Scale bars: (F-H) 100 μm . Copyrighted reprint¹²⁸; modified.

4.4.2 Confirmation of *in vivo* biocompatibility after graft implantation

After the intraoperative confirmation of the feasibility and tightness of the established anastomosis and the reendothelialized mBioVaSc-TERM® vessels, the scaffold was analyzed upon its vascular integrity and biocompatibility in successive studies for up to 120 days.

For the implantation studies with the mBioVaSc-TERM® connected to the animal's circulation inside the abdomen, the scaffold was prepared and the anastomosis sutured as described above. After confirmation of the vascular tightness and exclusion of leakage, the mBioVaSc-TERM® remained in the abdominal cavity next to the animal's intestine and the abdominal wall was sutured. After a short recovery period, the rats showed no signs of pain nor of altered behavior aside from early evident dizziness due to the anesthetics. Throughout the various implantation periods of 3 ($n = 4$), 7 ($n = 3$),

30 days (n = 5), and 120 days (n=3) the animals were monitored daily. Body weight measurement and score upon general social, feeding and movement behavior observation determined continuation or termination of the animal experiment (Fig. 17). Due to the stress of the surgical intervention all animals were scored with '2'. Administration of the anti-inflammatory and pain-relieving drug carprofen resulted in decreased signs of post-operative suffering and therefore a scoring of '1' or '0' within the first three days after surgery and no increase thereafter, except for one animal, that's body posture was bent. For all animals, beside one (Fig. 17; marked with *), normal weight gain and no altered behavior was observed as compared to control animals during the whole study. The mBioVaSc-TERM® was tolerated by the rats without any notable complications, incompatibility or rejection except for one animal. The weight gain of this one rat stagnated and exhibited signs of acute abdominal pain after seven days postoperatively and therefore was euthanized (Fig. 17; marked with *). Post mortem examination revealed that a progressing ileus had occurred in this animal. Presumably, the incidence was likely not directly linked to the compatibility of the scaffold but a common intestinal obstruction. Besides the one euthanized animal, the others were examined as scheduled.

was clearly detectable throughout the scaffolds vasculature from the side of anastomosis to the lumen's capillary bed (Fig. 18A).

After 7 days *in vivo*, the implanted scaffold was surrounded by loose connective tissue, thereby loosely adherent to the tissues around the implant, but easily dissected thereof (Fig. 18B). Nevertheless, it appeared macroscopically intact with its vasculature filled with blood.

Explanting the mBioVaSc-TERM® 30 days post implantation, it was entirely encapsulated by connective tissue and thereby adherent to the surrounding abdominal wall. While after short-term experiments the graft surrounding connective tissue was only thin and loose, after 30 days the surrounding tissue was thicker and the scaffold compressed instead of spread (Fig. 18C). The naturally produced connective tissue had to be removed in order to identify the mBioVaSc-TERM® inside the abdomen. Despite the fibrotic encapsulation, the anastomosis was still intact (Fig. 18C; inset). However, macroscopically no visible blood flow was detected anymore, not even in the larger vessels.

Implanted for 120 days, the mBioVaSc-TERM® was indistinguishably integrated within the connective tissue and thereby unrecoverable for detailed examination (Fig. 18D).

Enveloping the graft into a surgical fleece to separate it from the surrounding tissue resulted in the degradation of the graft after 30 days of implantation (Fig. 18E). Therefore, the scaffold was not considered for further analysis.

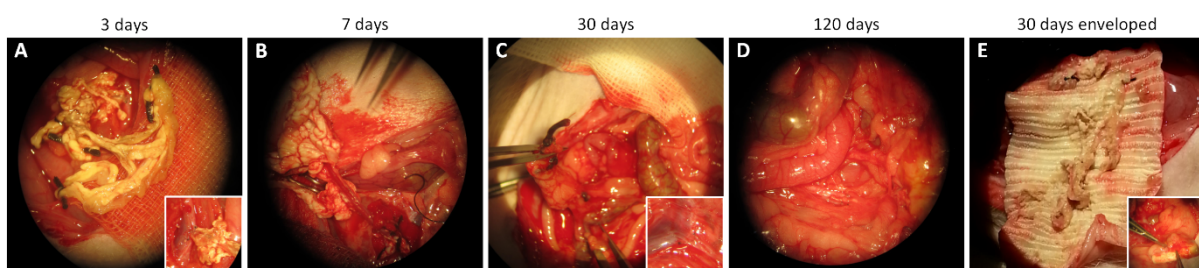


Figure 18. Macroscopic evaluation of the implanted mBioVaSc-TERM®.

After implantation period for (A) 3, (B) 7, (C) 30, and (D) 120 days the abdomen was opened by a laparotomy to recover the transplanted scaffold. Additionally, (E) the revascularized graft was enveloped with a surgical mesh and implanted for 30 days. The mBioVaSc-TERM® was evaluated macroscopically upon integrity, blood perfusion, and intact anastomosis.

4.4.4 Fading of functional markers on ECs and liver-like organoids

The vascularized scaffold was established in order to nourish and maintain engineered tissue *in vivo*. To proof that the mBioVaSc-TERM® was capable of being utilized for maintaining tissue culture *in vivo*, the vasculature was lined with hdmECs and spheroidal liver organoids were generated and implemented into the lumen of the vascularized scaffold.

Immunohistochemical analysis was performed to confirm that the vascular structures were lined with ECs and the luminal implemented liver-like organoids displayed cell type-specific markers as well as proliferative capabilities.

In particular, anti-CD31 staining was performed on cross sections as indicated by dotted lines on the macroscopic representation of the explanted mBioVaSc-TERM® after 3 days of implantation (Fig. 19A). On vessels proximal (Fig. 19B), distal (Fig. 19B'), and luminal (Fig. 19B'') to the anastomosis, CD31⁺ ECs were displayed to tightly line the vascular structures of different diameter. Additionally, integrated liver-like organoids in the *in vivo* study, were examined immunohistochemically for the cell characteristic markers of the three implemented organoid cell types. Hepatocytes were verified by CK18 (Fig. 19C), liver sinusoidal ECs by CD31 (Fig. 19D), and MSCs by CD90 (Fig. 19E). Furthermore, proliferative capabilities were examined by Ki67 (Fig. 19F) and apoptosis was observed by activated cleaved caspase 3 stain (Fig. 19G).

Similarly, after 7 days *in vivo*, the explanted scaffold was macroscopically mainly intact (Fig. 19H). The proximal (Fig. 19I) and distal vasculature (Fig. 19I') to the anastomosis depicted CD31-positive cells in all observed vessels. The CD31⁺ ECs lining capillaries inside the lumen of the scaffold could be clearly demonstrated (Fig. 19I''). However, some of the vascular structures appeared not be endothelialized completely suggesting a beginning vascular obliteration in retrospective consideration of the 30 day implantation results. The markers CK18 (Fig. 19J), CD31 (Fig. 19K), and CD90 (Fig. 19L) for the liver-like organoids were demonstrated as well as Ki67 (Fig. 19M) and activated cleaved caspase 3 (Fig. 19N). However, the detected signal for caspase 3 was increased whereas Ki67 was decreased compared to the 3 days implant. Furthermore, the structural integrity of the organoid appeared fragmented.

The progressive deterioration of the microscopically revealed structures proceeded over a time period for up to 30 days. Macroscopically, the original structure of the mBioVaSc-TERM® was not recovered after explantation (Fig. 19O). Immunohistochemical analysis revealed a fading of the endothelial barrier in the larger proximal (Fig. 19P) and distal (Fig. 19P') vessels and only a scattered CD31⁺ EC detection in the luminal capillaries (Fig. 19P''). The fate of the implemented liver organoids matched the EC-examination of the vascular structures of the implanted mBioVaSc-TERM® in terms of successive deterioration. Similar to the fading EC markers, a progressive structural dispersion of the implemented organoids and decreased signal intensity was observed on CK18 (Fig. 19Q), CD31 (Fig. 19R), and CD90 (Fig. 19S) staining. Equivalently, Ki67 (Fig. 19T) also decreased further, whereas activated cleaved caspase 3 (Fig. 19U) was further increased.

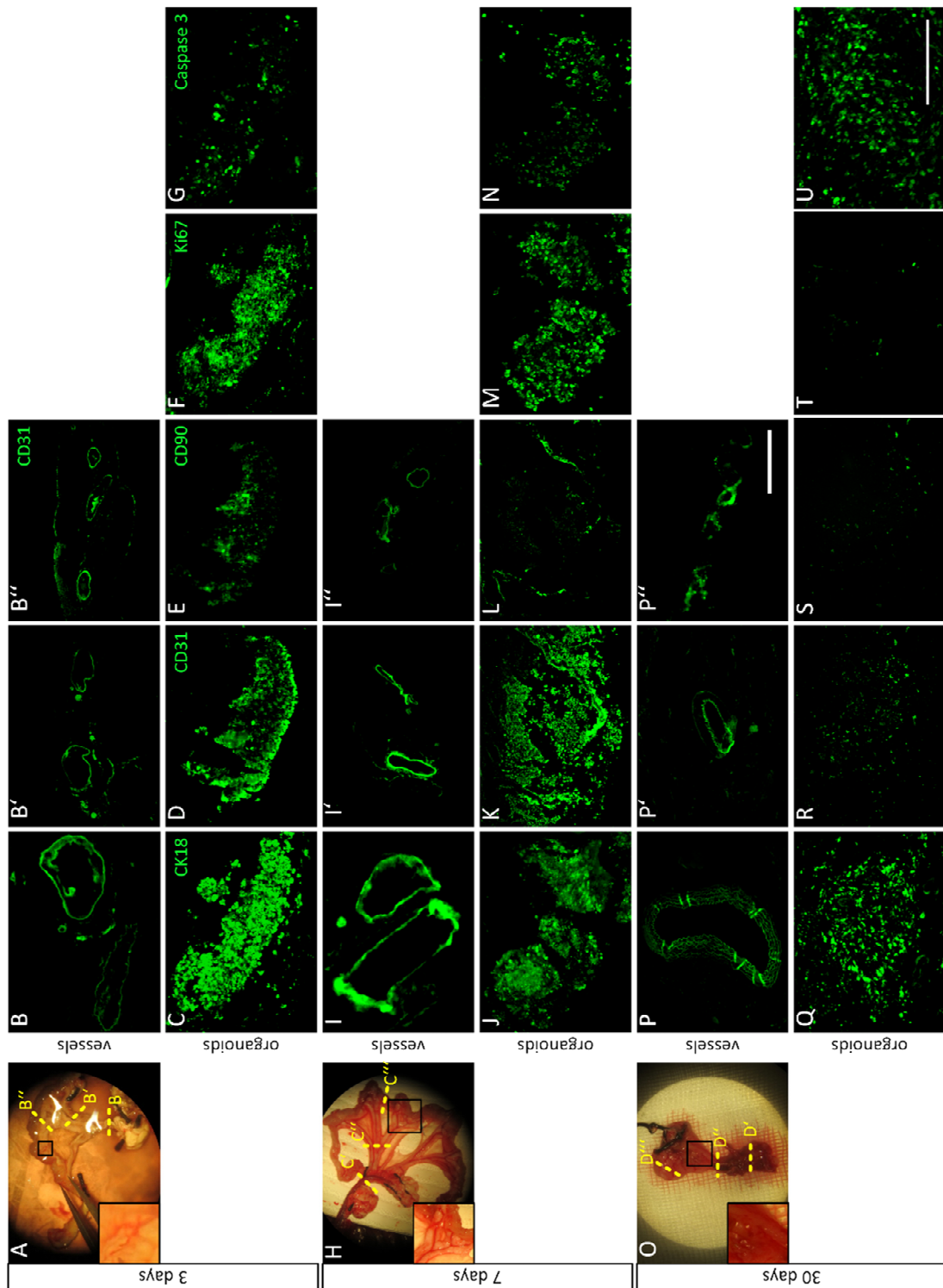


Figure 19. Graft explantation and immunohistological examination.

Characterization of the mBioVaSc-TERM® upon (A, H, O) macroscopic appearance and (B'-U) immunohistochemical analysis after implantation for (A-G) 3, (H-N) 7, and (O-U) 30 days. The insets show a magnification of the blood-perfused vascular tree. The dashed lines indicate the cross sections for staining against CD31: (B, I, P) proximal to the anastomosis, (B', I', P') on distal parts of the vasculature, and (B'', I'', P'') through the lumen. Liver-like organoids were implemented in the luminal compartment, confirmed by staining against: (C, J, Q) CK18, (D, K, R) CD31, and (E, L, S) CD90 for hepatocytes, endothelial cells, and mesenchymal stem cells, respectively. Highlighting proliferative cells by (F, M, T) Ki67 staining as well as apoptosis by (G, N, U) activated cleaved Caspase3. Scale bars: 100 μ m. Copyrighted reprint¹²⁸; modified.

In conclusion, for the mBioVaSc-TERM® the *in vivo* proof of concept for the feasibility of transplantation and short term implantation was demonstrated. The anastomosis and vasculature of the scaffold prove to be tight when connected to the animal's circulation and perfused with the host's blood. However, cell- and apoptosis-specific marker analysis during long-term implantation revealed fading vascular and organoid integrity.

Despite the given drawbacks after long term implantation, the impressive *in vitro* as well as the promising short term *in vivo* results depicted first steps for the mBioVaSc-TERM® towards a platform technology to generate implantable vascularized (endocrine) tissues that can be anastomosed to the host blood circulation for an immediate blood supply. Yet, long term *in vivo* stability and persistence of the scaffold have to be improved.

5. DISCUSSION

With increasing life expectancy in conjunction with the prevalence of risk factors such as diabetes, high blood pressure, obesity, smoking, environmental pollution etc. the amount of acute and chronic organ failures ascends¹⁴³. Organ impairments severely deteriorate quality of life and social status by negatively impacting or impeding daily activity, physical and psychological performance, and employment. A wide range of metabolic dysfunctions can be pharmaceutically compensated but the only definitive treatment is organ transplantation. Nevertheless, the availability of donor organs is limited¹⁴⁴. Hence, there is an increasing demand for improved tissue regeneration or bio-engineered tissue substitutes with clinical relevance being biocompatible, non-immunogenic, non-thrombogenic, but biologically functional. While recent advances in TE succeeded in the generation of flat 2D or hollow tissues^{145,146}, even towards clinical application^{76,147}, functional tissue engineering of complex solid organs is still unmet due to the lack of whole tissue nutrition. Nevertheless, progression towards whole organ generation is being made in small animal models by whole organ decellularization and recellularization of complex organs such as liver⁴⁶, lung^{187,47}, heart¹⁴⁸, kidney⁵⁷, and limbs⁵⁹. However, adequate vascularization to meet the demand for nutrient supply of the generated organ is the most critical issue that has not yet been solved to maintain the tissue viable. In this regard, tissue decellularization and recellularization appears most promising but is still in its infancy¹⁴⁹. For this reason, a consecutive built up of functional organ tissue seemed consequential, generating a vascularized matrix as framework for subsequent tissue establishment and maturation.

Resulting thereof, aim of this thesis was to purge a rat intestinal segment from host cells to serve as an acellular platform to reconstruct a transplantable vascularized tissue, depending on the demand of the therapeutic intention. This approach met the principles of TE²⁷ and RM^{28,29} laying the base for the generation of an advanced therapy medicinal product (ATMP). This technology might be utilized in future to replace and functionally restore impaired tissue, or to function as a drug delivery system to consistently assure the release of need-based pharmacologically active components *in vivo*.

With the BioVAsc-TERM®, Prof. Heike Walles already established of a vascularized platform technology for tissue engineering indicating the capacity for translating basic

research into clinical application¹¹³. Ongoing research continuously extends the applicability of the BioVaSc-TERM® and its related SIS onto the generation of further tissues and disease models such as skin¹⁵⁰, meniscus¹⁵¹, intestinal¹⁵², and various tumor models¹⁵³⁻¹⁵⁵. However, although the size of the porcine-derived scaffold enables the preclinical application in large animal models to anastomose the vascular tree of the BioVaSc-TERM® without mismatch, the application in small animal models is excluded due to its size. Nevertheless, preclinical studies in small animal models are preferential to large animal models for initial proof of concept¹⁵⁶. Furthermore, its size requires a vast amount of cells for recellularization, resulting in enormous effort, cost, and time for basic research. Therefore, technology transfer and miniaturization of the BioVaSc-TERM® as a platform technology is necessary to enable transplantation in small animal models for proof of concept studies.

5.1 Identification of a suitable tissue for miniaturization of the BioVaSc-TERM®

The advantages of the BioVaSc-TERM® were the versatility to reconstruct a wide range of tissues on a collagenous scaffold embedding a vascular network. After *in vitro* maturation in a perfusion bioreactor system applying tissue-specific stimulation, the established graft could then immediately be anastomosed to a patient's blood circulation to mediate sustained *in vivo* survivability. The underlying reason allowing immediate anastomosis and vascular blood supply was the preservation and utilization of the innate vascularization of the scaffold's 3D ECM structure. For miniaturization purpose, those properties had to be necessarily reflected.

Regarding scaffold size, the dimensions were considered to be as small as possible requiring only a minimum amount of cells for repopulation, enabling proof of concept studies in small animal models, and minimal invasive implantations in patients. Nevertheless, a sufficient amount of functional cells had to be implemented to assure a functional physiologic therapeutic effect. Furthermore, a vascular in- and outlet had to be feasible to be anastomosed without vascular offset to enable perfusion and prevent leakage or rupture.

A lot of synthetic scaffolds are biocompatible, highly reproducible in their preparation, and even their manufacturing can be automated for a large part¹⁵⁷. However, it is

technically not yet feasible to suffice the requirements mimicking a natural vascularization including one afferent and one efferent vessel interconnected by a dense capillary bed embedded in a 3D ECM meshwork.

Therefore, the natural jejunal segment indicated ideal properties as a biologically vascularized scaffold establishing a platform technology comprising a tubular collagen-based ECM with an embedded vascular network. Hence, for down scaling of the porcine-derived BioVaSc-TERM®, a naturally occurring ECM homologue from a small animal model had to be identified facilitating scaffold explantation, decellularization, and subsequent tissue graft reconstruction. The most important part thereby was the feasibility of the explantation while preserving the vascular structures for further processing.

The most prevalent small animal models employed for research, being mouse and rat, were considered first for evaluation of the feasibility of vascular cannulation and retention.

At first consideration, the mouse model was empirically assessed for miniaturization of a biologically vascularized scaffold due to its small size, prevalent usage, and low cost. Mouse whole organ decellularization via cannulation and partial recellularization was shown previously for heart¹⁵⁸ and lung^{159,160}. However, in the described studies, the cannulation was achieved via the heart. The vessels directly supplying the intestine were too thin and their diameter too narrow to introduce an indwelling cannula. As the vasculature cannot efficiently be utilized without cannulation, the initial selection of the mouse model as donor for scaffold miniaturization was dismissed due to the vasculature being inapplicable for stable permanent cannulation and thereby for perfusion decellularization and reestablishment of the vascular system.

The preservation of the vascular tree was the major requirement for the scaffold. Taxonomically, the next bigger prevalent small animal model of the murine family employed was the rat, which was successfully examined upon feasibility of vascular cannulation, perfusion, and scaffold explantation as represented in figure 4. Furthermore, the vascular network was prepared similar to the BioVaSc-TERM® possessing one main feeding vessel, a capillary network branching thereof enabling the supply of the scaffold, and finally leading into a draining vessel. The defined in- and outlet enabled *in vitro*

perfusion and later, after maturation of the graft, the reanastomosis to a vascular system *in vivo*.

However, for the generation of the porcine-derived scaffold, the vascular branches that are emerging directly from the superior mesenteric artery and those leading into the superior mesenteric vein were utilized for cannulation as feeding and draining vessels, respectively. By approaching the mesenteric branches of a 2.5 m long porcine jejunum¹⁶¹ three to four segments could be explanted. In contrast, the mesenteric branches leading into the rat intestinal segments were as well too thin to be cannulated. Nevertheless, the superior mesenteric artery, branching off from the abdominal aorta, and antidromic vein, which leads into the hepatic portal vein, were big enough for cannulation with the smallest available cannulas. However, the exploitation of the superior mesenteric vessels limited the amount of explanted intestinal segments. Nonetheless, the critical step for the usability of a suitable segment is the retention of the vascular circulation and its further accessibility for decellularization, recellularization, perfusion culture, and anastomosis. Therefore, after the feeding artery and draining vein were cannulated, one jejunal segment with an intact arteriovenous circulation was extracted per rat.

5.2 Establishment of a decellularization protocol for rat intestine

For further processing, a well-balanced decellularization protocol was critical for effectively removing cellular materials provoking an adverse inflammatory response upon implantation¹²³ while maintaining native ECM structure facilitating recellularization^{162,163}.

In TE, a multitude of various methods have been established for the decellularization of different tissues and organs¹⁶⁴ based on chemical, enzymatic, and mechanical procedures¹²⁶ targeting different components. Despite an extensive experience with decellularization of porcine jejunal segments¹¹³, the miniaturization was not accomplished by a simple “scale down” of the established protocols due to different scaffold parameters and properties, such as the vessel diameter, scaffold thickness, and cellular masses. The decellularization, recellularization, and cultivation procedures were adapted almost completely anew.

At the same time, Totonelli et al. published a protocol describing a rat intestinal decellularization method¹¹⁶. Consequently, the protocol described was reproduced, adopted on the in-house available laboratory equipment, and optimized upon cell, especially DNA removal as well as ECM preservation. The overall matrix composition appeared already well preserved and the original host DNA was removed to a great extent. The detergent concentrations and incubation times were only customized upon the in-house operational procedures but were kept to the described suggestion as close as feasible. With the DNase incubation adjustment to be performed at 37 °C instead of room temperature the enzymatic DNA cleavage activity was increased. However, with biocompatibility assays indicating poor cell survival of freshly seeded cells after processing of the intestinal segment, additional repeated washing steps were implemented to assure the removal of cytotoxic detergents.

A multistep perfusion decellularization protocol using a combination of chemical lysis, enzymatic DNA cleavage, and multiple washing steps was set up (Fig. 5A).

Initially, to minimize the incubation time with more detrimental chemicals, ultrapure water was utilized for osmotic cell lysis with barely disintegrating effects on ECM components and architecture¹²⁶. Considering osmotic cellular rupture, it was likely that cell-ECM contacts persisted with attached cell membrane fragments as well as conjugated intracellular proteins. Subsequently, harsher acting sodium deoxycholate (SDC) was used to solubilize residual cytoplasmic membranes, lipids, and DNA¹⁶⁵. Subsequent perfusion of a DNase solution enzymatically hydrolyzed residual high molecular weight deoxyribonucleotide chains^{166,167}. To improve DNase-mediated enzymatic activity of DNA lysis, the incubation was performed at 37 °C in contrast to previously published protocols, in which this step was performed at room temperature^{116,117}. The perfusion was steadily applied at constant flow causing a pressure gradient assuring and accelerating the delivery and penetration depth through the 3D ECM of the cell lysis reagents as well as flushing out of cellular debris^{126,168}. Mechanical properties of the ECM were shown not to be significantly affected by perfusion decellularization¹⁶⁹. Even though ionic detergents, such as SDC, sodium dodecyl sulfate, or Triton X-200, are commonly used for decellularization as they can thoroughly solubilize cell and nuclear membranes and completely denature proteins, these properties also account for damaging ECM proteins¹⁶⁵. SDC appeared to be the least detrimental of the ionic detergents but insufficient for complete removal of cellular components while damaging matrix

components. Alkaline solutions are rather suitable for the decellularization of dense structures as they harshly degrade structural matrix components. Non-ionic detergents, proteases, and chelators, however, are in general very mild and thereby ineffective in complete cellular remnant removal. To reduce the amount and exposure time of chemical agents, cellular disruption can be achieved beforehand by repeated freeze-thaw cycles instead of osmotic cell lysis. However, even though it does not significantly impair mechanical ECM properties, it leaves disruptions in the tissue ultrastructure^{168,170}. Finally, since decellularization was carried out under non-sterile conditions, the resulting scaffold was exposed to ionizing radiation (>25 kGy) for sterilization to assure sterility for cell culture and implantation. Disinfection and sterilization was shown not to alter cell adhesion capability onto the ECM¹⁷¹.

5.3 Scaffold characterization upon cell removal, structural preservation, and biocompatibility

With establishing a protocol for tissue decellularization the thereof emerging scaffold was thoroughly characterized in terms of cell and DNA removal, ECM preservation, as well as subsequently biocompatibility for recellularization. Qualitative analysis was carried out histologically. Quantitative examination was performed by spectrometric and colorimetric analysis. For ECM component preservation two of the main ECM proteins were examined: collagen and elastin. With about 30% of the total mass, collagen is the most prevalent ECM protein representing a main structural element as well as providing tensile strength and supporting cell adhesion, chemotaxis, migration, and tissue development^{172,173}. Elastin fibers are often associated with collagens providing elasticity to the incorporated tissues¹⁷⁴.

Even though the incubation time of SDC was reduced by initial utilization of ultrapure water for cell rupture, due to tight cell-matrix anchorage, loss of ECM was inevitable. Even though the loss in collagen and elastin were both statistically significant (Fig. 5I and J), it was structurally not relevant as observed in the histological (Fig. 5C', E', and F') and ultrastructural analysis (Fig. 5L-N) as critical structural ECM proteins could mostly be preserved, including the vascular basement membrane, highly important for cellular

proliferation, migration, and differentiation, serving as structural and functional guide for neovascularization¹⁷⁵.

Despite the ECM being the essential basis and framework for subsequent recellularization leading to a functional implant, the decellularization process was balanced primarily on full cellular removal avoiding immunogenic graft rejection. The preservation of the biochemical composition, 3D organization, and integrity of the ECM was subordinated to immunogenicity but of highest importance for subsequent recellularization.

Feulgen stain, spectroscopic determination, and electrophoretic analysis prove the DNA removal (Fig. 5D', G, and H). Whereas the native DNA was detected and represented as high molecular weight chromosomal DNA by electrophoretic analysis (Fig. 5G). Official benchmarks for effectively decellularized tissues for implantation are only hardly available. Besides guidelines on sterility¹⁶⁸ and endotoxin amount¹⁷⁶, recommended criteria are the lack of nuclei, and residual dsDNA below 50 ng per mg dry weight and 200 base pairs in length¹²⁶ to avoid host immune responses¹⁷⁷.

Besides host cellular DNA¹⁷⁸, also bacteria are capable of evoking immunogenic graft rejection or residual decellularization solutions might elicit local inflammation or necrosis. Originating from the intestine, endotoxins are complex lipopolysaccharides (LPS) which are a major part of the gram-negative bacteria cell wall and extensively abundant in the jejunum and colon¹⁷⁹. Despite the most amount of LPS being found at the villus tips¹⁷⁹ and thereby exposed while the perfusion decellularization process, residual LPS can elicit proinflammatory responses leading to systemic inflammation, with subsequently increased microvascular permeability and consecutive breakdown of microcirculatory flow significantly contributing to organ failure¹²¹. Furthermore, cytotoxicity tests^{180,181} indicated no cause of cellular damage when exposed to the acellular scaffold after its completed preparation indicating primarily no residual bile acids after sodium deoxycholate treatment during decellularization¹⁸².

Subsequently, for demonstrating biocompatibility, the scaffold was employed for initial recellularization. To indicate the capability of the mBioVaSc-TERM® to establish a platform technology for functional graft generation, the preserved basement membrane of the vascular tree was revascularized. Metabolic activity and cell viability were demonstrated by colorimetric MTT and vitality by CellTiter Glo analysis. In addition, *in vitro* cultured cells are usually more sensitive to toxic agents due to the direct exposure.

Therefore, a material considered as non-toxic after verification *in vitro*, is expected also to be innocuous *in vivo*¹⁸³.

Another critical marker for immunogenicity besides residual DNA is the alpha-Gal epitope on xenogenic cells^{184,185} most conveniently assayed quantitatively by ELISA¹⁸⁶. However, alpha-Gal analysis was not considered due to the manifold results attesting biocompatibility together with the similar positive experience made with the BioVaSc-TERM®. Inflammatory response to implanted biomaterials can also be determined *in vitro* by macrophage test systems, being developed in parallel^{187,188}. Acellular SIS-based matrices were demonstrated to not elicit immune reactions upon transplantation^{123,189} and to enhance survival of implemented cells¹⁹⁰.

Following the established decellularization protocol all reference points for acellularity, cytotoxicity, inflammation, and sterility were met for the mBioVaSc-TERM®.

In summary, a perfusion decellularization protocol for rat small intestine was established, based on a previously published method^{116,117}. Effectively preserving the original intestinal architecture while efficiently removing host cells resulted in an acellular scaffold of plain ECM meeting the demands and benchmarks for clinical applicability. Furthermore, biocompatibility was demonstrated indicating to capacity for recellularization of the mBioVaSc-TERM®.

5.4 Reestablishment of the vascular system

Despite initial general indication for biocompatibility, the proof for EC adhesion, growth, proliferation, migration, and maturation of a functional barrier was to be demonstrated.

The reconstitution of the vessel structures was required to assure a functional vascular network providing sufficient nutrient and oxygen supply for a complex dense 3D tissue. Furthermore, the endothelial barrier is critical for maintaining water and protein balance between the intra- and extravascular space. Beyond, haemocompatibility of a scaffold connected to the host blood circulation is critical for a functional implant avoiding immediate coagulation¹⁹¹. Therefore, lining the acellular vessel structures of the scaffold with an endothelial cell layer reduces the risk of thrombosis when implanted *in vivo*¹⁹². This accounts especially for decellularized biological matrices as they mainly consist of collagen – and as seen in the SEM images, the basal membrane is in some places widely

disrupted due to the decellularization process uncovering the underlying collagen network directly exposing a highly abundant matrix component with prothrombotic properties^{193,194}. Coagulation is part of the humoral defense specifically activated when blood interacts with subendothelial layered collagens and vWF¹⁹⁵ to stop blood loss. However, facing an implanted scaffold with vascular structures dominated by collagen the subsequent coagulation will result in thrombosis ultimately completely blocking the vascular access to the scaffold. Successively, the established tissue will become undernourished and finally apoptotic causing more harm to the patient.

Therefore, the vessel system of the scaffold was successfully recellularized with human dermal microvascular endothelial cells (hdmEC) establishing a functional tight endothelial barrier with antithrombotic properties¹⁹⁵ providing hemocompatibility.

5.4.1 Revascularization-capacity of the vascular structures with primary ECs

Before vascular recellularization of the scaffold, primary isolated hdmECs were lentivirally transduced for either GFP or RFP expression to enable live imaging. Thereafter, they were characterized upon their cellular markers¹⁹⁶ relevant for vasculogenesis, angiogenesis, mitogenesis, migration, permeability, cell-cell contact, blood vessel formation, as well as their ability to form functional barriers¹²⁹ (Fig. 6).

CD31 is a cell surface marker on endothelial cells for intercellular junctions, critical for angiogenesis, and a prevalently applied marker for EC identification. CD34 is mostly present on hematopoietic stem cells and capillary endothelial cells. CD31 and CD34, in combination, characterize vascular endothelial cells with high specificity. CD105, also known as Endoglin (ENG), is a membrane glycoprotein and auxiliary receptor for the TGF-beta receptor complex with a crucial role in angiogenic endothelial cells due to affecting cytoskeletal organization and migration during vascular remodeling. TIE2 is an angiopoietin receptor on the cell surface, crucial for blood vessel formation. The determined VE cadherin is crucial in vascular endothelial cell-cell adhesion and major determinant of endothelial permeability. CD146, the melanoma cell adhesion molecule (MCAM), is highly expressed in cells of the blood vessel wall, linking the cells actin cytoskeleton to laminin in the ECM. Only the examination of the VEGFR-2 led to almost no detection of positive cells presenting the receptor on their membrane surfaces.

VEGFR-2 is one of the VEGF receptors mediating most of the known cellular responses of VEGF, thereby highly important for vasculogenesis and angiogenesis, as well as mitogenesis and migration. However, upon cell confluency VEGFR-2 gets internalized by contact inhibition¹⁹⁷ potentially explaining the lack of positive detection by FACS analysis.

In total, the isolated cells were homogeneously positive for endothelial marker and especially functional markers such as cell-cell and cell-ECM adhesion, as well as important marker for angiogenesis and blood vessel formation. Furthermore, the capability to proliferate and to form a tight barrier was demonstrated by TEER and FITC permeability assays. Thereby, the genetically modified GFP/RFP-expressing ECs depicted a suitable source for revascularization enabling non-invasive live microscopy for validation of the recellularization.

Next, the capacity of the decellularized vascular structures of the mBioVaSc-TERM® to restore the intra-vascular barrier was determined by revascularization with ECs. A tight endothelial lining facilitates hemocompatibility of a collagenous scaffold, avoiding coagulation when in contact with blood¹⁹². Revascularization was already demonstrated for the BioVaSc-TERM® *in vitro*¹¹¹ as well as when anastomosed to the brachial vascular bundle of a human arm¹¹³. Furthermore, vascular structures of a rat-derived decellularized intestinal segment were already used to determine the angiogenic capacity *in vitro*¹⁹⁸. The rat-derived segment was to date only demonstrated to facilitate *in vitro* reendothelialization of individual vascular channel segments by demonstrating vessel formation, a competence for neovascularization¹⁹⁸ and to exhibit pro-angiogenic properties facilitating vessel ingrowth indicated by an *in vivo* chicken chorioallantoic membrane (CAM) assay¹¹⁶.

Pursuing full graft vascularization to generate fully vascularized tissues, thorough reendothelialization of the whole scaffold was demonstrated and arteriovenous circulation was validated in this work. Despite distinguishable reendothelialization of the former arterial and venous vessels by differently labeled ECs, arteries and veins were not fully reestablished as only ECs were utilized for revascularization.

Therefore, ECs were infused into and dispersed throughout the network of the retained vascular basement membrane system¹⁹⁹ (Fig. 7A and B). By preservation of the vascular basement membrane the cells were able to migrate and proliferate in the preformed vascular structures²⁰⁰ lining and restoring the vessels. Utilizing fluorescently labelled

cells, the former arterial and venous vessels were individually displayed as well as the interconnection of both in the capillary bed, demonstrating a circulatory network (Fig. 7G).

In summary, scaffold revascularization was established, demonstrating typical endothelial markers (Fig. 8B, C, E, and F), functionality (Fig. 9 and 10A), viability (Fig. 8A), vitality (Fig. 8D), and barrier integrity (Fig. 10B-D) of the ECs lining the arteriovenous network of the mBioVaSc-TERM®. Beyond, the recellularization capacity was subsequently demonstrated to enable complete revascularization of the vessel system.

5.4.2 Maturation of the vascular barrier by arteriovenous perfusion culture

With intraluminal flow modulating vascular permeability²⁰¹, vessels exposed to high shear stress by transporting large quantities of blood in short time are usually thick and hardly take part in nutrient exchange, while in the extensively branching capillary beds the blood flow is low enabling mass exchange. Flow in the capillaries is mainly determined by colloid osmotic and hydrostatic pressure²⁰².

Examining revascularization, the ECs were lining the arteriovenous tubular vascular network demonstrating typical endothelial markers, functionality, vitality, and viability while embedded in a 3D environment.

Supporting maturation of the vascular endothelial barrier, physiological *in vivo*-like conditions were mimicked using computer aided incubator and bioreactor systems (Fig. 7C and D). Temperature and gas were controlled as well as physiological pressure onto the vessels system was applied by pulsatile perfusion. The thereby occurring shear stress in the vasculature simulates the hemodynamic forces onto the endothelial cells stimulating maintenance of vascular homeostasis^{203,204}, vascular conductivity²⁰⁵, vascular barrier integrity⁷⁸, maintenance of vessel branches⁸⁵, as well as arteriogenesis²⁰⁶.

Vascular flow, arterial and venous circulation, and endothelial barrier integrity was demonstrated by intra vital fluorescence microscopy perfusing with PBS (Fig. 7E) and blood (Fig. 7F) as well as by determination of the venous return (Fig. 9). The perfusion through the whole scaffold, especially through the established arteriovenous loop, strongly depends on the integrity of the barrier function by the ECs, usually hardly

accomplished in decellularized tissues. In addition, also in native vasculature the capillary bed is naturally prone to leakage that is returned into the blood circulation via the lymphatic system⁶⁶.

The vascular endothelial barriers in capillaries function as a semipermeable membrane to control blood–tissue exchange of fluids, nutrients, and metabolic waste products while preventing pathogens or harmful materials in the circulation from entering into tissues by transporting cells of the immune system⁶⁶. Most of these characteristics were indicated in the mBioVaSc-TERM® after perfusion culture showing flow and culture media transport through the mesenteric vessels but leakage of fluid, indicated by phenol red leakage (Fig. 7E), through the capillary bed in the former gut lumen.

In native vasculature most of the leaked fluid is reabsorbed into the lymphatic system, which was not realizable for the mBioVaSc-TERM® cultured *in vitro* in the bioreactor setup. The amount of fluid reabsorbed into the venous capillaries is dependent on the colloid osmotic pressure gradient between intra- and extravascular space and hydrostatic pressure. At the arterial end of the capillaries, hydrostatic pressure prevails forcing fluid out of the vasculature. With fluid extrusion, hydrostatic pressure reduces within the capillary until colloid osmotic pressure overbalances hydrostatic pressure at the venous end leading to reabsorption of the fluid. However, since the arterial hydrostatic pressure is higher than the oncotic blood pressure, the net reabsorption is less than the net filtration. This discrepancy leads to a net excess filtration of about 15 % blood fluid remaining in the interstitial space collected by the lymphatic system⁶⁶. Dependent on the body posture and the thereby bearing pressure by body weight and muscular tonicity on the vasculature the interstitial fluid absorption is significantly affected introducing tissue pressure as a determinant for fluid reabsorption²⁰⁷.

Within the bioreactor setup, the same culture medium was present in all compartments, thereby, not establishing a gradient. This might explain the low venous return when perfusing with both, PBS and culture medium, as when perfusing with blood, the venous return was significantly increased, very likely due to blood plasma proteins creating a colloid osmotic pressure gradient.

Furthermore, the physiological venous blood pressure is low in contrast to the arterial pulse pressure in consequence of the cardiac cycle and the muscular arteries. Due to the low blood pressure, the blood return is reduced if not supported otherwise. In an

organism, this issue is overcome by pumping the blood towards the heart by vasoconstriction of the vessels themselves or by squeezing local veins during skeletal muscle contractions or breathing⁶⁶. In case of the mBioVaSc-TERM® cultured in the bioreactor system, smooth muscle cells were lacking as well as a “muscular pump” or “respiratory pump”. Nevertheless, while perfusing the arterial pedicle the perfusion pump of the bioreactor system created a negative pressure at the venous pedicle aiding venous pressure and venous return. To increase the venous return within the bioreactor improving vascular maturation, the intravascular hydrostatic also the necessary colloid osmotic pressure have to be established and maintained²⁰². This might be mitigated by using different media for vascular perfusion and for graft culture. Therefore, the total serum protein concentration inside the vessel has to be higher than extravascular to ensure osmotic fluid inflow after capillary filtration²⁰⁸. Similar effects were indicated perfusing the mBioVaSc-TERM® *in vitro* with whole blood: unobstructed flow through the vasculature, retention of proteins solved in blood, and venous return could be demonstrated by vital microscopy²⁰⁹ with FITC-coupled dextran and venous backflow quantification. Despite physiological capillary fluid exchange by plasma filtration from the intravascular space into the interstitial space venous backflow could be reestablished for up to 40 % compared to native tissue.

Heparinized whole-blood perfusion through the revascularized mBioVaSc-TERM® (Fig. 7F, 9, and 10D) revealed no thrombosis in the scaffold. Interestingly, perfusion of blood-isolated platelets also revealed no adhesion to the vessel when lined with ECs in contrast to EC-free scaffolds, which is essential for blood coagulation and assessable *in vitro*^{210,211}. Obviously, the used endothelial cells formed tight barriers and with endothelial lining of a scaffold platelet adhesion was diminished facing perfusion with whole-blood isolated platelets.

In summary, considering that the mBioVaSc-TERM® was cultured in a bioreactor system with culture media it was obvious to not be able to fully reestablish the native *in vivo* circulation and venous return: the oncotic pressure was similar intra- as well as extravascular due to ubiquitously available medium and vasoconstriction was not feasible due to missing smooth muscle cell layers. Nevertheless, mimicking native conditions perfusing with blood enabled a restoration of the venous return of 40 % compared to native tissue. Furthermore, endothelial barrier integrity as well as the retention of proteins and high molecular particles resembling the size of blood plasma proteins was

demonstrated inside the capillaries by intravital microscopy. Apart from media extrusion into interstitial space, a closed circulatory blood vessel circuit - an arteriovenous loop - was established.

5.4.3 iPS technology depicts an alternative cell source for vascularization

In this thesis, hPSCs that were differentiated into the mesothelium lineage were demonstrated to be differentiated into ECs, pericytes and SMCs within the mBioVaSc-TERM® providing 3D vessel structures. This fortified the established differentiation protocol by Thomas Colunga (Dalton Lab, PI: Prof. Dr. Stephen Dalton, Center for Molecular Medicine, University of Georgia, Georgia, USA) as well as the capacity of the mBioVaSc-TERM® as platform for vascular TE.

The visceral mesothelium is a thin epithelial layer surrounding internal organs²¹². During development, a fraction of those cells undergoes epithelial to mesenchymal transition invading the underlying tissue and contributes to the vascular system^{213,214}.

Cultured and differentiated in the vascular system of the mBioVaSc-TERM®, the spatial distribution of the cells resembled the native vessel composition (Fig. 11). However, the vessels were only sparsely populated and functionality of the muscular layer as e.g. by vasoconstriction or vasodilation was not performed even upon stimulation, presumably due to the imperfect cell layer. Optimizing recellularization efficiency as for the hdmECs, dense and functional cell layers should be attainable, reconstructing native-like vessels.

Moreover, hPSCs differentiated into the mesothelium lineage might be utilized to reestablish the visceral mesothelial layer - typically present on internal organs - around the mBioVaSc-TERM®. Enveloping the scaffold with a layer of mesothelial cells might reduce the incidence of peritoneal adhesions.

In summary, hPSC technology²¹⁵ was employed to differentiate cells towards ECs, pericytes, and SMCs from one common progenitor, lining the vessels of the mBioVaSc-TERM®. Implementation of those three different cell types potentially enables the generation of a diversified vascular network superior to EC only in terms of vascular stability and functionality. For clinical application, it is feasible to generate patient-specific iPSCs for subsequent differentiation into desired tissue graft and autologous stem cell therapy²¹⁶. However, this attempt is very laborious with enormous efforts necessary

for de-differentiation of somatic cells to pluripotency, differentiation towards the desired functional organ-specific cells, considering organs being multicellular tissue, and proving immunogenic and tumorigenic potential of the generated cells.

5.4.4 Advancements for mBioVaSc-TERM® revascularization

Despite the whole vascular tree of the mBioVaSc-TERM® seemed to be recellularized, not all capillary branches were observed to be perfused during intra vital microscopy (Fig. 10). Thrombosis could be excluded at this point causing the vascular obstruction as with plain culture media perfused coagulation cascade was not triggered. Nevertheless, blockage of the respective vessels was assumed, presumably during mass injection of the endothelial cells inside the vascular tree and microcirculation through the capillary bed. Thereby, cells might have blocked some capillaries for further perfusion. The lumen diameter of a capillary ranges from 5 - 10 μm , wide enough for an erythrocyte to pass⁶⁶ but easily blocked by mass endothelial cell infusion. Vessel blockage by manual mass EC infusion might be avoided by modifying the recellularization method by resuspending the ECs in higher volumes and slower successive infusion. Preliminary results showed endothelial cells slowly infused into the graft vasculature within the bioreactor by the perfusion pump with similar cellular distribution within the vascular system. Functionality and perfusability of the newly established vascularization method still has to be confirmed.

Furthermore, pursuing complete endothelialization, vascular progenitor cells were proven to be promising cell sources for *in vitro* vascularization in TE^{44,102} as they are even capable of restoring functional vascular endothelium²¹⁷ and enhancing neovascularization in an ischemic environment *in vivo*²¹⁸. The crucial influence of these progenitors in vascular repair and regeneration²¹⁹ could be exploited to close eventual gaps in the endothelial lining of the vascular branches by perfusion of vascular or endothelial progenitors after initial recellularization.

In addition, oxygenation of culture media²²⁰ might result in improved quality of grafts generated. With oxygen saturation being overall one of the most vital criteria, the warranty of physiological normoxic conditions is imperative for maintaining reproducible tissue viability. The implementation of oxygenated culture media inside the

bioreactor incubator setup as well as its sensory monitoring²²¹ would reduce fluctuations in oxygen concentration compared to oxygen diffusion through the aqueous culture media with only gaseous oxygen provided in the atmosphere of the incubator. Furthermore, avoiding the risk of hypoxic conditions might improve cell growth, differentiation, maintenance, and subsequently experimental validity.

Nevertheless, these results reflected the difficulty of the full restoration of the natural capillary network due to its complexity. However, the *in vitro* generation of vessels with capillary sized diameters is not feasible with currently available technology. Thus, biological materials - with progress on graft vascularization demonstrated in this work and the implications drawn on future advancements - represent the most promising source for vascular TE.

Taken together, via physiological perfusion culture the vascular scaffold was successfully reendothelialized with hdmECs, bearing perfusable and discriminable arteriovenous transitions in the capillary bed. A venous return was established utilizing colloid osmotic pressure perfusing with whole blood excluding undefined leakage besides the interstitial fluid homeostasis through the capillary diffusion. Thrombosis was not observed even with whole blood perfusion leading to the assumption that a tight haemocompatible vascular endothelial barrier was established, though hard to consistently prove considering the vast branched vessel network. The functional arteriovenous vascular reconstruction depicted by sophisticated techniques e.g. 3D light sheet and intravital microscopy impressively demonstrated a hallmark in vascular tissue engineering.

However, pursuing full graft vascularization, only an endothelialization was achieved. The additional implementation of pericytes and smooth muscle actin-positive cells as indicated by mesothelial cell differentiation (Fig. 10) might enable the generation of fully functional vessels and would depict a milestone in vascular tissue engineering. Nevertheless, for the newly established cell differentiation, the cell revascularization procedure has to be improved as the vessels were not completely lined as indicated by the immunohistological stainings (Fig. 11). The incomplete repopulation of the vascular structures had functional consequences indicated by the inability for vasoconstriction of the muscular layer, even upon stimulation (Fig. 11E). To perform muscular contraction there has to be a dense layer of tightly interconnected cells that was not yet achieved.

Considering the varying compositions of artery, arterioles, capillaries, venules, and veins²²² to be implemented into the complex branching vascular network of the mBioVaSc-TERM® the cellular composition might be more efficiently studied in simpler set-ups such as vessels with only one defined vascular structure. With the gained insight into vessel dissection, de- and recellularization a follow-up study focusing on single straight vessels might further promote vascular TE and advance its translation into clinical application, bearing in mind the huge clinical demand for functional biocompatible vascular grafts.

5.5 Application of the mBioVaSc-TERM® as a platform for multicellular co-culture

With revascularization of the mBioVaSc-TERM®, the scaffold was demonstrated to be suitable for cell culture and nutrient and gas supply was established to feed cells for tissue graft development on the ECM of the former gut lumen (Fig. 12). Expanding the applicability of the mBioVaSc-TERM®, after seeding ECs in the vessel structures various other cell types – including multicellular organoids – were co-cultured in the luminal compartment.

Therefore, culture conditions were individually adapted to the need of the implemented cell types, subsequently demonstrating maintained cell viability and function. Media composition was not trivial to compose as different cells with distinct demands for growth factors, cytokines, and hormones were cultured together.

Furthermore, the endothelial structures provided a distribution system to feed co-cultured cells but also to function as distribution system to deliver compounds to the cells for metabolic conversion and/or to spread secreted drugs throughout the vascular circulation.

The endothelial barrier integrity of the revascularized vessels of the mBioVaSc-TERM® was characterized to be tight enough to retain proteins above 40 kDa but enabled leakage from the capillaries for low molecular weight compounds. In reverse conclusion, it should also be feasible for secreted proteins to enter the vascular system via the capillary network enabling drug secreting cells to release compounds into the blood stream. The proof of the distribution of biologically active drugs via the

vascular system indicated the capability of the mBioVaSc-TERM® to be developed towards an implantable drug delivery system.

5.5.1 Example of mBioVaSc-TERM® application for liver-like organoid culture

To demonstrate the capacity of the mBioVaSc-TERM® to maintain highly metabolic active tissue viable and functional, liver-like organoids¹¹⁸ were integrated in the luminal scaffold (Fig. 13C) as tissue model that might serve for prospective toxicology and metabolism studies¹¹⁵.

In a preliminary work¹¹⁸ liver-like organoids were established by self-assembly of hepatocytes, liver sinusoidal ECs, and mesenchymal stem cells cultured in high cellular density (Fig. 13A and B). The metabolic and enzymatic activity and substrate conversion was described as well as the liver-specific protein production and metabolism¹¹⁵. After self-assembly of the different cell types to a dense organoid, they could only be maintained in culture for a maximum of 72 h due to increasing nutrient and oxygen deficiency leading to apoptosis and necrosis in the inner cell mass of the organoid. Acute nutrient and oxygen deficiency could be circumvented by implementing the organoids into a dynamic perfusion culture setup¹¹⁸. Combining the organoid technology with the mBioVaSc-TERM®, the perfusion culture within the vascularized scaffold (Fig. 13D) increased organoid culture for one week. However, functional analysis by HPLC of converted metabolites from the culture supernatant demonstrated that the capacity for liver-specific enzymatic conversion of the cultured organoids was only on a basal level (Fig. 13G). However, the hepatocyte 2D monoculture that was serving as control also demonstrated only basal enzymatic activity upon stimulation. In conclusion, the basal enzymatic activity of the organoids upon stimulation was likely not a result of the 3D co-culture but due to impaired hepatocytes that were implemented. Nevertheless, viability (Fig. 13E) and characteristic marker (Fig. 13F) of the liver-like organoid was maintained indicating a promising perspective to also demonstrate functionality in the near future.

5.5.2 Example of mBioVaSc-TERM® application as drug delivery system

A collaboration was aiming to unravel the molecular causes of skeletal muscle wasting and to deduce therapeutic strategies to neutralize the effect and ameliorate the condition. One strategy was the transplantation of a drug delivery system releasing inhibitors of proteins limiting muscle mass. Activin A and Myostatin are negatively regulating skeletal muscle mass²²³⁻²²⁵. Follistatin is an activin-binding protein inhibiting Activin A and Myostatin and thereby ameliorating their atrophic pathology²²⁶. Furthermore, Activin A facilitates capillary formation similarly to VEGF²²⁷. The mBioVaSc-TERM® was evaluated to be employed as drug delivery system. Considering animal studies in rat, there was no available rat model expressing the relevant phenotype. Therefore, the mBioVaSc-TERM® was considered for implantation of cells overexpressing Activin A and Myostatin to induce a muscle atrophic phenotype to be rescued subsequently.

For the proof of drug distribution throughout the vascular system, CHO cells were employed and genetically modified for drug secretion²²⁸. CHO cells depicted a prevalent model for the production of therapeutically applied proteins²²⁹.

Cultured inside the mBioVaSc-TERM®, the amount of secreted protein was determined by ELISA (Fig. 14A). Activin A and Myostatin secretion reached a certain concentration plateau in 2D and in 3D culture. However, the total amount of protein secreted in 3D was up to 200 % increased, compared to the 2D reference. An explanation of the significant increase in secretion despite similar cell number might be the perfusion culture. In contrast to static culture, within the bioreactor there was a steady medium turnover, thereby constantly reducing the local drug concentration presumably avoiding a saturation but facilitating constant release.

Furthermore, it was demonstrated that the secreted drugs did not only diffuse into the surrounding reactor compartment but were distributed throughout the bioreactor system. Therefore, the secreted drugs must have passed the endothelial barrier to reach into the intravascular compartment and subsequently being distributed throughout the bioreactor system. Translation these assumptions into a potential clinical application, secreted drugs from the mBioVaSc-TERM® might pass into the blood circulation and be distributed throughout the body. Whether a systemic effect might be elicited, still has to be determined by further studies.

Beyond secretion of the proteins, their biological activity was demonstrated as this is critical to elicit a therapeutic effect. Utilizing the effect of Activin A and Myostatin on inhibition of cell proliferation of MPC-11 cells¹²², the biological activity was demonstrated by applying the secretome of the genetically modified CHO cells onto MPC-11 cells to determine MPC-11 proliferation kinetics dependent on the applied supernatant concentration (Fig. 14B). The different biological efficiency of both proteins was represented by the distinct inhibitory effect on the proliferation kinetics in MPC-11 cells. As depicted in figure 14B, to decrease cellular MPC-11 vitality to the same level using Activin A and Myostatin, Activin A was diluted to a higher extent achieving similar cellular effects, reflecting the different effective concentrations of the proteins to induce a cellular response. Thereby, a shift in proliferation kinetics towards increased dilutions resulted.

In summary, not only cellular survival and secretion was demonstrated but also the biological activity of the secretome proving the concept of the mBioVaSc-TERM® to potentially serve as a drug delivery system. Furthermore, Activin A might enhance vascularization within the mBioVaSc.

Beyond, the implementation of genetically engineered autologous cells could be a viable strategy for clinical application and future cell therapy with the mBioVaSc-TERM®.

5.5.3 Example of mBioVaSc-TERM® application as endocrine tissue graft

The secretion of Activin A and Myostatin by the genetically modified CHO cells enabled the proof of concept for drug secretion and distribution throughout the vascular system of the mBioVaSc-TERM®. In contrast to constitutive secretion, numerous metabolic diseases demand a highly regulated release of factors. A constant secretion as with the constitutive producing cells generated above might have disadvantageous side effects. Therefore, the drug secretion has to be tightly regulated in a dose dependent manner by feedback mechanisms. However, the implementation of all the required feedback loop mechanisms by genetic engineering is highly laborious.

To demonstrate the capacity of the mBioVaSc-TERM® to maintain naturally drug secreting cell cluster viable and functional, porcine neonatal islet-like cell clusters¹⁴² (NICC) were employed (Fig. 15A). Islets constitute the endocrine function of the pancreas secreting hormones critical for glucose homeostasis¹⁰.

For insulin secretion, the total amount of secreted protein was not as high as for Activin A and Myostatin. However, the latter proteins were produced by genetically modified cells for constitutive expression and secretion whereas insulin secretion is highly regulated and the cells more demanding on the microenvironment of their cellular niche for survival and function. Furthermore, the employed islets were immature when isolated upon insulin secretory activity²³⁰, as indicated by the immunohistological staining hardly verifying insulin⁺ staining on the cultured NICCs (Fig. 15D). Nevertheless, the islets were viable in the luminal culture within the mBioVaSc-TERM® (Fig. 15B) as well as secretion of insulin was demonstrated in the co-culture setup. However, insulin secretion was stimulated only by 3, 5, and 10 mM glucose, proving too little to induce an elevated secretion rate above the base level (Fig. 15E). Furthermore, the impact of supplementary co-culture was determined by seeding additional ECs, MSCs or both, ECs and MSCs, in the luminal compartment of the mBioVaSc-TERM® (Fig. 15F). MSCs did not demonstrate to have an impact on insulin secretion of the NICCs. The co-culture with ECs clearly indicated a trend in increased insulin secretion. Though, no impact of ECs on increasing insulin secretion is known, it was likely that the raised insulin levels were due to elevated NICC viability by directly co-culturing ECs additional to the revascularized structures.

In summary, viability of cell cluster co-cultured with different cell types with distinct demands on the culture conditions was demonstrated as well as their secretion, proving the concept of the mBioVaSc-TERM® to potentially serve as a framework to establish an endo- or exocrine tissue.

Moreover, despite advances in clinical islet transplantation as the gold standard therapy, there is still a huge inefficiency due to a progressive loss of islets and islet function²³¹. As a far future perspective, instead of intravenous injection of islets, the mBioVaSc-TERM® might serve as a tailored microenvironment for islet survival and function with adjacent vascularization providing the functional stimuli and distribution network.

Concerning the realization of a secretory active organ-like tissue, a consecutive study aims to generate a vascularized 3D organ-model of the pancreas combining vascular TE and iPS cell technology. Based on the herein established concept, the mBioVaSc-TERM® will provide the framework for a 3D co-culture system of human iPS cells differentiated into pancreatic β -cells^{232,233} and acinar cells²³⁴, representing the endocrine and exocrine function of the pancreas, respectively.

5.5.4 Advancements for tissue graft generation and maintenance

The perfusion culture was demonstrated to be feasible and appeared superior to standard static culture regarding long-term vitality, viability, and functionality.

The co-culture of ECs within the luminal culture in addition to reendothelialized vessels indicated positive effects on vitality and thereby maintained functionality as shown for NICCs. Exploiting the capacity of ECs for angiogenesis¹⁹⁸, combined with the implementation of sprouting and tube forming EC-spheroids co-cultured with tissue-like organoids^{102,103}, intraluminal vascularization might be achieved. Inner-luminal vascularization interconnected to the capillary branches embedded inside the luminal ECM of the mBioVaSc-TERM® would establish a fully pervading vessel network throughout the luminal compartment. Thereby, promoting vascularization inside the luminal cavity beyond revascularization of the scaffold vasculature, might enable full thickness tissue graft generation.

Beyond, by improving the venous return with establishing a colloid osmotic gradient between intra- and extravascular space and utilizing the distinct afferent and efferent vessel system, drugs could be delivered via the simulated blood stream to a generated tissue within the luminal compartment of the mBioVaSc-TERM®. The returned compounds might be analyzed upon the capacity to pass the endothelial barrier and tissue-specific drug metabolism as well as the tissue itself can be analyzed upon the metabolic pathways induced by exposition to a certain drug in an *in vivo*-like situation. This technology might facilitate basic research on organ function and metabolic pathways as well as give further insight on disease patterns including vascular diseases. Constituting organ-specific tissue pervaded by endothelialized vessels, the mBioVaSc-TERM® might function as an *in vivo*-like test system utilized for drug screening, metabolism and toxicity studies as well as a cancer model enabling the examination of tumor vascularization and metastasis. Preliminary data shown in this thesis for the generation of liver and pancreatic tissue indicated promising results towards the future establishment of organ models for drug screening and toxicity tests.

Generating different tissues in different scaffolds and connecting both in a circuit within a bioreactor system, reciprocal effects might be determined representing a vascularized multi-organoid system.

In summary, to demonstrate the capacity of the mBioVaSc-TERM® as a platform technology for vascularized tissue graft generation, multicellular organoids, genetically modified cells for drug release or naturally hormone secreting cell cluster were maintained viable and functional in a co-culture setup. The biologically active secreted proteins were determined to be distributed throughout the whole bioreactor system. The different applications indicated further improvements but provided promising results to facilitate the generation of long-term functional graft tissue based on the mBioVaSc-TERM®.

5.6 Clinical relevance and capacity of the mBioVaSc-TERM® for *in vivo* application

The mBioVaSc-TERM® was demonstrated to be biocompatible and haemocompatible, to enable revascularization and facilitate physiological vascular perfusion, and to maintain tissue-like co-culture.

Next, the translation toward clinical applicability was evaluated, demonstrating *in vivo* proof of concept whether the mBioVaSc-TERM® is suitable as scaffold for tissue graft generation and further as Advanced Therapy Medicinal Product (ATMP). To determine the capacity as human cell therapy application, immunodeficient small animal models are most suitable to not compromise the proof of concept by heterologous immune rejection¹⁵⁶. In particular, the mBioVaSc-TERM® was revascularized with hdmECs classifying the graft as xenogenic when implanted in rats. Therefore, immune-compromised nude rats were employed to circumvent immunogenic rejections for proof of concept for implantation and *in vivo* application of the mBioVaSc-TERM®.

For further studies, autologous cells can be utilized, however, vascular integrity has to be proven for each EC source introduced.

Furthermore, concerning the generation of an ATMP, preclinical studies on safety, efficacy, and biodistribution are for practical and ethical reasons preferentially examined in small animal models.

5.6.1 Immediate and leakage-free vascular anastomosis of the mBioVaSc-TERM®

The preserved vascular structures of the mBioVaSc-TERM® enabled an immediate anastomosis to the circulation of rats for *in vivo* proof of concept studies. The capacity for vascular anastomosis displays a huge advantage over most attempts in vascular tissue engineering with only the establishment of an intrinsic vascularization but no directly connectable pedicles.

The porcine-derived BioVaSc-TERM® was already demonstrated to be connected to the brachial vascular bundle in the upper arm of a human patient¹¹³. However, the vessels of the rat-derived mBioVaSc-TERM® were distinctly smaller in diameter and thereby more demanding to suture. Furthermore, to avoid vascular offset, vessels of similar diameter are favorable for anastomosis. Microsurgical handling of a visceral surgeon enabled to suture the feeding and draining mesenteric vessels of the mBioVaSc-TERM® onto a rat's abdominal aorta as well as the caudal vena cava, respectively (Fig. 16).

For *in vivo* proof of concept, the mBioVaSc-TERM® was reendothelialized with hdmECs and implanted in nude rats. After anastomosis of the mBioVaSc-TERM® onto the rat vasculature, the mBioVaSc-TERM® was perfused by an unobstructed unidirectional blood flow as a part of the animal's blood circulation. With the mBioVaSc-TERM® directly anastomosed to the blood circulation, an immediate foreign body reaction was not expected due to the utilization of immunodeficient rat and the well described successful clinical application of decellularized ECM. The main concerns were leakage and insufficient scaffold haemocompatibility. Acute leakage could have resulted in bleeding to death of the patient and incomplete lining of the vascular structures with ECs could have resulted in acute thrombosis sealing off the blood supply within the graft and in the worst case leading to an embolus outside the scaffold.

The *in vitro* tested vascular tightness and haemocompatibility of the reendothelialized vascular tree were confirmed *in vivo*, preventing leakage and acute thrombosis. Furthermore, the rats with implanted grafts showed no signs of rejection nor intolerance, besides one complication (Fig. 17), presumably due to an intestinal obstruction in consequence of the surgical intervention during the implantation.

5.6.2 Potential integration of the mBioVaSc-TERM® into surrounding tissue

It is described in literature that implanted biomaterials elicit foreign body response and monocyte and macrophage-like cells are recruited to the site of the implant facilitating ECM turnover or encapsulation within the first 3 days *in vivo*. At day 7, these implants are completely sealed off by a definitive fibrotic capsule²³⁵.

In contrast, the mBioVaSc-TERM®, which is composed of naturally occurring ECM and reendothelialized to provide vascular tightness and haemocompatibility did not elicit any signs of foreign body reaction nor graft remodeling or turnover within the first 3 days (Fig. 18A).

Even after 7 days *in vivo*, the mBioVaSc-TERM® was only faintly covered by loose connective tissue and the vascular function seemingly unimpaired (Fig. 18B). As this did not correlate with the typical development of immunogenic rejection of fibrotic connective tissue encapsulation to shield the material from the body²³⁶ it was more likely to resemble impaired healing potentially triggering similar mechanisms like peritoneal adhesion.

30 days post implantation, the scaffold was entirely encapsulated and adherent to the surrounding tissue but still easily dissected therefrom (Fig. 18C). This was in line with peritoneal healing, depicting critical progression of adhesion formation after seven days²³⁷.

Beyond this time frame, when implanted for 120 days *in vivo*, the graft was indistinguishably incorporated into the tissue (Fig. 18D). With exclusion of fibrotic encapsulation, the graft being inseparable from original tissues indicated graft integration into the organism.

These results were in line with other implantation studies described in literature^{238,239}. In fact, connective tissue overgrowth was utilized therein enabling vascular sprouts to surround and infiltrate the transplant. Thereby, a prevascularization of an originally avascular biomaterial was achieved. This strategy for TE requires an implantation *in vivo* for 2 – 6 weeks, dependent on scaffold size, until the material is encapsulated by connective tissue and vascular sprouts have grown towards the material²⁴⁰. The synthetic biomaterials then is explanted to serve now as a prevascularized scaffold allowing the incorporation of cellular components in close proximity to vascular structures *in vitro*.

Next, the prevascularized graft is finally implanted again. Due to the beforehand established prevascularization, the connection of the vascular structures within the graft and the host vasculature will now occur quicker enabling nutrient supply and minimized graft necrosis. Nevertheless, two surgeries are necessary and after explantation and reimplantation the ingrown vessels do not provide a connection to the circulation any more, which has to be reestablished by sprouting anew.

Comparing the established mBioVaSc-TERM® with other engineered scaffolds²³⁵, the innate vascularization enabled direct anastomosis for immediate nutrient supply, and the use of naturally occurring decellularized scaffolds could be considered preferable in terms of biocompatibility, immunogenic rejection and foreign body reaction. Thereby, the mBioVaSc-TERM® appeared superior to synthetic avascular scaffolds.

However, the exploitation of biomaterial encapsulation indicates that the *in vivo* overgrowth of the mBioVaSc-TERM® might be advantageous for long-term functional tissue integration. In contrast, sealing the mBioVaSc-TERM® off the surrounding tissue by enveloping it in a surgical mesh resulted in degradation of the scaffold (Fig. 18E) indicating that the surrounding tissue elicited no adverse effects onto graft survival but appeared beneficial.

Another explanation for connective tissue surrounding the implanted graft is peritoneal adhesion formation. Naturally, internal organs are anchored within the body but still can move freely to a certain degree not sticking to each other to ensure a functional motility especially for the intestine. The “slippery surface” on the internal organs is provided by a mesothelial cell layer²⁴¹ secreting a surface active phospholipid-based surfactant²⁴² with fibrinolytic activity protecting against adhesions and thromboses²⁴³. Upon injury or inflammation a regeneration cascade is triggered and peritoneal healing is normally completed within 7 – 10 days²⁴⁴ by differentiation of underlying mesenchymal cells²⁴⁵. Otherwise, if regeneration is impeded, scarring occurs inducing peritoneal adhesion formation²⁴⁵.

Furthermore, due to surgical trauma such as tissue desiccation, irradiation, hemorrhage, ischemia, and reactions to foreign materials introduced during the procedure such as glove powder, sutures, and gauze the host abdominal organs likely get affected and normal healing mechanism becomes impaired and shifts towards adhesion formation²⁴⁶.

Even in clinical routine the incidence of peritoneal adhesion occurrence after abdominal surgery is 93 %. However, in most cases, they do not cause severe symptoms. Nevertheless, they might progressively become larger and tighter provoking chronic abdominal pain to the point of intestinal obstruction even years after the surgery requiring a second operation to break the adhesion²⁴⁷.

In case of the mBioVaSc-TERM®, considering the 1.5 – 2 hours surgical implantation procedure for anastomosis and implantation of the mBioVaSc-TERM® it was very likely for a surgical intervention-caused inflammation to occur. Furthermore, during decellularization all cells including the naturally present mesothelial cells secreting the protective surfactant were removed. Thereby, upon implantation, the graft was unprotected with the exposed bare ECM of the mBioVaSc-TERM® incapable of regeneration, most likely triggering peritoneal scarring in consequence of the missing surfactant and surfactant producing cells. Consequently, excessive ECM is likely to be deposited successively establishing a fibrous bridge between tissues²⁴⁴. Thereby, the scaffold was exposed to matrix turnover, scarring and thus fibrous tissue deposition anchoring the graft to its abdominal environment²⁴⁸ and ultimately integrated or disintegrated dependent on the biocompatibility and vitality of the graft tissue.

For the mBioVaSc-TERM®, adhesion, anchorage, and incorporation are not generally disadvantageous. In contrast, the overgrowth of implanted biomaterials with collagenous tissue and cell infiltration was exploited to create living autologous tissue²⁴⁹ with the mechanical properties and functions of the primarily implanted biomaterial²⁵⁰. However, further analysis has to demonstrate whether the mBioVaSc-TERM® was integrated within the tissue with sprouting vessels or whether the surrounding tissue was fibrotic deposition triggered by peritoneal adhesion. Furthermore, functional tissue has to be implemented inside the mBioVaSc-TERM® to demonstrate the *in vivo* capacity as a viable tissue graft. Examining graft function over time *in vivo* will determine the main criterion for evaluation of clinical mBioVaSc-TERM® applicability.

5.6.3 Alternative implantation sites avoiding the risk for peritoneal adhesion

Despite integration of the mBioVaSc-TERM® within the surrounding tissue not being disadvantageous, as this procedure is deliberately exploited for synthetic biomaterials to

establish prevascularization, there is a high risk for peritoneal adhesions causing secondary damage. This might have been occurred to the one laboratory animal that developed an ileus²⁵¹.

With peritoneal adhesions being a clinically relevant problem²⁵², adhesion risk might be reduced by optimizing the implantation procedure or explore another implantation site, subsequently also diminishing the incidence of secondary intestinal obstructions.

In the small animal model rat there is hardly an alternative location for anastomosis. A rat jugular vein and carotid artery at the neck were no option as there was no space for the actual mBioVaSc-TERM® to be placed. The iliac vein and artery in the lower abdomen or femoral vessels in the upper legs could be considered. However, the latter might already be too small for anastomosis and even despite preparing the graft small enough that it could be placed in a leg muscle pocket, it would be exposed to a lot of force applied by the surrounding leg musculature potentially destructing the scaffold.

In large animal models, however, the above mentioned options will be feasible due to the different size proportions of graft and recipient and therefore depict viable alternatives to the intraabdominal space.

5.6.4 Barriers guarding the graft from ECM remodeling and deposition

Besides relocating the implantation site various peritoneal adhesion prevention therapies are in development²⁵³. The implementation of solid barriers to physically separate two tissues depicted the clinically most successful adhesion barriers in current clinical applications²⁵³.

Hence, to diminish the prevalent hazard a barrier to shield the implant was employed that was also supposed to enable easier graft recovery and subsequent analysis. The GORE® DUALMESH® biomaterial was used to promote host tissue incorporation on one side while minimizing tissue attachment on the other²⁵⁴. However, employing the GORE® DUALMESH® biomaterial did not reduce tissue encapsulation. In contrast, when enveloped in a surgical mesh the biomaterial pouch was completely encapsulated. Moreover, the scaffold within the biomaterial pouch was degraded (Fig. 18E).

Examining the pathologic state of the implant, foreign body response is usually described as a non-specific immune response by the infiltration of inflammatory cells to destroy and

remove foreign materials²⁵⁵. The enveloped scaffold was very likely in the process of being phagocytosed and removed. This indicated that the long-term sealing off from the surrounding environment was obviously disadvantageous in terms of tissue survival and integration. In contrast, the scaffold which was not enveloped was completely integrated without signs of adverse reactions by the animal. In both cases, similar mechanisms, chemical mediators, matrix metalloproteinases, and macrophages present in blood and the peritoneal fluid²⁵⁶ were likely responsible for tissue remodeling. However, the degraded scaffold being enveloped and sealed off from the environment indicated that the triggering effect was elicited by factors circulating in the bloodstream.

Vascular sprouting from the surrounding host tissue into the graft might potentially have occurred improving graft integration. The immediate anastomosis establishing blood circulation throughout the graft might facilitate short-term survival of the implanted tissue. However, for long-term tissue integration, additional sprouting and expansion of the vascular network might be necessary. The establishment and implementation of further strategies to increase sprouting and enhance vascularization seems advantageous for graft survival.

Other strategies than enveloping the scaffold with a definite barrier to separate graft from host might be more promising in minimizing the risk for pathologic adhesions while preserving the mBioVaSc-TERM® from degradation but allowing tissue integration. Approaches resembling a more natural strategy or employing a naturally-derived protectant might be superior in protecting the internal organs from adhesions but still enabling long-term integration of the mBioVaSc-TERM® without introducing an artificial material eliciting foreign body reaction.

Instead of solid barriers, fluids and gels are described as absorbable surfactant lubricants²⁵⁷ to reduce the incidence of adhesions until the natural barrier of affected areas is regenerated after a surgical intervention. Embedded in hydrogels or applied independently, medication was developed targeting the molecular mechanisms of to significantly decrease adhesion formation²⁵⁸. Hellebrekers *et al.* reviewed fibrinolytic agents aiming for the prevention of the onset of adhesion or the immediate lysis of excessive ECM deposition counteracting developing fibrous bridge formation.

A TE approach suggested the implementation of mesothelial cells²⁵³ on the scaffold surface providing a natural biological barrier. hPSCs demonstrated the capacity to be

differentiated into the mesothelium lineage and might then be utilized to reestablish the visceral mesothelial layer on the mBioVaSc-TERM®, as present on internal organs reducing the incidence of peritoneal adhesion. Regarding clinical application, autologous cells implemented potentially provoke immune reactions. However, autologous mesothelial cell isolation requires the determination of suitable sites for taking biopsies, the establishment of protocols for cell isolation, characterization and massive cellular expansion to an adequate amount to repopulate the graft in suitable co-culture conditions. Starting with the determination of an accessible location for taking a biopsy for cell extraction, the whole process will be extremely laborious. The generation of mesothelial cells from iPS cells might be a potential alternative, however, similarly laborious and requires proof of safety of the iPS cells²⁵⁹.

Besides the implementation of cells facilitating surface functionalization, the capability of functionalizing the mBioVaSc-TERM® ECM with the respective proteins could be determined alternatively.

In summary, without a mesh envelope constituting a definite barrier, the graft was integrated into the surrounding tissue, while the mesh enveloped graft was degraded. Nevertheless, minimizing the risk of peritoneal adhesion by employing another biodegradable envelope or biological surface modification might depict a viable solution still enabling long-term tissue integration.

5.6.5 Vascular regression during long-term mBioVaSc-TERM® implantation

During short-term *in vivo* implantation the blood flow appeared unobstructed within the vascular tree of the mBioVaSc-TERM® and no acute signs of inflammation were indicated. However, after long-term implantation the blood flow inside the scaffold vasculature was halted and the endothelial integrity degraded.

In contrast to the analysis of the *in vivo* implanted mBioVaSc-TERM® that demonstrated a gradually fading endothelialization, during seven weeks *in vitro* culture of the reendothelialized mBioVaSc-TERM® no vascular degradation was observed.

In both setups the mBioVaSc-TERM® was employed as a vascularized platform with only the vascular tree cultured with cells. There was no further demand for neither oxygen nor nutrition besides the ECs and there was no VEGF secretion for vascular stabilization from

subsequent cells and tissue co-culture. Even during embryogenesis vascular development responds dynamically to the needs of the surrounding tissue for nutrients and environmental factors upon blood flow by vascular growth or regression²⁶⁰. Thereby, the *in vivo* response to a structure without demand for oxygen supply was the regression of the respective vasculature²⁶¹. However, during *in vitro* culture, VEGF was constitutively added to the culture media, sustaining the vascularization. With a stable vascular network established *in vitro*, angiogenic vascular remodeling and expansion²⁶² was not investigated in particular.

With vascular regression observed *in vivo*, a strategy to circumvent endothelial degradation might be the implementation of co-cultured cells or an organ-like tissue inside the former intestinal lumen of the mBioVaSc-TERM® to induce a demand for nutrients as well as hypoxia inside the tissue establishing an oxygen tension ultimately preventing vascular regression and inducing vascular ingrowth²⁶³.

The vascular tree is highly adaptable and vascular remodeling including angiogenesis as well as vascular regression frequently occur during physiological processes as wound healing and inflammation²⁶⁴. Vascular remodeling is mainly triggered by VEGF. Simplified, an excess of VEGF results in angiogenic sprouting, while a lack leads to regression initiated by apoptosis of ECs. The latter is explained by anti-apoptotic characteristics of VEGF promoting cell survival while inhibiting caspase activation²⁶⁵. ECs express endogenous VEGF, however, only to maintain expression of VEGF receptor and cell adhesion molecules²⁶⁶.

The first sign for vascular regression is stagnancy of the blood flow in the respective vessels. Subsequently, the vascular wall components become gradually removed: the ECs undergo apoptosis²⁶⁷, whereas the fate of the pericytes is controversially discussed whether they also become apoptotic or dedifferentiate into fibroblast and migrate into the connective tissue²⁶⁴. Finally, residual debris of coagulated blood and apoptotic cells gets cleared by phagocytosis²⁶⁸. An empty basement membrane is the only remnant remaining from the former vessel. This phenomenon described, explains the observed gradual long-term decline of the mBioVaSc-TERM® vascularization *in vivo*.

Without sufficient stimuli to sustain the vascularization of the mBioVaSc-TERM® and promote sprouting ingrowth, successive regression and degeneration was a natural

consequence. Harboring only endothelialization, the graft was missing relevant tissue to be nurtured, therefore implant was of no purpose leading to regression.

Liver-like organoids were implemented, but presumably too little to induce a relevant demand for vascular ingrowth countering the vascular regression. If the luminal compartment would be filled with organoids, an established full thickness tissue might pose a high enough demand for vascular sprouting. Hypoxic cells express angiogenic molecules, such as VEGF, to stimulate the migration of endothelial precursors for vasculogenesis and thereby reduce the oxygen tension towards blood vessels²⁶⁹.

VEGF release from the mBioVaSc-TERM® to prevent vascular regression²⁷⁰ and to stimulate further angiogenesis²⁶⁴ and vascular ingrowth might enhance vascular stability and graft survival. VEGF supply might also be provided by coupling the protein to the ECM facilitating a release over time or by implementing VEGF-secreting cells. Cells utilized for tissue generation might be genetically modified for additional VEGF secretion to perform their tissue-specific function in addition to VEGF release. Thereby, sustained vascular integrity might be demonstrated as well as sustained functionality of the implanted graft tissue. Furthermore, if the function of implemented cells or tissue is vital for host survival as in a rescue model the urge to maintain the graft viable might even be elevated. However, additional *in vitro* analysis have to be performed to establish and characterize the graft prelamina to further *in vivo* studies.

Additional TE vascularization strategies such as further intra luminal endothelial cell co-culture, the implementation of vascular spheroids¹⁰² or vascular growth factors could enhance full tissue vascularization inside the luminal cavity interconnected with the perfused vascular network of the mBioVaSc-TERM®. Thereby, the intra luminal space of the mBioVaSc-TERM® can serve as a fully vascularized and systemically interconnected microenvironment for cells performing tissue specific function or demand-tailored drug delivery.

5.6.6 *In vivo* implantation demonstrated proof of concept but need for optimization towards a functional tissue graft or drug delivery system

Despite the long history and advancements in TE, mainly thin layered or hollow tissue graft are clinically applicable due to the urgent need for dense vascularization within in full thickness organ grafts.

Similarly for drug delivery, an implantable self-sustained on-demand system remains to be established. Amongst the first drug delivery systems, therapeutic agents coupled onto polymers provided a controlled release mathematically predictable upon dose and period. Stimuli-responsiveness allowed the timely and spatially specific drug release from polymers²⁷¹. However, polymers for drug delivery depict a single use application and require subsequent administration when consumed. With the rising prevalence of chronic disorders, however, the demand for sustainable devices continually rises. Despite pharmacological advancements upon absorption, distribution, metabolism, and excretion (ADME) of pharmaceutical compounds and promising drug delivery strategies²⁷², there are still hardly drug delivery devices in clinical trials for pharmacokinetic evaluation²⁷³. Lack of efficacy and toxicity appear to remain unmet for clinical applicability and product approval²⁷⁴.

Investigating the capacity of the mBioVaSc-TERM® as a platform technology, short-term *in vivo* proof of concept was demonstrated depicting promising results. The tight reendothelialized vessels enabled unobstructed blood perfusion anastomosed to the rat vasculature to facilitate nutrient and oxygen supply for the graft. Thereafter, the scaffold was applied in long-term implantation and analyzed upon the utilization as a cell-based implant.

Liver-like organoid culture within the mBioVaSc-TERM® lumen indicated the maintenance of *in vivo* tissue culture, though, only in short-term. Beyond 7 days *in vivo*, the implemented organoids demonstrated increased apoptosis (Fig. 19). Further vascularization inside the lumen might promote tissue survival and enable the full thickness tissue generation. Moreover, long-term culture of the liver-like organoids remains to be stabilized *in vitro* upon vitality and functionality.

In comparison, a small diameter scaffold, prevascularized by implantation of the hollow capsule until encapsulated with deposited ECM and vascular ingrowth, was utilized for

maintaining pancreatic islets viable and functional for more than 120 days^{17,238}. During the implantation period the recipient diabetic rats remained normoglycemic and vessels were demonstrated in close proximity to the insulin secreting cells in subsequent analysis²³⁸. This indicated the importance of prevascularization and the implementation of a functional tissue to pose a demand for nutrient supply and offer a benefit for the patient.

The capacity of the mBioVaSc-TERM® to serve as platform enabling the generation of a metabolic active vascularized organ and be utilized for drug release was indicated *in vitro*. Advancing from the identified drawbacks, improving long term stability *in vivo*, and demonstrating functional *in vivo* tissue substitution or drug delivery, the mBioVaSc-TERM® technology might be considered for establishing an ATMP serving as tissue graft or drug delivery system.

Demonstrating safety of the implemented cells to remain within the scaffold, fluorescently labelled cells might be cultured inside the mBioVaSc-TERM® lumen, enabling cell tracking to determine whether the cells migrate outside the graft. Secretion of fluorescent proteins or fluorescently labeled proteins would allow for tracking the distribution of the cell secretome, proving applicability as drug delivery system. Both approaches are feasible as the in-house available *In Vivo* Imaging System (IVIS) enables non-invasive imaging and monitoring.

Furthermore, demonstrating drug secretion and distribution *in vivo*, besides cells secreting fluorescent proteins a variety of available cell sources might be implemented demonstrating functional and bioactive proof of concept. Therefore the generated Activin A- or Myostatin-secreting CHO cells, the liver-like organoids might be examined upon human albumin secretion, or factor VIII secreting cells generated in a project for hemophilia A treatment. Either cell type is accessible for implementation in the mBioVaSc-TERM® with its secretome specifically detectable from blood samples taken after implantation and verified by commonly available ELISA or western blot techniques. Examination of blood samples enables the functional proof concept without end point analysis and thereby an extensive time course of steady analysis of availability of the secreted protein. Furthermore, dose and concentration of the secreted protein can be determined offering valuable clues to the cellular amount necessary for implantation to reach an effective drug level for therapeutic efficacy.

5.8 Summary

In this thesis, a rat jejunal segment was identified as suitable scaffold to function as a vascularized platform technology for TE and as drug delivery system. The miniaturized rat-derived version of the BioVaSc-TERM® provided similar properties as the porcine-derived scaffold, including an innate vascular network embedded in a natural ECM providing supply for a 3D cell co-culture environment. Despite the smaller scale, cannulation, decellularization, revascularization, *in vitro* perfusion culture, tissue generation, and anastomosis for *in vivo* application was still feasible.

With an improved decellularization protocol, the ECM components as well as the vascular structures were preserved, while host cells were removed.

Next, the acellular scaffold was characterized and recellularized after demonstration of biocompatibility. Thereby a tight endothelial barrier was established and the reendothelialized vascular network enabled physiological pulsatile perfusion culture of the arteriovenous circulation, prevented leakage, and facilitated venous return.

Subsequently, reseeded with multicellular organoids or drug secreting cells, the capacity of the mBioVaSc-TERM® as a platform technology for tissue culture and drug delivery was indicated *in vitro* demonstrating proof of concept.

Finally, the scaffold was employed for *in vivo* studies. The feeding and draining vessels of the mBioVaSc-TERM® were connected to the blood circulation of the host via anastomosis facilitating immediate blood supply. As indicated *in vitro*, also *in vivo* the tight endothelial barrier demonstrated hemocompatibility and prevented leakage, confirming vascular integrity. Short-term implantation indicated promising results for translating the mBioVaSc-TERM® into clinical application. Nevertheless, unimpeded blood perfusion only sustained during short-term studies. Analysis of long-term implantation indicated tissue integration, however, also cellular regression.

5.9 Conclusion

In conclusion, the fundamentals for a vascularized scaffold as a platform for cell, tissue/organ culture, and drug delivery was established. Based upon a decellularized rat jejunal segment with a preserved feeding and draining vascular tree, promising *in vitro*

results were achieved. For the first time, full vascularization of a 3D graft with an intact arteriovenous loop through a capillary network was demonstrated.

Despite highlighting the arteriovenous circulation within the scaffold to supply implemented co-cultures as well as the feasibility of the anastomosis to enable immediate supply *in vivo*, the effective advantage of both still has to be demonstrated for the mBioVaSc-TERM®.

Furthermore, improvement of vascular stability and the advancement of the 3D co-culture within the intraluminal compartment has to be further pursued to establish and sustain a functional full thickness, fully vascularized organ-like tissue graft.

To be considered for future ATMP development, the depicted drawbacks, in particular sustained long-term integrity *in vivo*, need to be overcome to facilitate translation into clinical applicability.

Altogether, the herein observed discrepancy between results obtained *in vitro* and *in vivo* is characteristic for TE grafts demonstrating impressive success *in vitro* and promising *in vivo* data in the short-term. However, most TE grafts unconvincingly fail in translation from bench to bedside.

Nevertheless, due to the promising proof of concept and the displayed capacity of the mBioVaSc to function as a platform for tissue grafts and drug delivery systems, the established technology will surely impact TE and RM.

5.10 Outlook on future perspectives

The mBioVaSc TERM® can be employed in basic research to examine 3D tissue culture, cell-cell and cell-matrix interactions, metabolic and toxicological surveys, and transplant development with the possibility for preclinical small animal model implantations granting faster results due to its smaller size, lower cell amount necessary for confluent culture and easier handling. The miniaturized biologically vascularized scaffold as platform technology for the generation of functional tissue grafts or the application as drug delivery system could serve as a powerful tool for TERM substituting for a loss of tissue/function or serving as a secretory active gland, dependent on the clinical and pharmaceutical issue. Upon successful proof of concept a translation into long-term small animal and preclinical large animal studies has to be evaluated.

Despite the success in reendothelialization, the established process might be improved by slower and prolonged EC infusion as well as the subsequent perfusion with circulating endothelial progenitor cells to enhance endothelialization and hemocompatibility²⁷⁵. Furthermore, fully functional mature vessels were not re-established. Mature vessels – typically composed of varying layers of smooth muscle cells, pericytes, and ECs – are more stable while newly formed vessels are less resistant to vascular regression²⁷⁰. Although a functional endothelial layer covered the retained basement membrane, sufficient for most capillaries, the absence of pericytes leads to increased leakage of plasma and blood cells²⁷⁶ impairing the maintenance of a colloid osmotic pressure. For implementation of pericytes, protocols for isolation, characterization, culture²⁷⁷, and therapeutic application²⁷⁸ are described. Moreover, the larger vessels within the mBioVaSc-TERM® lack SMCs promoting vascular sprouting, angiogenesis, maturation, functionality, and stability²⁷⁷ as well as pericytes contributing to vessel maturity, structure, and stability²⁷⁹. Beyond, embryonic stem and iPSC⁶⁷ cells depict a potentially infinite source of autologous cells for regeneration pushing towards clinical application³⁰. Furthermore, a differentiation protocol for hPSCs towards ECs, SMCs, and pericytes was established, enabling the generation of the respective vascular cells from one common source. The preliminary data gained with differentiated hPSCs demonstrated already promising results.

In addition to improving vascular stability of the vessels embedded within the scaffold ECM, the capillary network is aimed to be expanded to sprout into the intraluminal compartment to fully pervade a full thickness tissue. Intraluminal tissue vascularization within the mBioVaSc-TERM® might be achieved by implementation of vascular cells within the tissue exploiting their capacity for self-arrangement demonstrated by various cell seeding, spheroid-generation, and micro-tissue aggregation approaches^{280,281}.

The achieved success in decellularization and revascularization of a vastly branched vascular network encourages the attempt to generate custom-tailored vessels, e.g. for bypass surgeries. Certainly, the complexity of the branched capillary bed is irrelevant when generating a single straight tubular structure, however, the seemingly straightforward task proved as sophisticated endeavor as many attempts in TE failed despite an urgent demand in clinical application²⁸². Nevertheless, considering the gained

experience on decellularization, acellular vessels might be established as base framework and assembled with primary isolated endothelial cells and pericytes or respective cellular progenitors composing autologous vascular grafts. New bioreactor devices might have to be developed adaptable to the vessel size. Further functional tests will have to be included, e.g. coagulation assays, the proof of the graft's ability on vasoconstriction and -dilation²⁸³, as well as demonstrating the capability to withstand the physiological shear stress at the desired implantation site. Nevertheless, with the prevalent experience on de- and recellularization of vascular structures and the great interdisciplinary team of medical, biomedical, biological and material scientists as well as engineers, realization can confidently be approached. Thereafter, more studies on cellular reciprocal effects will be feasible due to the simpler setup.

Employing immunodeficient RNU rats²⁸⁴ for initial implantation studies enabled the evaluation of the proof of concept of the clinical applicability of the mBioVaSc-TERM®. Considering further studies, the use of autologous cells circumvents the need for the recipient to be immune-deprived.

In case of a loss of function or tissue replacement with no cells or not enough viable autologous cells extractable for sufficient expansion and graft establishment an allo- or xenogenic source will be inevitable. Thereby, immunosuppression becomes mandatory to protect the graft from the host immune response even though the application of immunosuppressants is adverse due to its side effects²⁸⁵. In this regard, the feasibility of the implementation of localized immunosuppression was discussed lately to avoid systemic effects while protecting the graft²⁸⁶. With yet only preliminary data available, localized immunosuppression emerged as a promising strategy for allo- or xenogenic graft transplantation if the utilization of autologous cells is not feasible.

Finally, for translation into clinical applicability, long-term implantation studies in small animal models and subsequently in large animals need to be feasible to prove immunogenicity, on-target toxicology, dose titration, and pharmacokinetics¹⁵⁶ of the mBioVaSc-TERM® when developed towards an ATMP as functional drug delivery system.

REFERENCES

- 1 Frantz, C., Stewart, K. M. & Weaver, V. M. The extracellular matrix at a glance. *Journal of cell science* **123**, 4195-4200, doi:10.1242/jcs.023820 (2010).
- 2 Hynes, R. O. The extracellular matrix: not just pretty fibrils. *Science (New York, N.Y.)* **326**, 1216-1219, doi:10.1126/science.1176009 (2009).
- 3 Nelson, C. M. & Bissell, M. J. Of extracellular matrix, scaffolds, and signaling: tissue architecture regulates development, homeostasis, and cancer. *Annual review of cell and developmental biology* **22**, 287-309, doi:10.1146/annurev.cellbio.22.010305.104315 (2006).
- 4 Xu, R., Boudreau, A. & Bissell, M. J. Tissue architecture and function: dynamic reciprocity via extra- and intra-cellular matrices. *Cancer metastasis reviews* **28**, 167-176, doi:10.1007/s10555-008-9178-z (2009).
- 5 Thorne, J. T. *et al.* Dynamic reciprocity between cells and their microenvironment in reproduction. *Biology of reproduction* **92**, 25, doi:10.1095/biolreprod.114.121368 (2015).
- 6 Jarvelainen, H., Sainio, A., Koulou, M., Wight, T. N. & Penttinen, R. Extracellular matrix molecules: potential targets in pharmacotherapy. *Pharmacological reviews* **61**, 198-223, doi:10.1124/pr.109.001289 (2009).
- 7 Mott, J. D. & Werb, Z. Regulation of matrix biology by matrix metalloproteinases. *Current opinion in cell biology* **16**, 558-564, doi:10.1016/j.ceb.2004.07.010 (2004).
- 8 Aitken, K. J. & Bagli, D. J. The bladder extracellular matrix. Part I: architecture, development and disease. *Nature reviews. Urology* **6**, 596-611, doi:10.1038/nrurol.2009.201 (2009).
- 9 Martin, P. & Nunan, R. Cellular and molecular mechanisms of repair in acute and chronic wound healing. *The British journal of dermatology* **173**, 370-378, doi:10.1111/bjd.13954 (2015).
- 10 Roder, P. V., Wu, B., Liu, Y. & Han, W. Pancreatic regulation of glucose homeostasis. *Experimental & molecular medicine* **48**, e219, doi:10.1038/emm.2016.6 (2016).
- 11 Schiel, R., Bambauer, R. & Steveling, A. Technology in Diabetes Treatment: Update and Future. *Artificial organs*, doi:10.1111/aor.13296 (2018).
- 12 Starzl, T. E. & Makowka, L. Organ transplantation--then and now. *Hospital physician* **23**, 28-33, 36 (1987).
- 13 Montana, E., Bonner-Weir, S. & Weir, G. C. Beta cell mass and growth after syngeneic islet cell transplantation in normal and streptozocin diabetic C57BL/6 mice. *The Journal of clinical investigation* **91**, 780-787, doi:10.1172/jci116297 (1993).
- 14 Kawahara, T. *et al.* Portal vein thrombosis is a potentially preventable complication in clinical islet transplantation. *American journal of transplantation : official journal of the American Society of Transplantation and the American Society of Transplant Surgeons* **11**, 2700-2707, doi:10.1111/j.1600-6143.2011.03717.x (2011).
- 15 Husain, S. R., Han, J., Au, P., Shannon, K. & Puri, R. K. Gene therapy for cancer: regulatory considerations for approval. *Cancer gene therapy* **22**, 554-563, doi:10.1038/cgt.2015.58 (2015).
- 16 Welman, T., Michel, S., Segaren, N. & Shanmugarajah, K. Bioengineering for Organ Transplantation: Progress and Challenges. *Bioengineered* **6**, 257-261, doi:10.1080/21655979.2015.1081320 (2015).
- 17 Pepper, A. R. *et al.* Transplantation of Human Pancreatic Endoderm Cells Reverses Diabetes Post Transplantation in a Prevascularized Subcutaneous Site. *Stem cell reports* **8**, 1689-1700, doi:10.1016/j.stemcr.2017.05.004 (2017).
- 18 Kaul, H. & Ventikos, Y. On the genealogy of tissue engineering and regenerative medicine. *Tissue Eng Part B Rev* **21**, 203-217, doi:10.1089/ten.TEB.2014.0285 (2015).
- 19 Ratner, H., Schoen, Lemons. *Biomaterials Science—An Introduction to Materials in Medicine*. (Academic Press, 1996).

- 20 Chick, L. R. Brief history and biology of skin grafting. *Ann Plast Surg* **21**, 358-365 (1988).
- 21 Jaklenc, A., Stamp, A., Deweerdt, E., Sherwin, A. & Langer, R. Progress in the tissue engineering and stem cell industry "are we there yet?". *Tissue Eng Part B Rev* **18**, 155-166, doi:10.1089/ten.TEB.2011.0553 (2012).
- 22 Hesiod. *Theogony* (700 BC).
- 23 Noh, S. *et al.* in *Clinical Regenerative Medicine in Urology* (ed Bup Wan Kim) 105-123 (Springer Singapore, 2018).
- 24 Langer, R. & Vacanti, J. P. Tissue engineering. *Science (New York, N.Y.)* **260**, 920-926 (1993).
- 25 Berthiaume, F., Maguire, T. J. & Yarmush, M. L. Tissue engineering and regenerative medicine: history, progress, and challenges. *Annual review of chemical and biomolecular engineering* **2**, 403-430, doi:10.1146/annurev-chembioeng-061010-114257 (2011).
- 26 Tabisz, B. *et al.* Site-Directed Immobilization of BMP-2: Two Approaches for the Production of Innovative Osteoinductive Scaffolds. *Biomacromolecules* **18**, 695-708, doi:10.1021/acs.biomac.6b01407 (2017).
- 27 Lanza, R., Langer, R. & Vacanti, J. *Principles of Tissue Engineering*. (Academic Press, 2007).
- 28 Daar, A. S. & Greenwood, H. L. A proposed definition of regenerative medicine. *Journal of tissue engineering and regenerative medicine* **1**, 179-184, doi:10.1002/term.20 (2007).
- 29 Mason, C. & Dunnill, P. A brief definition of regenerative medicine. *Regenerative medicine* **3**, 1-5, doi:10.2217/17460751.3.1.1 (2008).
- 30 Mao, A. S. & Mooney, D. J. Regenerative medicine: Current therapies and future directions. *Proceedings of the National Academy of Sciences of the United States of America* **112**, 14452-14459, doi:10.1073/pnas.1508520112 (2015).
- 31 Marklein, R. A. & Burdick, J. A. Controlling stem cell fate with material design. *Advanced materials (Deerfield Beach, Fla.)* **22**, 175-189, doi:10.1002/adma.200901055 (2010).
- 32 Bader, A. & Macchiarini, P. Moving towards in situ tracheal regeneration: the bionic tissue engineered transplantation approach. *Journal of cellular and molecular medicine* **14**, 1877-1889, doi:10.1111/j.1582-4934.2010.01073.x (2010).
- 33 Kim, B. S. & Mooney, D. J. Development of biocompatible synthetic extracellular matrices for tissue engineering. *Trends in biotechnology* **16**, 224-230 (1998).
- 34 Drury, J. L. & Mooney, D. J. Hydrogels for tissue engineering: scaffold design variables and applications. *Biomaterials* **24**, 4337-4351 (2003).
- 35 De France, K. J., Xu, F. & Hoare, T. Structured Macroporous Hydrogels: Progress, Challenges, and Opportunities. *Advanced healthcare materials*, doi:10.1002/adhm.201700927 (2017).
- 36 Baker, B. M. *et al.* Sacrificial nanofibrous composites provide instruction without impediment and enable functional tissue formation. *Proceedings of the National Academy of Sciences of the United States of America* **109**, 14176-14181, doi:10.1073/pnas.1206962109 (2012).
- 37 Fisher, M. B., Henning, E. A., Soegaard, N., Esterhai, J. L. & Mauck, R. L. Organized nanofibrous scaffolds that mimic the macroscopic and microscopic architecture of the knee meniscus. *Acta biomaterialia* **9**, 4496-4504, doi:10.1016/j.actbio.2012.10.018 (2013).
- 38 Lee, J. M. & Yeong, W. Y. Design and Printing Strategies in 3D Bioprinting of Cell-Hydrogels: A Review. *Advanced healthcare materials* **5**, 2856-2865, doi:10.1002/adhm.201600435 (2016).
- 39 Charbe, N., McCarron, P. A. & Tambuwala, M. M. Three-dimensional bio-printing: A new frontier in oncology research. *World journal of clinical oncology* **8**, 21-36, doi:10.5306/wjco.v8.i1.21 (2017).
- 40 Mertsching, H., Weimer, M., Kersen, S. & Brunner, H. Human skin equivalent as an alternative to animal testing. *GMS Krankenhaushygiene interdisziplinär* **3**, Doc11 (2008).
- 41 Dewan, A. K., Gibson, M. A., Elisseeff, J. H. & Trice, M. E. Evolution of autologous chondrocyte repair and comparison to other cartilage repair techniques. *BioMed research international* **2014**, 272481, doi:10.1155/2014/272481 (2014).
- 42 Dai, Y. & Foley, A. Tissue engineering approaches to heart repair. *Critical reviews in biomedical engineering* **42**, 213-227 (2014).

- 43 Monteiro, L. M., Vasques-Novoa, F., Ferreira, L., Pinto-do, O. P. & Nascimento, D. S. Restoring heart function and electrical integrity: closing the circuit. *NPJ Regen Med* **2**, 9, doi:10.1038/s41536-017-0015-2 (2017).
- 44 Fang, N. T. *et al.* Construction of tissue-engineered heart valves by using decellularized scaffolds and endothelial progenitor cells. *Chinese medical journal* **120**, 696-702 (2007).
- 45 Cheung, D. Y., Duan, B. & Butcher, J. T. Current progress in tissue engineering of heart valves: multiscale problems, multiscale solutions. *Expert opinion on biological therapy* **15**, 1155-1172, doi:10.1517/14712598.2015.1051527 (2015).
- 46 Uygun, B. E. *et al.* Organ reengineering through development of a transplantable recellularized liver graft using decellularized liver matrix. *Nature medicine* **16**, 814-820, doi:10.1038/nm.2170 (2010).
- 47 Ott, H. C. *et al.* Regeneration and orthotopic transplantation of a bioartificial lung. *Nature medicine* **16**, 927-933, doi:10.1038/nm.2193 (2010).
- 48 Raeder, R. H., Badylak, S. F., Sheehan, C., Kallakury, B. & Metzger, D. W. Natural anti-galactose alpha1,3 galactose antibodies delay, but do not prevent the acceptance of extracellular matrix xenografts. *Transplant immunology* **10**, 15-24 (2002).
- 49 Calve, S., Odelberg, S. J. & Simon, H. G. A transitional extracellular matrix instructs cell behavior during muscle regeneration. *Developmental biology* **344**, 259-271, doi:10.1016/j.ydbio.2010.05.007 (2010).
- 50 Badylak, S., Liang, A., Record, R., Tullius, R. & Hodde, J. Endothelial cell adherence to small intestinal submucosa: an acellular bioscaffold. *Biomaterials* **20**, 2257-2263 (1999).
- 51 Hodde, J. Naturally occurring scaffolds for soft tissue repair and regeneration. *Tissue engineering* **8**, 295-308, doi:10.1089/107632702753725058 (2002).
- 52 Groeber, F., Kahlig, A., Loff, S., Walles, H. & Hansmann, J. A bioreactor system for interfacial culture and physiological perfusion of vascularized tissue equivalents. *Biotechnology journal* **8**, 308-316, doi:10.1002/biot.201200160 (2013).
- 53 Pellegata, A. F., Tedeschi, A. M. & De Coppi, P. Whole Organ Tissue Vascularization: Engineering the Tree to Develop the Fruits. *Frontiers in bioengineering and biotechnology* **6**, 56, doi:10.3389/fbioe.2018.00056 (2018).
- 54 Atala, A., Bauer, S. B., Soker, S., Yoo, J. J. & Retik, A. B. Tissue-engineered autologous bladders for patients needing cystoplasty. *Lancet (London, England)* **367**, 1241-1246, doi:10.1016/s0140-6736(06)68438-9 (2006).
- 55 Raya-Rivera, A. *et al.* Tissue-engineered autologous urethras for patients who need reconstruction: an observational study. *Lancet (London, England)* **377**, 1175-1182, doi:10.1016/s0140-6736(10)62354-9 (2011).
- 56 Law, J. X., Liau, L. L., Aminuddin, B. S. & Ruzsyzmah, B. H. Tissue-engineered trachea: A review. *International journal of pediatric otorhinolaryngology* **91**, 55-63, doi:10.1016/j.ijporl.2016.10.012 (2016).
- 57 Song, J. J. *et al.* Regeneration and experimental orthotopic transplantation of a bioengineered kidney. *Nature medicine* **19**, 646-651, doi:10.1038/nm.3154 (2013).
- 58 Stabler, C. T. *et al.* Revascularization of decellularized lung scaffolds: principles and progress. *American journal of physiology. Lung cellular and molecular physiology* **309**, L1273-1285, doi:10.1152/ajplung.00237.2015 (2015).
- 59 Jank, B. J. *et al.* Engineered composite tissue as a bioartificial limb graft. *Biomaterials* **61**, 246-256, doi:10.1016/j.biomaterials.2015.04.051 (2015).
- 60 Wells, J. M. & Melton, D. A. Vertebrate endoderm development. *Annual review of cell and developmental biology* **15**, 393-410, doi:10.1146/annurev.cellbio.15.1.393 (1999).
- 61 Heinemann, T. & Honnefelder, L. Principles of ethical decision making regarding embryonic stem cell research in Germany. *Bioethics* **16**, 530-543 (2002).
- 62 Dulak, J., Szade, K., Szade, A., Nowak, W. & Jozkowicz, A. Adult stem cells: hopes and hypes of regenerative medicine. *Acta biochimica Polonica* **62**, 329-337, doi:10.18388/abp.2015_1023 (2015).

- 63 Rezza, A., Sennett, R. & Rendl, M. Adult stem cell niches: cellular and molecular components. *Current topics in developmental biology* **107**, 333-372, doi:10.1016/b978-0-12-416022-4.00012-3 (2014).
- 64 Takahashi, K. & Yamanaka, S. Induction of pluripotent stem cells from mouse embryonic and adult fibroblast cultures by defined factors. *Cell* **126**, 663-676, doi:10.1016/j.cell.2006.07.024 (2006).
- 65 Vivien, C. J., Hudson, J. E. & Porrello, E. R. Evolution, comparative biology and ontogeny of vertebrate heart regeneration. *NPJ Regenerative medicine* **1**, 16012, doi:10.1038/npjregenmed.2016.12 (2016).
- 66 OpenStax. *Anatomy & Physiology*. (OpenStax CNX, 2013).
- 67 Lengner, C. J. iPS cell technology in regenerative medicine. *Annals of the New York Academy of Sciences* **1192**, 38-44, doi:10.1111/j.1749-6632.2009.05213.x (2010).
- 68 Macchiarini, P. *et al.* Clinical transplantation of a tissue-engineered airway. *Lancet (London, England)* **372**, 2023-2030, doi:10.1016/s0140-6736(08)61598-6 (2008).
- 69 Bujia, J., Wilmes, E., Hammer, C. & Kastenbauer, E. Tracheal transplantation: demonstration of HLA class II subregion gene products on human trachea. *Acta oto-laryngologica* **110**, 149-154 (1990).
- 70 Grillo, H. C. Tracheal replacement: a critical review. *The Annals of thoracic surgery* **73**, 1995-2004 (2002).
- 71 Scherer, M. A. *et al.* Experimental bioprosthetic reconstruction of the trachea. *Archives of oto-rhino-laryngology* **243**, 215-223 (1986).
- 72 Nakanishi, R., Hashimoto, M., Muranaka, H. & Yasumoto, K. Effect of cryopreservation period on rat tracheal allografts. *The Journal of heart and lung transplantation : the official publication of the International Society for Heart Transplantation* **20**, 1010-1015 (2001).
- 73 Shi, H., Xu, H., Lu, D. & Wu, J. Animal models of tracheal allotransplantation using vitrified cryopreservation. *The Journal of thoracic and cardiovascular surgery* **138**, 1222-1226, doi:10.1016/j.jtcvs.2009.05.028 (2009).
- 74 Deschamps, C. *et al.* Cryopreservation of canine trachea: functional and histological changes. *The Annals of thoracic surgery* **47**, 208-212 (1989).
- 75 Lenot, B., Macchiarini, P., Dulmet, E., Weiss, M. & Darteville, P. Tracheal allograft replacement. An unsuccessful method. *European journal of cardio-thoracic surgery : official journal of the European Association for Cardio-thoracic Surgery* **7**, 648-652 (1993).
- 76 Macchiarini, P., Walles, T., Biancosino, C. & Mertsching, H. First human transplantation of a bioengineered airway tissue. *The Journal of thoracic and cardiovascular surgery* **128**, 638-641, doi:10.1016/j.jtcvs.2004.02.042 (2004).
- 77 Walles, T. *et al.* Experimental generation of a tissue-engineered functional and vascularized trachea. *The Journal of thoracic and cardiovascular surgery* **128**, 900-906, doi:10.1016/j.jtcvs.2004.07.036 (2004).
- 78 Yuan, S. Y. & Rigor, R. R. in *Regulation of Endothelial Barrier Function* (Morgan & Claypool Life Sciences Copyright (c) 2011 by Morgan & Claypool Life Sciences., 2010).
- 79 Ribatti, D., Nico, B. & Crivellato, E. The development of the vascular system: a historical overview. *Methods in molecular biology (Clifton, N.J.)* **1214**, 1-14, doi:10.1007/978-1-4939-1462-3_1 (2015).
- 80 Lammert, E., Cleaver, O. & Melton, D. Induction of pancreatic differentiation by signals from blood vessels. *Science (New York, N.Y.)* **294**, 564-567, doi:10.1126/science.1064344 (2001).
- 81 Wang, H. U., Chen, Z. F. & Anderson, D. J. Molecular distinction and angiogenic interaction between embryonic arteries and veins revealed by ephrin-B2 and its receptor Eph-B4. *Cell* **93**, 741-753 (1998).
- 82 Zhong, T. P., Childs, S., Leu, J. P. & Fishman, M. C. Gridlock signalling pathway fashions the first embryonic artery. *Nature* **414**, 216-220, doi:10.1038/35102599 (2001).
- 83 Risau, W. & Flamme, I. Vasculogenesis. *Annual review of cell and developmental biology* **11**, 73-91, doi:10.1146/annurev.cb.11.110195.000445 (1995).

- 84 Risau, W. Mechanisms of angiogenesis. *Nature* **386**, 671-674, doi:10.1038/386671a0 (1997).
- 85 le Noble, F. *et al.* Control of arterial branching morphogenesis in embryogenesis: go with the flow. *Cardiovascular research* **65**, 619-628, doi:10.1016/j.cardiores.2004.09.018 (2005).
- 86 Metz, R. P., Patterson, J. L. & Wilson, E. Vascular smooth muscle cells: isolation, culture, and characterization. *Methods in molecular biology (Clifton, N.J.)* **843**, 169-176, doi:10.1007/978-1-61779-523-7_16 (2012).
- 87 Marieb, E. N., Wilhelm, P. B., Hoehn, K., Hutchinson, M. & Mallatt, J. *Human Anatomy & Physiology*. (Benjamin-Cummings Publishing Company, 2013).
- 88 Folkman, J. & Hochberg, M. Self-regulation of growth in three dimensions. *The Journal of experimental medicine* **138**, 745-753 (1973).
- 89 Tian, L. & George, S. C. Biomaterials to prevascularize engineered tissues. *Journal of cardiovascular translational research* **4**, 685-698, doi:10.1007/s12265-011-9301-3 (2011).
- 90 Lesman, A. *et al.* Engineering vessel-like networks within multicellular fibrin-based constructs. *Biomaterials* **32**, 7856-7869, doi:10.1016/j.biomaterials.2011.07.003 (2011).
- 91 Lovett, M., Lee, K., Edwards, A. & Kaplan, D. L. Vascularization strategies for tissue engineering. *Tissue Eng Part B Rev* **15**, 353-370, doi:10.1089/ten.TEB.2009.0085 (2009).
- 92 Radisic, M. *et al.* Biomimetic approach to cardiac tissue engineering: oxygen carriers and channeled scaffolds. *Tissue engineering* **12**, 2077-2091, doi:10.1089/ten.2006.12.2077 (2006).
- 93 Richardson, T. P., Peters, M. C., Ennett, A. B. & Mooney, D. J. Polymeric system for dual growth factor delivery. *Nature biotechnology* **19**, 1029-1034, doi:10.1038/nbt1101-1029 (2001).
- 94 Balamurugan, A. N. *et al.* Bioartificial pancreas transplantation at prevascularized intermuscular space: effect of angiogenesis induction on islet survival. *Pancreas* **26**, 279-285 (2003).
- 95 Rucker, C., Kirch, H., Pullig, O. & Walles, H. Strategies and First Advances in the Development of Prevascularized Bone Implants. *Current molecular biology reports* **2**, 149-157, doi:10.1007/s40610-016-0046-2 (2016).
- 96 Montano, I. *et al.* Formation of human capillaries in vitro: the engineering of prevascularized matrices. *Tissue engineering. Part A* **16**, 269-282, doi:10.1089/ten.TEA.2008.0550 (2010).
- 97 Hegen, A. *et al.* Efficient in vivo vascularization of tissue-engineering scaffolds. *Journal of tissue engineering and regenerative medicine* **5**, e52-62, doi:10.1002/term.336 (2011).
- 98 Takebe, T. *et al.* Engineering of human hepatic tissue with functional vascular networks. *Organogenesis* **10**, 260-267, doi:10.4161/org.27590 (2014).
- 99 Wenger, A. *et al.* Modulation of in vitro angiogenesis in a three-dimensional spheroidal coculture model for bone tissue engineering. *Tissue engineering* **10**, 1536-1547, doi:10.1089/ten.2004.10.1536 (2004).
- 100 Borges, J. *et al.* Engineered adipose tissue supplied by functional microvessels. *Tissue engineering* **9**, 1263-1270, doi:10.1089/10763270360728170 (2003).
- 101 Unger, R. E. *et al.* Tissue-like self-assembly in cocultures of endothelial cells and osteoblasts and the formation of microcapillary-like structures on three-dimensional porous biomaterials. *Biomaterials* **28**, 3965-3976, doi:10.1016/j.biomaterials.2007.05.032 (2007).
- 102 Finkenzeller, G., Torio-Padron, N., Momeni, A., Mehlhorn, A. T. & Stark, G. B. In vitro angiogenesis properties of endothelial progenitor cells: a promising tool for vascularization of ex vivo engineered tissues. *Tissue engineering* **13**, 1413-1420, doi:10.1089/ten.2006.0369 (2007).
- 103 Wenger, A. *et al.* Development and characterization of a spheroidal coculture model of endothelial cells and fibroblasts for improving angiogenesis in tissue engineering. *Cells, tissues, organs* **181**, 80-88, doi:10.1159/000091097 (2005).
- 104 Lokmic, Z., Stillaert, F., Morrison, W. A., Thompson, E. W. & Mitchell, G. M. An arteriovenous loop in a protected space generates a permanent, highly vascular, tissue-engineered construct. *FASEB journal : official publication of the Federation of American Societies for Experimental Biology* **21**, 511-522, doi:10.1096/fj.06-6614com (2007).

- 105 Manasseri, B. *et al.* Microsurgical arterovenous loops and biological templates: a novel in vivo chamber for tissue engineering. *Microsurgery* **27**, 623-629, doi:10.1002/micr.20415 (2007).
- 106 Morritt, A. N. *et al.* Cardiac tissue engineering in an in vivo vascularized chamber. *Circulation* **115**, 353-360, doi:10.1161/circulationaha.106.657379 (2007).
- 107 Beier, J. P. *et al.* De novo generation of axially vascularized tissue in a large animal model. *Microsurgery* **29**, 42-51, doi:10.1002/micr.20564 (2009).
- 108 Laschke, M. W. *et al.* Angiogenesis in tissue engineering: breathing life into constructed tissue substitutes. *Tissue engineering* **12**, 2093-2104, doi:10.1089/ten.2006.12.2093 (2006).
- 109 Chen, X. *et al.* Prevascularization of a fibrin-based tissue construct accelerates the formation of functional anastomosis with host vasculature. *Tissue engineering. Part A* **15**, 1363-1371, doi:10.1089/ten.tea.2008.0314 (2009).
- 110 Warnke, P. H. *et al.* Growth and transplantation of a custom vascularised bone graft in a man. *Lancet (London, England)* **364**, 766-770, doi:10.1016/s0140-6736(04)16935-3 (2004).
- 111 Mertsching, H., Walles, T., Hofmann, M., Schanz, J. & Knapp, W. H. Engineering of a vascularized scaffold for artificial tissue and organ generation. *Biomaterials* **26**, 6610-6617, doi:10.1016/j.biomaterials.2005.04.048 (2005).
- 112 Schultheiss, D. *et al.* [Biological vascularized matrix (BioVaM): a new method for solving the perfusion problems in tissue engineering]. *Der Urologe. Ausg. A* **43**, 1223-1228, doi:10.1007/s00120-004-0702-7 (2004).
- 113 Mertsching, H. *et al.* Generation and transplantation of an autologous vascularized bioartificial human tissue. *Transplantation* **88**, 203-210, doi:10.1097/TP.0b013e3181ac15e1 (2009).
- 114 Burkard, A. *et al.* Generation of proliferating human hepatocytes using Upcyte(R) technology: characterisation and applications in induction and cytotoxicity assays. *Xenobiotica; the fate of foreign compounds in biological systems* **42**, 939-956, doi:10.3109/00498254.2012.675093 (2012).
- 115 Ramachandran, S. D. *et al.* Applicability of second-generation upcyte(R) human hepatocytes for use in CYP inhibition and induction studies. *Pharmacology research & perspectives* **3**, e00161, doi:10.1002/prp2.161 (2015).
- 116 Totonelli, G. *et al.* A rat decellularized small bowel scaffold that preserves villus-crypt architecture for intestinal regeneration. *Biomaterials* **33**, 3401-3410, doi:10.1016/j.biomaterials.2012.01.012 (2012).
- 117 Maghsoudlou, P., Totonelli, G., Loukogeorgakis, S. P., Eaton, S. & De Coppi, P. A decellularization methodology for the production of a natural acellular intestinal matrix. *Journal of visualized experiments : JoVE*, doi:10.3791/50658 (2013).
- 118 Ramachandran, S. D. *et al.* In Vitro Generation of Functional Liver Organoid-Like Structures Using Adult Human Cells. *PLoS one* **10**, e0139345, doi:10.1371/journal.pone.0139345 (2015).
- 119 Strauss, O., Phillips, A., Ruggiero, K., Bartlett, A. & Dunbar, P. R. Immunofluorescence identifies distinct subsets of endothelial cells in the human liver. *Scientific reports* **7**, 44356, doi:10.1038/srep44356 (2017).
- 120 Brede, C. *et al.* Mapping immune processes in intact tissues at cellular resolution. *The Journal of clinical investigation* **122**, 4439-4446, doi:10.1172/jci65100 (2012).
- 121 Schick, M. A. *et al.* Phosphodiesterase-4 inhibition as a therapeutic approach to treat capillary leakage in systemic inflammation. *The Journal of physiology* **590**, 2693-2708, doi:10.1113/jphysiol.2012.232116 (2012).
- 122 Phillips, D. J., Brauman, J. N., Mason, A. J., de Kretser, D. M. & Hedger, M. P. A sensitive and specific in vitro bioassay for activin using a mouse plasmacytoma cell line, MPC-11. *The Journal of endocrinology* **162**, 111-116 (1999).
- 123 Ingulli, E. Mechanism of cellular rejection in transplantation. *Pediatric nephrology (Berlin, Germany)* **25**, 61-74, doi:10.1007/s00467-008-1020-x (2010).
- 124 Bell, D. A., Morrison, B. & VandenBygaart, P. Immunogenic DNA-related factors. Nucleosomes spontaneously released from normal murine lymphoid cells stimulate proliferation and

- immunoglobulin synthesis of normal mouse lymphocytes. *The Journal of clinical investigation* **85**, 1487-1496, doi:10.1172/jci114595 (1990).
- 125 Bastian, D., Borel, H., Sasaki, T., Steinberg, A. D. & Borel, Y. Immune response to nucleic acid antigens and native DNA by human peripheral blood lymphocytes in vitro. *Journal of immunology (Baltimore, Md. : 1950)* **135**, 1772-1777 (1985).
- 126 Crapo, P. M., Gilbert, T. W. & Badylak, S. F. An overview of tissue and whole organ decellularization processes. *Biomaterials* **32**, 3233-3243, doi:10.1016/j.biomaterials.2011.01.057 (2011).
- 127 Meyer, U., Meyer, T., Handschel, J. & Wiesmann, H. P. *Fundamentals of Tissue Engineering and Regenerative Medicine*. (Springer Berlin Heidelberg, 2009).
- 128 Kress, S. *et al.* Evaluation of a Miniaturized Biologically Vascularized Scaffold in vitro and in vivo. *Scientific reports* **8**, 4719, doi:10.1038/s41598-018-22688-w (2018).
- 129 Schnoor, M. *et al.* Cortactin deficiency is associated with reduced neutrophil recruitment but increased vascular permeability in vivo. *The Journal of experimental medicine* **208**, 1721-1735, doi:10.1084/jem.20101920 (2011).
- 130 Resnick, N. *et al.* Fluid shear stress and the vascular endothelium: for better and for worse. *Progress in biophysics and molecular biology* **81**, 177-199 (2003).
- 131 von Horn, C. & Minor, T. Isolated kidney perfusion: the influence of pulsatile flow. *Scandinavian journal of clinical and laboratory investigation* **78**, 131-135, doi:10.1080/00365513.2017.1422539 (2018).
- 132 Kannan, R. Y., Salacinski, H. J., Sales, K., Butler, P. & Seifalian, A. M. The roles of tissue engineering and vascularisation in the development of micro-vascular networks: a review. *Biomaterials* **26**, 1857-1875, doi:10.1016/j.biomaterials.2004.07.006 (2005).
- 133 Sarin, H. Physiologic upper limits of pore size of different blood capillary types and another perspective on the dual pore theory of microvascular permeability. *Journal of angiogenesis research* **2**, 14, doi:10.1186/2040-2384-2-14 (2010).
- 134 Shelton, E. L. & Bader, D. M. Thymosin beta4 mobilizes mesothelial cells for blood vessel repair. *Annals of the New York Academy of Sciences* **1269**, 125-130, doi:10.1111/j.1749-6632.2012.06713.x (2012).
- 135 Kikuchi, K. *et al.* tcf21+ epicardial cells adopt non-myocardial fates during zebrafish heart development and regeneration. *Development (Cambridge, England)* **138**, 2895-2902, doi:10.1242/dev.067041 (2011).
- 136 Elmadbouh, I. *et al.* Mesothelial cell transplantation in the infarct scar induces neovascularization and improves heart function. *Cardiovascular research* **68**, 307-317, doi:10.1016/j.cardiores.2005.05.022 (2005).
- 137 Ozerdem, U., Grako, K. A., Dahlin-Huppe, K., Monosov, E. & Stallcup, W. B. NG2 proteoglycan is expressed exclusively by mural cells during vascular morphogenesis. *Developmental dynamics : an official publication of the American Association of Anatomists* **222**, 218-227, doi:10.1002/dvdy.1200 (2001).
- 138 Wong, T., McGrath, J. A. & Navsaria, H. The role of fibroblasts in tissue engineering and regeneration. *The British journal of dermatology* **156**, 1149-1155, doi:10.1111/j.1365-2133.2007.07914.x (2007).
- 139 Rui, L. Energy metabolism in the liver. *Comprehensive Physiology* **4**, 177-197, doi:10.1002/cphy.c130024 (2014).
- 140 Rodriguez, J. *et al.* Myostatin and the skeletal muscle atrophy and hypertrophy signaling pathways. *Cellular and molecular life sciences : CMLS* **71**, 4361-4371, doi:10.1007/s00018-014-1689-x (2014).
- 141 Buerck, L. W. *et al.* LEA29Y expression in transgenic neonatal porcine islet-like cluster promotes long-lasting xenograft survival in humanized mice without immunosuppressive therapy. *Scientific reports* **7**, 3572, doi:10.1038/s41598-017-03913-4 (2017).

- 142 Jimenez-Vera, E., Davies, S., Phillips, P., O'Connell, P. J. & Hawthorne, W. J. Long-term cultured neonatal islet cell clusters demonstrate better outcomes for reversal of diabetes: in vivo and molecular profiles. *Xenotransplantation* **22**, 114-123, doi:10.1111/xen.12151 (2015).
- 143 Murray, C. J. L. & Lopez, A. D. *The Global burden of disease : a comprehensive assessment of mortality and disability from diseases, injuries, and risk factors in 1990 and projected to 2020*. (Harvard School of Public Health, 1996).
- 144 Mahillo, B., Carmona, M., Alvarez, M., Noel, L. & Matesanz, R. Global Database on Donation and Transplantation: goals, methods and critical issues (www.transplant-observatory.org). *Transplantation reviews (Orlando, Fla.)* **27**, 57-60, doi:10.1016/j.trre.2013.01.001 (2013).
- 145 Gabouev, A. I. *et al.* In vitro construction of urinary bladder wall using porcine primary cells reseeded on acellularized bladder matrix and small intestinal submucosa. *The International journal of artificial organs* **26**, 935-942 (2003).
- 146 Jensen, T. *et al.* Biomimetic and synthetic esophageal tissue engineering. *Biomaterials* **57**, 133-141, doi:10.1016/j.biomaterials.2015.04.004 (2015).
- 147 Mostow, E. N., Haraway, G. D., Dalsing, M., Hodde, J. P. & King, D. Effectiveness of an extracellular matrix graft (OASIS Wound Matrix) in the treatment of chronic leg ulcers: a randomized clinical trial. *Journal of vascular surgery* **41**, 837-843, doi:10.1016/j.jvs.2005.01.042 (2005).
- 148 Ott, H. C. *et al.* Perfusion-decellularized matrix: using nature's platform to engineer a bioartificial heart. *Nature medicine* **14**, 213-221, doi:10.1038/nm1684 (2008).
- 149 Badylak, S. F., Taylor, D. & Uygun, K. Whole-organ tissue engineering: decellularization and recellularization of three-dimensional matrix scaffolds. *Annual review of biomedical engineering* **13**, 27-53, doi:10.1146/annurev-bioeng-071910-124743 (2011).
- 150 Groeber, F. *et al.* A first vascularized skin equivalent for as an alternative to animal experimentation. *Altex* **33**, 415-422, doi:10.14573/altex.1604041 (2016).
- 151 Kremer, A. *et al.* Three-Dimensional Coculture of Meniscal Cells and Mesenchymal Stem Cells in Collagen Type I Hydrogel on a Small Intestinal Matrix-A Pilot Study Toward Equine Meniscus Tissue Engineering. *Tissue engineering. Part A*, doi:10.1089/ten.TEA.2016.0317 (2017).
- 152 Schweinlin, M. *et al.* Development of an Advanced Primary Human In Vitro Model of the Small Intestine. *Tissue engineering. Part C, Methods* **22**, 873-883, doi:10.1089/ten.TEC.2016.0101 (2016).
- 153 Gottlich, C. *et al.* A Combined 3D Tissue Engineered In Vitro/In Silico Lung Tumor Model for Predicting Drug Effectiveness in Specific Mutational Backgrounds. *Journal of visualized experiments : JoVE*, e53885, doi:10.3791/53885 (2016).
- 154 Moll, C. *et al.* Tissue engineering of a human 3D in vitro tumor test system. *Journal of visualized experiments : JoVE*, doi:10.3791/50460 (2013).
- 155 Stratmann, A. T. *et al.* Establishment of a human 3D lung cancer model based on a biological tissue matrix combined with a Boolean in silico model. *Molecular oncology* **8**, 351-365, doi:10.1016/j.molonc.2013.11.009 (2014).
- 156 Lehmann, J., Schulz, R. M. & Sanzenbacher, R. [Strategic considerations on the design and choice of animal models for non-clinical investigations of cell-based medicinal products]. *Bundesgesundheitsblatt, Gesundheitsforschung, Gesundheitsschutz* **58**, 1215-1224, doi:10.1007/s00103-015-2239-x (2015).
- 157 Kew, S. J. *et al.* Synthetic collagen fascicles for the regeneration of tendon tissue. *Acta biomaterialia* **8**, 3723-3731, doi:10.1016/j.actbio.2012.06.018 (2012).
- 158 Lu, T. Y. *et al.* Repopulation of decellularized mouse heart with human induced pluripotent stem cell-derived cardiovascular progenitor cells. *Nature communications* **4**, 2307, doi:10.1038/ncomms3307 (2013).
- 159 Daly, A. B. *et al.* Initial binding and recellularization of decellularized mouse lung scaffolds with bone marrow-derived mesenchymal stromal cells. *Tissue engineering. Part A* **18**, 1-16, doi:10.1089/ten.TEA.2011.0301 (2012).

- 160 Wallis, J. M. *et al.* Comparative assessment of detergent-based protocols for mouse lung decellularization and re-cellularization. *Tissue engineering. Part C, Methods* **18**, 420-432, doi:10.1089/ten.TEC.2011.0567 (2012).
- 161 Drake, R. L., Vogl, W., Tibbitts, A. W. M. & Richardson, P. *Gray's anatomy for students*. 273–275 (Elsevier/Churchill Livingstone, 2005).
- 162 Rieder, E. *et al.* Decellularization protocols of porcine heart valves differ importantly in efficiency of cell removal and susceptibility of the matrix to recellularization with human vascular cells. *The Journal of thoracic and cardiovascular surgery* **127**, 399-405, doi:10.1016/j.jtcvs.2003.06.017 (2004).
- 163 Kajbafzadeh, A. M., Javan-Farazmand, N., Monajemzadeh, M. & Baghayee, A. Determining the optimal decellularization and sterilization protocol for preparing a tissue scaffold of a human-sized liver tissue. *Tissue engineering. Part C, Methods* **19**, 642-651, doi:10.1089/ten.TEC.2012.0334 (2013).
- 164 Arenas-Herrera, J. E., Ko, I. K., Atala, A. & Yoo, J. J. Decellularization for whole organ bioengineering. *Biomedical materials (Bristol, England)* **8**, 014106, doi:10.1088/1748-6041/8/1/014106 (2013).
- 165 Gilbert, T. W., Sellaro, T. L. & Badylak, S. F. Decellularization of tissues and organs. *Biomaterials* **27**, 3675-3683, doi:10.1016/j.biomaterials.2006.02.014 (2006).
- 166 Grauss, R. W. *et al.* Histological evaluation of decellularised porcine aortic valves: matrix changes due to different decellularisation methods. *European journal of cardio-thoracic surgery : official journal of the European Association for Cardio-thoracic Surgery* **27**, 566-571, doi:10.1016/j.ejcts.2004.12.052 (2005).
- 167 Fitzpatrick, J. C., Clark, P. M. & Capaldi, F. M. Effect of decellularization protocol on the mechanical behavior of porcine descending aorta. *International journal of biomaterials* **2010**, doi:10.1155/2010/620503 (2010).
- 168 Keane, T. J., Swinehart, I. T. & Badylak, S. F. Methods of tissue decellularization used for preparation of biologic scaffolds and in vivo relevance. *Methods (San Diego, Calif.)* **84**, 25-34, doi:10.1016/j.ymeth.2015.03.005 (2015).
- 169 Montoya, C. V. & McFetridge, P. S. Preparation of ex vivo-based biomaterials using convective flow decellularization. *Tissue engineering. Part C, Methods* **15**, 191-200, doi:10.1089/ten.tec.2008.0372 (2009).
- 170 Hussein, K. H., Park, K. M., Kang, K. S. & Woo, H. M. Biocompatibility evaluation of tissue-engineered decellularized scaffolds for biomedical application. *Materials science & engineering. C, Materials for biological applications* **67**, 766-778, doi:10.1016/j.msec.2016.05.068 (2016).
- 171 Hodde, J. P., Record, R. D., Tullius, R. S. & Badylak, S. F. Retention of endothelial cell adherence to porcine-derived extracellular matrix after disinfection and sterilization. *Tissue engineering* **8**, 225-234, doi:10.1089/107632702753724996 (2002).
- 172 Leitinger, B. & Hohenester, E. Mammalian collagen receptors. *Matrix biology : journal of the International Society for Matrix Biology* **26**, 146-155, doi:10.1016/j.matbio.2006.10.007 (2007).
- 173 Rozario, T. & DeSimone, D. W. The extracellular matrix in development and morphogenesis: a dynamic view. *Developmental biology* **341**, 126-140, doi:10.1016/j.ydbio.2009.10.026 (2010).
- 174 Wise, S. G. & Weiss, A. S. Tropoelastin. *The international journal of biochemistry & cell biology* **41**, 494-497, doi:10.1016/j.biocel.2008.03.017 (2009).
- 175 Miosge, N. The ultrastructural composition of basement membranes in vivo. *Histology and histopathology* **16**, 1239-1248 (2001).
- 176 Daly, K. A. *et al.* The host response to endotoxin-contaminated dermal matrix. *Tissue engineering. Part A* **18**, 1293-1303, doi:10.1089/ten.TEA.2011.0597 (2012).
- 177 Keane, T. J., Londono, R., Turner, N. J. & Badylak, S. F. Consequences of ineffective decellularization of biologic scaffolds on the host response. *Biomaterials* **33**, 1771-1781, doi:10.1016/j.biomaterials.2011.10.054 (2012).

- 178 Gilbert, T. W., Freund, J. M. & Badylak, S. F. Quantification of DNA in biologic scaffold materials. *The Journal of surgical research* **152**, 135-139, doi:10.1016/j.jss.2008.02.013 (2009).
- 179 Ge, Y., Ezzell, R. M. & Warren, H. S. Localization of endotoxin in the rat intestinal epithelium. *The Journal of infectious diseases* **182**, 873-881, doi:10.1086/315784 (2000).
- 180 Ziats, N. P., Miller, K. M. & Anderson, J. M. In vitro and in vivo interactions of cells with biomaterials. *Biomaterials* **9**, 5-13 (1988).
- 181 Murray, P. E., Garcia Godoy, C. & Garcia Godoy, F. How is the biocompatibility of dental biomaterials evaluated? *Medicina oral, patologia oral y cirugia bucal* **12**, E258-266 (2007).
- 182 Dettin, M. *et al.* Natural Scaffolds for Regenerative Medicine: Direct Determination of Detergents Entrapped in Decellularized Heart Valves. *BioMed research international* **2017**, 9274135, doi:10.1155/2017/9274135 (2017).
- 183 Cenni, E. *et al.* Established cell lines and primary cultures in testing medical devices in vitro. *Toxicology in vitro : an international journal published in association with BIBRA* **13**, 801-810 (1999).
- 184 Ekser, B. & Cooper, D. K. Overcoming the barriers to xenotransplantation: prospects for the future. *Expert review of clinical immunology* **6**, 219-230 (2010).
- 185 Naso, F., Gandaglia, A., Iop, L., Spina, M. & Gerosa, G. Alpha-Gal detectors in xenotransplantation research: a word of caution. *Xenotransplantation* **19**, 215-220, doi:10.1111/j.1399-3089.2012.00714.x (2012).
- 186 Naso, F., Gandaglia, A., Iop, L., Spina, M. & Gerosa, G. First quantitative assay of alpha-Gal in soft tissues: presence and distribution of the epitope before and after cell removal from xenogeneic heart valves. *Acta biomaterialia* **7**, 1728-1734, doi:10.1016/j.actbio.2010.11.030 (2011).
- 187 Jannasch, M. *et al.* A comparative multi-parametric in vitro model identifies the power of test conditions to predict the fibrotic tendency of a biomaterial. *Scientific reports* **7**, 1689, doi:10.1038/s41598-017-01584-9 (2017).
- 188 Jannasch, M. *et al.* In vitro chemotaxis and tissue remodeling assays quantitatively characterize foreign body reaction. *Altex* **34**, 253-266, doi:10.14573/altex.1610071 (2017).
- 189 Lesage, F. *et al.* Minimal modulation of the host immune response to SIS matrix implants by mesenchymal stem cells from the amniotic fluid. *Hernia : the journal of hernias and abdominal wall surgery* **21**, 973-982, doi:10.1007/s10029-017-1635-6 (2017).
- 190 Kutschka, I. *et al.* Collagen matrices enhance survival of transplanted cardiomyoblasts and contribute to functional improvement of ischemic rat hearts. *Circulation* **114**, 1167-1173, doi:10.1161/circulationaha.105.001297 (2006).
- 191 Kumar, V. A., Brewster, L. P., Caves, J. M. & Chaikof, E. L. Tissue Engineering of Blood Vessels: Functional Requirements, Progress, and Future Challenges. *Cardiovascular engineering and technology* **2**, 137-148, doi:10.1007/s13239-011-0049-3 (2011).
- 192 McGuigan, A. P. & Sefton, M. V. The influence of biomaterials on endothelial cell thrombogenicity. *Biomaterials* **28**, 2547-2571, doi:<http://dx.doi.org/10.1016/j.biomaterials.2007.01.039> (2007).
- 193 Neeves, K. B. Collagen-induced thrombosis in large vessels using native prothrombotic substrates. *Thrombosis research* **131**, 1-2, doi:10.1016/j.thromres.2012.11.007 (2013).
- 194 Zhu, S. & Diamond, S. L. Contact activation of blood coagulation on a defined kaolin/collagen surface in a microfluidic assay. *Thrombosis research* **134**, 1335-1343, doi:10.1016/j.thromres.2014.09.030 (2014).
- 195 Palta, S., Saroa, R. & Palta, A. Overview of the coagulation system. *Indian journal of anaesthesia* **58**, 515-523, doi:10.4103/0019-5049.144643 (2014).
- 196 Miettinen, M., Lindenmayer, A. E. & Chaubal, A. Endothelial cell markers CD31, CD34, and BNH9 antibody to H- and Y-antigens--evaluation of their specificity and sensitivity in the diagnosis of vascular tumors and comparison with von Willebrand factor. *Modern pathology : an official journal of the United States and Canadian Academy of Pathology, Inc* **7**, 82-90 (1994).

- 197 Lampugnani, M. G., Orsenigo, F., Gagliani, M. C., Tacchetti, C. & Dejana, E. Vascular endothelial cadherin controls VEGFR-2 internalization and signaling from intracellular compartments. *The Journal of cell biology* **174**, 593-604, doi:10.1083/jcb.200602080 (2006).
- 198 Dew, L., English, W. R., Chong, C. K. & MacNeil, S. Investigating Neovascularization in Rat Decellularized Intestine: An In Vitro Platform for Studying Angiogenesis. *Tissue engineering. Part A* **22**, 1317-1326, doi:10.1089/ten.TEA.2016.0131 (2016).
- 199 Kalluri, R. Basement membranes: structure, assembly and role in tumour angiogenesis. *Nature reviews. Cancer* **3**, 422-433, doi:10.1038/nrc1094 (2003).
- 200 Ausprunk, D. H. & Folkman, J. Migration and proliferation of endothelial cells in preformed and newly formed blood vessels during tumor angiogenesis. *Microvascular research* **14**, 53-65 (1977).
- 201 Yuan, Y., Granger, H. J., Zawieja, D. C. & Chilian, W. M. Flow modulates coronary venular permeability by a nitric oxide-related mechanism. *The American journal of physiology* **263**, H641-646 (1992).
- 202 Scallan, J., Huxley, V. H. & Korthuis, R. J. in *Capillary Fluid Exchange: Regulation, Functions, and Pathology* (Morgan & Claypool Life Sciences Copyright (c) 2010 by Morgan & Claypool Life Sciences., 2010).
- 203 Hattori, K. *et al.* Microfluidic perfusion culture chip providing different strengths of shear stress for analysis of vascular endothelial function. *Journal of bioscience and bioengineering* **118**, 327-332, doi:10.1016/j.jbiosc.2014.02.006 (2014).
- 204 Tousoulis, D., Kampoli, A. M., Tentolouris, C., Papageorgiou, N. & Stefanadis, C. The role of nitric oxide on endothelial function. *Current vascular pharmacology* **10**, 4-18 (2012).
- 205 von Horn, C. & Minor, T. Isolated kidney perfusion: the influence of pulsatile flow. *Scandinavian journal of clinical and laboratory investigation*, 1-5, doi:10.1080/00365513.2017.1422539 (2018).
- 206 Schaper, W. & Scholz, D. Factors regulating arteriogenesis. *Arteriosclerosis, thrombosis, and vascular biology* **23**, 1143-1151, doi:10.1161/01.atv.0000069625.11230.96 (2003).
- 207 Youmans, J. B., Wells, H. S., Donley, D., Miller, D. G. & Frank, H. THE EFFECT OF POSTURE (STANDING) ON THE SERUM PROTEIN CONCENTRATION AND COLLOID OSMOTIC PRESSURE OF BLOOD FROM THE FOOT IN RELATION TO THE FORMATION OF EDEMA. *The Journal of clinical investigation* **13**, 447-459, doi:10.1172/jci100597 (1934).
- 208 Weisberg, H. F. Osmotic pressure of the serum proteins. *Annals of clinical and laboratory science* **8**, 155-164 (1978).
- 209 Norman, K. Techniques: Intravital microscopy--a method for investigating disseminated intravascular coagulation? *Trends in pharmacological sciences* **26**, 327-332, doi:10.1016/j.tips.2005.04.002 (2005).
- 210 Zhou, J. *et al.* Impact of heart valve decellularization on 3-D ultrastructure, immunogenicity and thrombogenicity. *Biomaterials* **31**, 2549-2554, doi:10.1016/j.biomaterials.2009.11.088 (2010).
- 211 Baptista, P. M. *et al.* The use of whole organ decellularization for the generation of a vascularized liver organoid. *Hepatology (Baltimore, Md.)* **53**, 604-617, doi:10.1002/hep.24067 (2011).
- 212 Mutsaers, S. E. & Wilkosz, S. Structure and function of mesothelial cells. *Cancer treatment and research* **134**, 1-19 (2007).
- 213 Rinkevich, Y. *et al.* Identification and prospective isolation of a mesothelial precursor lineage giving rise to smooth muscle cells and fibroblasts for mammalian internal organs, and their vasculature. *Nature cell biology* **14**, 1251-1260, doi:10.1038/ncb2610 (2012).
- 214 Wilm, B., Ipenberg, A., Hastie, N. D., Burch, J. B. & Bader, D. M. The serosal mesothelium is a major source of smooth muscle cells of the gut vasculature. *Development (Cambridge, England)* **132**, 5317-5328, doi:10.1242/dev.02141 (2005).

- 215 Kavyasudha, C. *et al.* Clinical Applications of Induced Pluripotent Stem Cells - Stato Attuale. *Advances in experimental medicine and biology* **1079**, 127-149, doi:10.1007/5584_2018_173 (2018).
- 216 Diecke, S., Jung, S. M., Lee, J. & Ju, J. H. Recent technological updates and clinical applications of induced pluripotent stem cells. *The Korean journal of internal medicine* **29**, 547-557, doi:10.3904/kjim.2014.29.5.547 (2014).
- 217 Liao, S. *et al.* Endothelial Progenitor Cells for Ischemic Stroke: Update on Basic Research and Application. *Stem cells international* **2017**, 2193432, doi:10.1155/2017/2193432 (2017).
- 218 Kawamoto, A. *et al.* Intramyocardial transplantation of autologous endothelial progenitor cells for therapeutic neovascularization of myocardial ischemia. *Circulation* **107**, 461-468 (2003).
- 219 Lu, W. & Li, X. PDGFs and their receptors in vascular stem/progenitor cells: Functions and therapeutic potential in retinal vasculopathy. *Molecular aspects of medicine*, doi:10.1016/j.mam.2017.10.001 (2017).
- 220 Place, T. L., Domann, F. E. & Case, A. J. Limitations of oxygen delivery to cells in culture: An underappreciated problem in basic and translational research. *Free radical biology & medicine* **113**, 311-322, doi:10.1016/j.freeradbiomed.2017.10.003 (2017).
- 221 Sardesai, N., Rao, G. & Kostov, Y. Versatile common instrumentation for optical detection of pH and dissolved oxygen. *The Review of scientific instruments* **86**, 074302, doi:10.1063/1.4926542 (2015).
- 222 Tucker, W. D. & Bhimji, S. S. in *Anatomy, Blood Vessels* (StatPearls Publishing LLC., 2017).
- 223 Lee, S. J. *et al.* Regulation of muscle mass by follistatin and activins. *Molecular endocrinology (Baltimore, Md.)* **24**, 1998-2008, doi:10.1210/me.2010-0127 (2010).
- 224 Latres, E. *et al.* Activin A more prominently regulates muscle mass in primates than does GDF8. *Nature communications* **8**, 15153, doi:10.1038/ncomms15153 (2017).
- 225 Durieux, A. C. *et al.* Ectopic expression of myostatin induces atrophy of adult skeletal muscle by decreasing muscle gene expression. *Endocrinology* **148**, 3140-3147, doi:10.1210/en.2006-1500 (2007).
- 226 Mariot, V. *et al.* Downregulation of myostatin pathway in neuromuscular diseases may explain challenges of anti-myostatin therapeutic approaches. *Nature communications* **8**, 1859, doi:10.1038/s41467-017-01486-4 (2017).
- 227 Maeshima, K., Maeshima, A., Hayashi, Y., Kishi, S. & Kojima, I. Crucial role of activin a in tubulogenesis of endothelial cells induced by vascular endothelial growth factor. *Endocrinology* **145**, 3739-3745, doi:10.1210/en.2004-0213 (2004).
- 228 Le Fourn, V., Girod, P. A., Buceta, M., Regamey, A. & Mermod, N. CHO cell engineering to prevent polypeptide aggregation and improve therapeutic protein secretion. *Metabolic engineering* **21**, 91-102, doi:10.1016/j.ymben.2012.12.003 (2014).
- 229 Wurm, F. M. Production of recombinant protein therapeutics in cultivated mammalian cells. *Nature biotechnology* **22**, 1393-1398, doi:10.1038/nbt1026 (2004).
- 230 Kemter, E. *et al.* INS-eGFP transgenic pigs: a novel reporter system for studying maturation, growth and vascularisation of neonatal islet-like cell clusters. *Diabetologia* **60**, 1152-1156, doi:10.1007/s00125-017-4250-2 (2017).
- 231 Ahearn, A. J., Parekh, J. R. & Posselt, A. M. Islet transplantation for Type 1 diabetes: where are we now? *Expert review of clinical immunology* **11**, 59-68, doi:10.1586/1744666x.2015.978291 (2015).
- 232 Rezania, A. *et al.* Maturation of human embryonic stem cell-derived pancreatic progenitors into functional islets capable of treating pre-existing diabetes in mice. *Diabetes* **61**, 2016-2029, doi:10.2337/db11-1711 (2012).
- 233 Rezania, A. *et al.* Reversal of diabetes with insulin-producing cells derived in vitro from human pluripotent stem cells. *Nature biotechnology* **32**, 1121-1133, doi:10.1038/nbt.3033 (2014).
- 234 Takizawa-Shirasawa, S. *et al.* FGF7 and cell density are required for final differentiation of pancreatic amylase-positive cells from human ES cells. *Cell and tissue research* **354**, 751-759, doi:10.1007/s00441-013-1695-6 (2013).

- 235 Campbell, J. H., Efendy, J. L., Han, C., Girjes, A. A. & Campbell, G. R. Haemopoietic origin of myofibroblasts formed in the peritoneal cavity in response to a foreign body. *Journal of vascular research* **37**, 364-371, doi:10.1159/000025752 (2000).
- 236 Anderson, J. M. Biological Responses to Materials. *Annual Review of Materials Research* **31**, 81-110, doi:10.1146/annurev.matsci.31.1.81 (2001).
- 237 Maciver, A. H., McCall, M. & James Shapiro, A. M. Intra-abdominal adhesions: cellular mechanisms and strategies for prevention. *International journal of surgery (London, England)* **9**, 589-594, doi:10.1016/j.ijsu.2011.08.008 (2011).
- 238 Pileggi, A. *et al.* Reversal of diabetes by pancreatic islet transplantation into a subcutaneous, neovascularized device. *Transplantation* **81**, 1318-1324, doi:10.1097/01.tp.0000203858.41105.88 (2006).
- 239 Pepper, A. R. *et al.* A prevascularized subcutaneous device-less site for islet and cellular transplantation. *Nature biotechnology* **33**, 518-523, doi:10.1038/nbt.3211 (2015).
- 240 Gruionu, G., Stone, A. L., Schwartz, M. A., Hoying, J. B. & Williams, S. K. Encapsulation of ePTFE in prevascularized collagen leads to peri-implant vascularization with reduced inflammation. *Journal of biomedical materials research. Part A* **95**, 811-818, doi:10.1002/jbm.a.32925 (2010).
- 241 Michailova, K. N. & Usunoff, K. G. Serosal membranes (pleura, pericardium, peritoneum). Normal structure, development and experimental pathology. *Advances in anatomy, embryology, and cell biology* **183**, i-vii, 1-144, back cover (2006).
- 242 Hills, B. A. Lubrication of visceral movement and gastric motility by peritoneal surfactant. *Journal of gastroenterology and hepatology* **11**, 797-803 (1996).
- 243 van Hinsbergh, V. W., Kooistra, T., Scheffer, M. A., Hajo van Bockel, J. & van Muijen, G. N. Characterization and fibrinolytic properties of human omental tissue mesothelial cells. Comparison with endothelial cells. *Blood* **75**, 1490-1497 (1990).
- 244 Boland, G. M. & Weigel, R. J. Formation and prevention of postoperative abdominal adhesions. *The Journal of surgical research* **132**, 3-12, doi:10.1016/j.jss.2005.12.002 (2006).
- 245 Duron, J. J. Postoperative intraperitoneal adhesion pathophysiology. *Colorectal disease : the official journal of the Association of Coloproctology of Great Britain and Ireland* **9 Suppl 2**, 14-24, doi:10.1111/j.1463-1318.2007.01343.x (2007).
- 246 Imudia, A. N., Kumar, S., Saed, G. M. & Diamond, M. P. Pathogenesis of Intra-abdominal and pelvic adhesion development. *Seminars in reproductive medicine* **26**, 289-297, doi:10.1055/s-0028-1082387 (2008).
- 247 Ellis, H. The clinical significance of adhesions: focus on intestinal obstruction. *The European journal of surgery. Supplement. : = Acta chirurgica. Supplement*, 5-9 (1997).
- 248 diZerega, G. S. The peritoneum and its response to surgical injury. *Progress in clinical and biological research* **358**, 1-11 (1990).
- 249 Campbell, G. R. *et al.* The peritoneal cavity as a bioreactor for tissue engineering visceral organs: bladder, uterus and vas deferens. *Journal of tissue engineering and regenerative medicine* **2**, 50-60, doi:10.1002/term.66 (2008).
- 250 Hayashida, K., Kanda, K., Yaku, H., Ando, J. & Nakayama, Y. Development of an in vivo tissue-engineered, autologous heart valve (the biovalve): preparation of a prototype model. *The Journal of thoracic and cardiovascular surgery* **134**, 152-159, doi:10.1016/j.jtcvs.2007.01.087 (2007).
- 251 von Dembowski, T. Über die Ursachen der peritonealen Adhäsionen nach chirurgischen Eingriffen mit Rücksicht auf die Frage des Ileus nach Laparotomien. *Langenbeck's Archives of Surgery* **37** (1889).
- 252 Menzies, D. & Ellis, H. Intestinal obstruction from adhesions--how big is the problem? *Annals of the Royal College of Surgeons of England* **72**, 60-63 (1990).
- 253 Ward, B. C. & Panitch, A. Abdominal adhesions: current and novel therapies. *The Journal of surgical research* **165**, 91-111, doi:10.1016/j.jss.2009.09.015 (2011).

- 254 Koehler, R. H. *et al.* Minimal adhesions to ePTFE mesh after laparoscopic ventral incisional hernia repair: reoperative findings in 65 cases. *JSLs : Journal of the Society of Laparoendoscopic Surgeons* **7**, 335-340 (2003).
- 255 Coleman, D. L., King, R. N. & Andrade, J. D. The foreign body reaction: a chronic inflammatory response. *Journal of biomedical materials research* **8**, 199-211, doi:10.1002/jbm.820080503 (1974).
- 256 Holmdahl, L. & Ivarsson, M. L. The role of cytokines, coagulation, and fibrinolysis in peritoneal tissue repair. *The European journal of surgery = Acta chirurgica* **165**, 1012-1019, doi:10.1080/110241599750007810 (1999).
- 257 Giusto, G. *et al.* A pectin-honey hydrogel prevents postoperative intraperitoneal adhesions in a rat model. *BMC veterinary research* **13**, 55, doi:10.1186/s12917-017-0965-z (2017).
- 258 Hellebrekers, B. W., Trimbos-Kemper, T. C., Trimbos, J. B., Emeis, J. J. & Kooistra, T. Use of fibrinolytic agents in the prevention of postoperative adhesion formation. *Fertility and sterility* **74**, 203-212 (2000).
- 259 Masuda, S. *et al.* Eliminating residual iPS cells for safety in clinical application. *Protein & cell* **6**, 469-471, doi:10.1007/s13238-015-0170-4 (2015).
- 260 Ashton, N. Oxygen and the growth and development of retinal vessels. In vivo and in vitro studies. The XX Francis I. Proctor Lecture. *American journal of ophthalmology* **62**, 412-435 (1966).
- 261 Keshet, E. Preventing pathological regression of blood vessels. *The Journal of clinical investigation* **112**, 27-29, doi:10.1172/jci19093 (2003).
- 262 Patan, S. Vasculogenesis and angiogenesis. *Cancer treatment and research* **117**, 3-32 (2004).
- 263 Zimna, A. & Kurpisz, M. Hypoxia-Inducible Factor-1 in Physiological and Pathophysiological Angiogenesis: Applications and Therapies. *BioMed research international* **2015**, 549412, doi:10.1155/2015/549412 (2015).
- 264 Baluk, P. *et al.* Regulated angiogenesis and vascular regression in mice overexpressing vascular endothelial growth factor in airways. *The American journal of pathology* **165**, 1071-1085, doi:10.1016/s0002-9440(10)63369-x (2004).
- 265 Jin, K. *et al.* Caspase-3 and the regulation of hypoxic neuronal death by vascular endothelial growth factor. *Neuroscience* **108**, 351-358 (2001).
- 266 E, G. *et al.* Endogenous vascular endothelial growth factor-A (VEGF-A) maintains endothelial cell homeostasis by regulating VEGF receptor-2 transcription. *The Journal of biological chemistry* **287**, 3029-3041, doi:10.1074/jbc.M111.293985 (2012).
- 267 Baffert, F. *et al.* Cellular changes in normal blood capillaries undergoing regression after inhibition of VEGF signaling. *American journal of physiology. Heart and circulatory physiology* **290**, H547-559, doi:10.1152/ajpheart.00616.2005 (2006).
- 268 Ausprunk, D. H., Falterman, K. & Folkman, J. The sequence of events in the regression of corneal capillaries. *Laboratory investigation; a journal of technical methods and pathology* **38**, 284-294 (1978).
- 269 Hoper, J. & Jahn, H. Influence of environmental oxygen concentration on growth and vascular density of the area vasculosa in chick embryos. *International journal of microcirculation, clinical and experimental* **15**, 186-192 (1995).
- 270 Benjamin, L. E. The controls of microvascular survival. *Cancer metastasis reviews* **19**, 75-81 (2000).
- 271 Liechty, W. B., Kryscio, D. R., Slaughter, B. V. & Peppas, N. A. Polymers for drug delivery systems. *Annual review of chemical and biomolecular engineering* **1**, 149-173, doi:10.1146/annurev-chembioeng-073009-100847 (2010).
- 272 Jain, K. K. Current status and future prospects of drug delivery systems. *Methods in molecular biology (Clifton, N.J.)* **1141**, 1-56, doi:10.1007/978-1-4939-0363-4_1 (2014).
- 273 Chien, J. Y. & Ho, R. J. Drug delivery trends in clinical trials and translational medicine: evaluation of pharmacokinetic properties in special populations. *Journal of pharmaceutical sciences* **100**, 53-58, doi:10.1002/jps.22253 (2011).

- 274 Ho, R. J. & Chien, J. Y. Drug delivery trends in clinical trials and translational medicine: Updated
analysis of ClinicalTrials.gov database. *Journal of pharmaceutical sciences* **98**, 1928-1934,
doi:10.1002/jps.21649 (2009).
- 275 Meier, L. A. *et al.* Blood outgrowth endothelial cells alter remodeling of completely biological
engineered grafts implanted into the sheep femoral artery. *Journal of cardiovascular
translational research* **7**, 242-249, doi:10.1007/s12265-013-9539-z (2014).
- 276 Hellstrom, M. *et al.* Lack of pericytes leads to endothelial hyperplasia and abnormal vascular
morphogenesis. *The Journal of cell biology* **153**, 543-553 (2001).
- 277 Patel, J. J., Srivastava, S. & Siow, R. C. Isolation, Culture, and Characterization of Vascular
Smooth Muscle Cells. *Methods in molecular biology (Clifton, N.J.)* **1430**, 91-105,
doi:10.1007/978-1-4939-3628-1_6 (2016).
- 278 Esteves, C. L. & Donadeu, F. X. Pericytes and their potential in regenerative medicine across
species. *Cytometry. Part A : the journal of the International Society for Analytical Cytology*,
doi:10.1002/cyto.a.23243 (2017).
- 279 Simonavicius, N. *et al.* Pericytes promote selective vessel regression to regulate vascular
patterning. *Blood* **120**, 1516-1527, doi:10.1182/blood-2011-01-332338 (2012).
- 280 Laschke, M. W. & Menger, M. D. Prevascularization in tissue engineering: Current concepts
and future directions. *Biotechnology advances* **34**, 112-121,
doi:10.1016/j.biotechadv.2015.12.004 (2016).
- 281 Carrabba, M. & Madeddu, P. Current Strategies for the Manufacture of Small Size Tissue
Engineering Vascular Grafts. *Frontiers in bioengineering and biotechnology* **6**, 41,
doi:10.3389/fbioe.2018.00041 (2018).
- 282 Nicolini, F. *et al.* Coronary Artery Bypass Grafting with Arterial Conduits in the Elderly.
International heart journal **58**, 647-653, doi:10.1536/ihj.16-468 (2017).
- 283 Groneberg, D. *et al.* Smooth muscle-specific deletion of nitric oxide-sensitive guanylyl cyclase
is sufficient to induce hypertension in mice. *Circulation* **121**, 401-409,
doi:10.1161/circulationaha.109.890962 (2010).
- 284 Rolstad, B. The athymic nude rat: an animal experimental model to reveal novel aspects of
innate immune responses? *Immunological reviews* **184**, 136-144 (2001).
- 285 Bamoulid, J. *et al.* The need for minimization strategies: current problems of
immunosuppression. *Transplant international : official journal of the European Society for
Organ Transplantation* **28**, 891-900, doi:10.1111/tri.12553 (2015).
- 286 Song, Y. *et al.* Feasibility of localized immunosuppression: 3. Preliminary evaluation of
organosilicone constructs designed for sustained drug release in a cell transplant environment
using dexamethasone. *Die Pharmazie* **67**, 394-399 (2012).

APPENDIX

Copyright permission of reprints

Figure 1:

Reprinted by permission from Springer Nature: Springer Singapore Clinical Regenerative Medicine in Urology by Sujin Noh, Noehyun Myung, Myeongji Park, Seulgi Kim, Sung-Uk Zhang, Hyun-Wook © 2018.

Figure 2:

Reprinted from Pearson Education, Inc. publishing as Benjamin Cummings, Human Anatomy & Physiology by Elaine N. Marieb, Susan J. Mitchell, Lori A. Smith © 2013.

Figure 5, 7(A, D-G), 8-10, 14, 16, 19:

Modified and reprinted from Springer Nature, Scientific Reports, Volume 8, Article number: 4719 (2018), Evaluation of a Miniaturized Biologically Vascularized Scaffold *in vitro* and *in vivo*, by Sebastian Kress, Johannes Baur, Christoph Otto, Natalie Burkard, Joris Braspenning, Heike Walles, Joachim Nickel & Marco Metzger. This work is licensed under the Creative Commons Attribution 4.0 International License (<http://creativecommons.org/licenses/by/4.0/>).

Figure 7:

(B) Modified and reprinted from Biomaterials, Volume 26, Issue 14, by Ruben Y. Kannan, Henryk J. Salacinski, Kevin Sales, Peter Butler & Alexander M. Seifalian, The roles of tissue engineering and vascularisation in the development of micro-vascular networks: a review, Pages 1857-1875, © 2005, with permission from Elsevier.

Name, Vorname: Kress, Sebastian
Straße: Friedrichstraße 13
PLZ und Ort: 97082 Würzburg
Tel.: 0931 201 73461
E-Mail: sebastian.kress@uni-wuerzburg.de

Erklärungen nach §4 Abs. 3 Satz 3, 5, 8 der Promotionsordnung der Fakultät für Biologie

Affidavit

I hereby declare that my thesis entitled: „Development and proof of concept of a biological vascularized cell-based drug delivery system” is the result of my own work.

I did not receive any help or support from commercial consultants. All sources and / or materials applied are listed and specified in the thesis.

Furthermore I verify that the thesis has not been submitted as part of another examination process neither in identical nor in similar form.

Eidesstattliche Erklärung

Hiermit erkläre ich an Eides statt, die Dissertation: „Entwicklung und Proof of Concept eines biologischen, vaskularisierten, zellbasierten Drug-Delivery-Systems“, eigenständig, d. h. insbesondere selbständig und ohne Hilfe eines kommerziellen Promotionsberaters, angefertigt und keine anderen, als die von mir angegebenen Quellen und Hilfsmittel verwendet zu haben.

Ich erkläre außerdem, dass die Dissertation weder in gleicher noch in ähnlicher Form bereits in einem anderen Prüfungsverfahren vorgelegen hat.

Würzburg, den 08.11.2018

Unterschrift

Danksagung

Zuallererst möchte ich mich aufs herzlichste bei Frau Prof. Dr. Heike Walles bedanken, mir die Möglichkeit gegeben zu haben meine Dissertation an ihrem Lehrstuhl für Tissue Engineering und Regenerative Medizin anzufertigen. Bereits schon während des Studiums durfte ich dich in Vorlesungen und dann einem Praktikum kennen lernen nachdem du aus Stuttgart nach Würzburg kamst. Aufgrund deiner positiven und inspirierenden Art und der spannenden Arbeitsthemen wollte ich bereits schon gerne während Bachelor- oder Masterarbeit mit dir zusammenarbeiten. Zur Dissertation konnte ich dies nun endlich. Hierbei durfte ich von deinem Wissen und deiner Erfahrung profitieren und konnte stets auf deine Unterstützung mit vielen wertvollen Vorschlägen und Ideen vertrauen (sowie dem ein oder anderen Arschtritt). Danke.

Des Weiteren danke ich Herrn Prof. Dr. Georg Krohne für die Betreuung meiner Arbeit als Zweitgutachter und dem zur Verfügung stellen seiner Abteilung für Elektronenmikroskopie.

Ich danke dem Land Bayern und der Bayerischen Forschungsstiftung für die Förderung des „Forschungsverbunds Muskelschwund (Sarkopenie) und Osteoporose – Folgen eingeschränkter Regeneration im Alter (FORMOsA)“, Förderkennzeichen AZ-1044-12.

Dr. Joachim Nickel möchte ich für die stete Motivation, positive Unterstützung und das Engagement selbstständiges Arbeiten zu vermitteln danken. Joachim, ich wollte speziell dich zum direkten Ansprechpartner und Betreuer im Labor, da ich in meinem Praktikum bei dir deinen weiten Erfahrungsschatz und tiefes Fachwissen zu jedweder Fragestellung, sei es praktisch oder theoretisch, bewunderte. Letztendlich bedanke ich mich für die lustigen Sprüche, deine Versuche mich nach Rückschlägen wiederaufzubauen und weiter zu ermutigen, und den steten Ansporn mit der Arbeit fertig zu werden.

Für das Durchführen der Tierversuche danke ich Dr. Marco Metzger. Deine Expertise und Hilfe war unerlässlich das Projekt so weit voran zu treiben. Darüber hinaus bin ich dankbar für die geknüpften Kooperation mit Prof. S. Dalton, wodurch sehr viel Arbeit auf mich zu kam.

Frau Dr. Daniela Z. danke ich mich vor der Arbeitslosigkeit in die Vollbeschäftigung gerettet zu haben um mich näher mit das Pankreas auseinanderzusetzen. Einem vortrefflichen Organ, das gepaart mit der Möglichkeit mein Methodenspektrum auf iPS-

Technologie zu erweitern, beispielhaft dazu dient eventuell funktionelle Differenzierungen über wochen(end)lange Versuche nachzuweisen.

Mein persönlicher Dank, mich durch die nicht immer einfache Zeit begleitet und mir jederzeit mit Rat und Tat zur Seite gestanden zu haben, gilt all denen die hier nicht einzeln aufgelistet sein mussten.